

AD-A184 865

1

DTIC FILE COPY



DTIC  
ELECTE  
OCT 0 1 1987  
S D  
dD

DYNAMICS OF PROPELLANT  
FEEDLINE SYSTEMS  
  
THESIS  
  
William F. Berrier, Jr.  
First Lieutenant, USAF  
  
AFIT/GA/AA/85D-2

DISTRIBUTION STATEMENT A  
Approved for public release  
Distribution Unlimited

DEPARTMENT OF THE AIR FORCE  
AIR UNIVERSITY  
**AIR FORCE INSTITUTE OF TECHNOLOGY**

Wright-Patterson Air Force Base, Ohio

87 9 25 072

1

DTIC  
ELECTE  
OCT 0 1 1987  
S D  
D

DYNAMICS OF PROPELLANT

FEEDLINE SYSTEMS

THESIS

William F. Berrier, Jr.  
First Lieutenant, USAF

AFIT/GA/AA/85D-2

Approved for public release; distribution unlimited

DYNAMICS OF PROPELLANT  
FEEDLINE SYSTEMS

THESIS

Presented to the Faculty of the School of Engineering  
of the Air Force Institute of Technology

Air University

In Partial Fulfillment of the  
Requirements for the Degree of  
Master of Science in Astronautical Engineering



William F. Berrier, Jr., B.S.  
First Lieutenant, USAF

May 1987

Accession For	
NTIS GRA&I	<input checked="" type="checkbox"/>
DTIC TAB	<input type="checkbox"/>
Unannounced	<input type="checkbox"/>
Justification	
By	
Date	
Doc	

A-1

### Acknowledgements

In the course of performing this investigation and writing this thesis, I find myself deeply indebted to a number of people. Special thanks go to my faculty advisor, Dr. Milton E. Franke, for his infinite patience and for his help in establishing the direction and organization of this work. Also, I am grateful to the members of GA-85D, especially Capt. Robert Bandstra, for being there, both in class and out. And finally, I wish to thank my family and friends for the support and encouragement I received. All of these people helped me through a long and trying period of my life.

William F. Berrier, Jr.

## Table of Contents

	Page
Acknowledgements	ii
List of Figures	iv
List of Tables	viii
Notation	ix
Abstract	xi
I. Introduction	1
II. Method of Characteristics	4
Equations of Motion	4
Finite Difference Equations	6
III. Boundary Equations	9
Known End Conditions	9
Series Connection	10
Valve-in-line	11
Cavitation	12
Accumulator	14
IV. System Analysis	16
Single Pipe Models	16
Multiple Pipe Models	19
V. Results	29
Single Pipe Verification for Valve Closure	29
Single Pipe Verification for Cavitation	39
Multiple Pipe Verification of Valve-in-line	50
Verification of Multiple Pipe Valve Closure	56
Saturn V Feedline	67
VI. Conclusions	84
Bibliography	85
Appendix A: Program User's Guide	87
Appendix B: Additional Boundary Conditions	102
Vita	104

## List of Figures

Figure		Page
2-1	x-t grid for pipe divided into N reaches	7
3-1	Characteristic lines at pipe ends	9
3-2	Series Connection	10
3-3	Valve-in-line	10
4-1	Upstream pressure for simulation 2	19
4-2	Valve Characteristic, $\tau$	21
4-3	Pulser valve	27
5-1	Results by Wylie and Streeter (L=600 m, a=1200 m/s, D=0.5 m, $t_c=2.1$ s, $E_m=1.5$ , f=0.018)	30
5-2	Program results for single pipe closure (L=600 m, a=1200 m/s, D=0.5 m, $t_c=2.1$ s, $E_m=1.5$ , f=0.018)	30
5-3	Program results for changes in $E_m$ (L=600 m, a=1200 m/s, D=0.5 m, $t_c=2.1$ s, f=0.018)	32
5-4	Program results for changes in $t_c$ (L=600 m, a=1200 m/s, D=0.5 m, $E_m=1.5$ , f=0.018)	32
5-5	Program results for changes in friction factor (L=600 m, a=1200 m/s, D=0.5 m, $t_c=2.1$ s, $E_m=1.5$ )	36
5-6	Program results for changes in pipe length (L=600 m, a=1200 m/s, D=0.5 m, $t_c=2.1$ s, $E_m=1.5$ , f=0.018)	36
5-7	Wylie's results for two locations (L=3048 m, a=981 m/s, D=0.61 m, $Q_0=0.89$ m <sup>3</sup> /s, $H_v=-10.06$ m)	39
5-8	Program results for cavitation simulation 1 (x=813 m, L=3048 m, a=981 m/s, D=0.61 m, $Q_0=0.89$ m <sup>3</sup> /s, $H_v=-10.06$ m)	40
5-9	Program results for simulation 1 (x=1627 m, L=3048 m, a=981 m/s, D=0.61 m, $Q_0=0.89$ m <sup>3</sup> /s, $H_v=-10.06$ m)	40
5-10	Wylie's results for simulation 2 ( $H_v=-10.1$ m)	42
5-11	Program results for simulation 2 (x=1160 m, L=1450 m, a=1290 m/s, D=0.1 m, $Q_0=0.0158$ m <sup>3</sup> /s, $H_v=-10.1$ m)	43
5-12	Program results for simulation 2 (x=1160 m, L=1450 m, a=1290 m/s, D=0.1 m, $Q_0=0.0158$ m <sup>3</sup> /s, $H_v=-10.1$ m)	43

Figure		Page
5-13	Program results for simulation 1 (L=3048 m, a=981 m/s, D=0.61 m, Q <sub>0</sub> =0.89 m <sup>3</sup> /s, H <sub>v</sub> =-100 m)	45
5-14	Program results for simulation 1 (x=813 m, L=3048 m, a=981 m/s, D=0.61 m, Q <sub>0</sub> =0.89 m <sup>3</sup> /s, H <sub>v</sub> =-5.03 m)	45
5-15	Program results using Euler's method (x=813 m, L=3048 m, a=981 m/s, D=0.61 m, Q <sub>0</sub> =0.89 m <sup>3</sup> /s, H <sub>v</sub> =-10.06 m)	47
5-16	Program results using forward integration (x=813 m, L=3048 m, a=981 m/s, D=0.61 m, Q <sub>0</sub> =0.89 m <sup>3</sup> /s, H <sub>v</sub> =-10.06 m)	47
5-17	Program results for simulation 1 with air release (x=813 m, L=3048 m, a=981 m/s, D=0.61 m, Q <sub>0</sub> =0.89 m <sup>3</sup> /s, H <sub>v</sub> =-10.06 m)	49
5-18	Results for air release and reduced time-step (x=813 m, L=3048 m, a=981 m/s, D=0.61 m, Q <sub>0</sub> =0.89 m <sup>3</sup> /s, H <sub>v</sub> =-10.06 m)	49
5-19	Swaffield's results at the valve for case 1 (L <sub>2,3</sub> =9.87 m, a=918 m/s, D=0.0508 m, P <sub>v</sub> =700 Pa, t <sub>c</sub> =0.081 s)	51
5-20	Program results at the valve for case 1 (L <sub>2,3</sub> =9.87 m, a=918 m/s, D=0.0508 m, P <sub>v</sub> =700 Pa, t <sub>c</sub> =0.081 s)	51
5-21	Swaffield's results for case 2 (L <sub>2,3</sub> =9.87 m, a=918 m/s, D=0.0508 m, P <sub>v</sub> =700 Pa, t <sub>c</sub> =0.16 s)	53
5-22	Program results for case 2, 50.8 mm from valve (L <sub>2,3</sub> =9.87 m, a=918 m/s, D=0.0508 m, P <sub>v</sub> =700 Pa, t <sub>c</sub> =0.16 s)	54
5-23	Program results for case 2, 4.04 m from valve (L <sub>2,3</sub> =9.87 m, a=918 m/s, D=0.0508 m, P <sub>v</sub> =700 Pa, t <sub>c</sub> =0.16 s)	54
5-24	Swaffield's results for case 3 (L <sub>2,3</sub> =9.87 m, a=918 m/s, D=0.0508 m, P <sub>v</sub> =700 Pa, t <sub>c</sub> =0.14 s)	55
5-25	Program results for case 3 (L <sub>2,3</sub> =9.87 m, a=918 m/s, D=0.0508 m, P <sub>v</sub> =700 Pa, t <sub>c</sub> =0.081 s)	55
5-26	Program results for case 1 of multipipe closure (L <sub>1</sub> =351 m, L <sub>2</sub> =483 m, L <sub>3</sub> =115 m, a=1200 m/s, H <sub>0</sub> =289 m)	59
5-27	Program results for case 2 of multipipe closure (L <sub>1</sub> =351 m, L <sub>2</sub> =483 m, L <sub>3</sub> =115 m, a=1200 m/s, H <sub>0</sub> =400 m)	63
5-28	Program results for case 3 of multipipe closure (L <sub>1</sub> =351 m, L <sub>2</sub> =483 m, L <sub>3</sub> =115 m, a=1200 m/s, H <sub>0</sub> =200 m)	63
5-29	Program results for case 4 of multipipe closure (L <sub>1</sub> =351 m, L <sub>2</sub> =483 m, L <sub>3</sub> =115 m, a=1200 m/s, H <sub>0</sub> =289 m, hard closure)	65

Figure		Page
5-30	Program results for case 5 of multipipe closure ( $L_1=351$ m, $L_2=483$ m, $L_3=115$ m, $a=1200$ m/s, $H_0=289$ m, soft closure)	65
5-31	Results of run 1 for Saturn V feedline ( $P_0=621$ kPa, $t_c=1.5$ s, $E_m=1.2$ )	69
5-32	Results of run 2 for Saturn V feedline ( $P_0=621$ kPa, $t_c=1.5$ s, $E_m=1.2$ )	69
5-33	Results of run 3 for Saturn V feedline ( $P_0=621$ kPa, $t_c=1.5$ s, $E_m=1.0$ )	71
5-34	Results of run 4 for Saturn V feedline ( $P_0=621$ kPa, $t_c=1.5$ s, $E_m=1.5$ )	71
5-35	Results of run 5 for Saturn V feedline ( $P_0=896$ kPa, $t_c=1.5$ s, $E_m=1.2$ )	73
5-36	Results of run 6 for Saturn V feedline ( $P_0=621$ kPa, $t_c=1.5$ s, $E_m=1.2$ , $\omega=2.5$ Hz)	73
5-37	Results of run 7 for Saturn V feedline ( $P_0=621$ kPa, $t_c=1.5$ s, $E_m=1.2$ , $\omega=10$ Hz)	75
5-38	Results of run 8 for Saturn V feedline ( $P_0=621$ kPa, $t_c=1.5$ s, $E_m=1.2$ , $\omega=25$ Hz)	75
5-39	Results of run 9 for Saturn V feedline ( $P_0=621$ kPa, $t_c=1.5$ s, $E_m=1.0$ , $\omega=2.5$ Hz)	77
5-40	Results of run 10 for Saturn V feedline ( $P_0=621$ kPa, $t_c=1.5$ s, $E_m=1.2$ , $\omega=2.5$ Hz)	77
5-41	Results of run 11 for Saturn V feedline ( $P_0=896$ kPa, $t_c=1.5$ s, $E_m=1.0$ , $\omega=10$ Hz)	78
5-42	Results of run 12 for Saturn V feedline ( $P_0=621$ kPa, $t_c=1.5$ s, $E_m=1.0$ , vol.= $0.0$ m <sup>3</sup> )	80
5-43	Results of run 13 for Saturn V feedline ( $P_0=621$ kPa, $t_c=1.5$ s, $E_m=1.0$ , vol.= $0.018$ m <sup>3</sup> )	80
5-44	Results of run 14 for Saturn V feedline ( $P_0=621$ kPa, $t_c=1.5$ s, $E_m=1.0$ , vol.= $0.036$ m <sup>3</sup> )	80
5-45	Results of run 15 for Saturn V feedline ( $P_0=621$ kPa, $t_c=1.5$ s, $E_m=1.0$ , vol.= $0.054$ m <sup>3</sup> )	81
5-46	Results of run 16 for Saturn V feedline ( $P_0=896$ kPa, $t_c=1.5$ s, $E_m=1.0$ , vol.= $0.0$ m <sup>3</sup> )	81



Figure		Page
5-47	Results of run 17 for Saturn V feedline ( $P_0=896$ kPa, $t_c=1.5$ s, $E_m=1.0$ , vol.= $0.054$ m <sup>3</sup> )	83
5-48	Results of run 18 for Saturn V feedline ( $P_0=621$ kPa, $t_c=1.5$ s, $E_m=1.0$ , $\omega=2.5$ Hz, vol.= $0.054$ m <sup>3</sup> )	83
A-1	Program Flow Chart	88
B-1	Branch Connection	102

List of Tables

Table	Page
I. Input Variations for Single Pipe Closure	17
II. Flow Parameters for Valve-in-line	20
III. Pipeline Parameters for Valve-in-line	20
IV. System Data for Series Closure	21
V. Input Variations for Series Closure	22
VI. Feedline Configuration Data	25
VII. Input Parameters for Saturn V Feedline	28
VIII. Comparison of Results for Head at the Valve during Series Closure	57

### Notation

A	Cross sectional area of the pipe
a	Velocity of pressure pulse
a'	Compliance
B	Pipeline constant
B <sub>0</sub> , B <sub>1</sub> , B <sub>2</sub> , B <sub>3</sub>	Pump curve constants
C <sub>M</sub> , C <sub>p</sub>	Known constants in characteristic equations
C <sub>v</sub>	Known constant in valve equation
D	Pipe diameter
E	Young's modulus
E <sub>m</sub>	Exponent from valve closure equation
e	Pipe thickness
FF	Pipeline constant
f	Darcy-Weisbach friction factor
H	Piezometric head
H*	Absolute piezometric head
g	gravitational acceleration
K	Bulk modulus
L	Pipe length
L <sub>1</sub> , L <sub>2</sub>	Equation identifiers for the method of characteristics
N	Number of reaches a pipe is divided into for computation
P	Pressure
Q	Volume flow rate at a section
R	Pipeline constant
t	Time
t <sub>c</sub>	Time until complete closure of a valve

$V$	Mean velocity at a point
$V_g$	Volume of gas at a section
$x$	Distance along a pipe
$z$	Height above or below some reference plane
$\alpha$	Slope of a pipe
$\alpha_0$	Void fraction
$\zeta$	Interpolation constant
$\lambda$	Unknown multiplier from method of characteristics
$\rho$	Mass density
$\tau$	Dimensionless valve characteristic
$\omega$	Frequency

Subscripts

A, B, C	Known points in the characteristic grid
d	Downstream
o	Initial value
P	Solution point in x-t plane
R, S	Interpolated points for characteristic grid
t, x	Denote partial differentiation
u	Upstream
v	At vapor conditions
1, 2, etc.	Labels indicating a particular pipe within a system

Abstract

In this investigation, a generalized computer code for the simulation of fluid transients was assembled, verified, and applied. The solution method developed for the program was based on a method of characteristics solution of the equations of motion for one-dimensional fluid flow in pipelines. The differential equations were solved using a first-order finite difference technique. Boundary conditions for the equations of motion were developed or directly included from available component models. The computer routines were verified by comparison of results with published results from several sources. The agreement between the results of this study and the published data was quite good for a wide range of boundary conditions and pipe systems. Recommendations were made for improvement of some models and the replacement of others to further improve the accuracy of the results.

# DYNAMICS OF PROPELLANT FEEDLINE SYSTEMS

## I. Introduction

Fluid systems in use by the aerospace industry are often characterized by high volume flow rates or high system pressures. Furthermore, these operating conditions are coupled with small permissible ranges of variation from the design flow and pressure operating points (1:1). The net result of the two factors is a large potential for performance degradation due to fluid transients. Within the space program, a sometimes spectacular manifestation of this phenomena is combustion instability, a performance problem frequently caused by wave motion occurring within the propellant feed system of liquid rocket engines (2:1).

Previous Work. Many attempts have been made to model the dynamics of liquid propellant feedlines. All of the models developed to date, however, can be categorized either as a linearized network model or as a time-step simulation. The network models achieve a solution by linearizing the equations of motion, then treating the transient as a perturbation on some mean flow. Time-step simulations on the other hand employ nonlinear finite difference forms of the equations of motion, usually obtained by the method of characteristics (3:1).

One of the first to apply linearized flow equations to feedlines was Rubin (4). He employed both fluid dynamic theories and electrical circuit analogies to achieve a solution. Ryan (5) made use of a linearized model to investigate structural instabilities coupled to fluid transients in the S-IIc engines of the Saturn V. About that same time Johnson (6) attempted to produce a generalized computer program based on linear

equations to predict longitudinal instability in propulsion systems. More recently, Holster and Astleford (7) developed a general analytical model based on the linerized flow equations developed by D'Souza and Oldenburger (8).

As for time-step simulations, Woods (9) applied the method of characteristics to a frictionless model to study fluid fluctuations in feedlines. Wood et al. (1) developed a more general nonlinear distributed parameter model which the authors named the "wave-plan" method. The "wave-plan" method was developed to predict unsteady flow in liquid filled lines and was later used to create a generalized digital computer program (10) to analyze fluid transients in liquid rocket feedlines. Fashbaugh and Streeter (11) made use of the method of characteristics to develop their own digital computer program to investigate transients in propellant feedlines of the Titan II missile. However, one of the most recent digital computer programs that made use of the method of characteristics did not arise out of a study of propellant feedlines. During the Aircraft Hydraulic Systems Dynamic Analysis Project, the McDonnell Aircraft Company developed four digital computer programs for simulating a number of different aspects of the dynamics of aircraft hydraulic systems. One of the four programs, named Hydraulic Transients (HYTRAN) (12), simulates and predicts the dynamic response of a hydraulic system to sudden changes in load flow demand. HYTRAN, however, is a very complex computer program, where the user must be very familiar with transient phenomena in hydraulic systems and know how to interpret the results.

Objectives. The time-step simulations which have been encountered in the literature, so far, tended to be either very complex or overly

restrictive. Therefore, the objective of this investigation was to assemble, verify, and apply a simple but flexible computer program for the analysis of fluid transients in pipelines. Routines in the program were adapted from existing code whenever possible. In addition, this investigation was to provide a source from which future investigators could draw references on work of a similar nature.

Approach. The approach used in this investigation was not completely new, rather, it was a variation on the method used in several of the works presented earlier. The investigation conducted for this thesis proceeded through three main steps. Step one was the derivation of the equations that would form the basis of the computer program. First the finite difference forms of the equations of motion were derived by the method of characteristics (13, 14). Then, a number of boundary conditions which commonly occur in propellant feedlines were developed to provide for a complete solution. The second step of this study was to present the systems to be modeled. It was at this point, that the input data for each system was described and the appropriate boundary conditions assigned. And finally, the last step was to analyze the results obtained by running computer simulations which made use of the systems modeled in step two. The results of the simulations were compared with published data when possible.



## II. Method of Characteristics

In this section a numerical solution of the equations that were used to model unsteady flow in pipelines is developed by the method of characteristics. This technique was used to transform partial differential equations which had no general solution into particular total differential equations that did. The equations that resulted were then integrated to provide finite difference equations by which the pressure and flow velocity within a pipeline could be obtained numerically. The process by which these equations were derived was not new, however the final form of the finite difference equations used for the calculations was different. Unlike previous derivations, the final form was in terms of pressure and volume flow rate, not head or pressure and velocity.

### Equations of Motion

In this study, transient fluid flow was represented by a one-dimensional model with time,  $t$ , and distance along the pipe axis,  $x$ , as independent variables, and pressure,  $P$ , and mean sectional velocity,  $V$ , as dependent variables. The partial differential equations may be derived by the application of the momentum and of the continuity principles to a constant area section of pipe having a length,  $dx$  (13:694). The derivation which follows is similar to derivations presented by Swaffield (13), Wylie and Streeter (14), and Watters (15).

The equations of motion:

$$L_1 = P_x / \rho + g \sin \alpha + V V_x + V_t + f V |V| / 2D = 0 \quad (2.1)$$

and continuity:

$$L_2 = P_t + \rho a^2 V_x + V P_x = 0 \quad (2.2)$$

are the equations which will be used in this development.

The method of characteristics proceeds by making a linear combination of Eq. (2.1) and (2.2) using an unknown multiplier,  $\lambda$ .

$$L=L_1+\lambda L_2=[P_x/\rho+gsina+VV_x+fV V /2D]+\lambda[P_t+\rho a^2V_x+VP_x]=0 \quad (2.3)$$

Regrouping terms,

$$\lambda[P_x(V+1/\lambda\rho)+P_t]+[V_x(V+\lambda\rho a^2)+V_t]+gsina+fV|V|/2D=0 \quad (2.4)$$

Eq. (2.4) can be simplified by the appropriate selection of the two particular values of  $\lambda$ . Since  $P$  and  $V$  are functions of  $x$  and  $t$ , from calculus

$$dP/dt=P_x dx/dt+P_t \quad dV/dt=V_x dx/dt+V_t \quad (2.5)$$

Upon examination of equations (2.4) and (2.5),

$$dx/dt=V+1/\lambda\rho=V+\lambda\rho a^2 \quad (2.6)$$

Thus, Eq. (2.4) becomes the ordinary differential equation

$$\lambda dP/dt+dV/dt+gsina+fV|V|/2D=0 \quad (2.7)$$

Eq. (2.6) can be solved to obtain the two particular values of  $\lambda$ ,

$$\lambda = \pm 1/\rho a \quad (2.8)$$

Substituting Eq. (2.8) back into Eq. (2.6) produces

$$dx/dt=V \pm a \quad (2.9)$$

To complete the transformation, Eq. (2.8) is substituted into Eq.

(2.7). The characteristic equations which result are:

$$dV/dt+(1/\rho a)dP/dt+gsina+fV|V|/2D=0 \quad (2.10)$$

$$dx/dt=V+a \quad (2.11)$$

$$dV/dt-(1/\rho a)dP/dt+gsina+fV|V|/2D=0 \quad (2.12)$$

$$dx/dt=V-a \quad (2.13)$$

where Eq. (2.10) and (2.12) are valid only when the respective equations, Eq. (2.11) and (2.13) are valid.

### Finite Difference Equations

Due to the nonlinear nature of the characteristic equations, a finite difference approach is used to obtain a numerical solution. To this point the derivation has paralleled the development presented by Watters (15). However, Watters completed his derivation after replacing pressure by piezometric head,  $P = \rho g(H-z)$ . Wylie and Streeter (14) make the same substitution much earlier in their derivation. This development, though, will retain the pressure throughout, in a manner similar to the development by Swaffield (13).

By multiplying Eq. (2.10) through (2.13) by  $dt$ , and integrating the equations using a first-order approximation, the finite difference forms are:

$$V_P - V_R + (P_P - P_R) / \rho a + g \sin \alpha (t_P - t_R) + f V_R |V_R| (t_P - t_R) / 2D = 0 \quad (2.14)$$

$$x_P - x_R = (V_R + a)(t_P - t_R) \quad (2.15)$$

$$V_P - V_S - (P_P - P_S) / \rho a + g \sin \alpha (t_P - t_S) + f V_S |V_S| (t_P - t_S) / 2D = 0 \quad (2.16)$$

$$x_P - x_S = (V_S - a)(t_P - t_S) \quad (2.17)$$

Solving for  $V_P$  and writing Eq. (2.14) and (2.16) in terms of volume flow rate in place of velocity

$$Q_P = C_P - B P_P \quad (2.18)$$

$$Q_P = C_M + B P_P \quad (2.19)$$

In which

$$C_P = Q_R - B P_R - R_R - FF Q_R |Q_R| \quad (2.20)$$

$$C_M = Q_S - B P_S - R_S - FF Q_S |Q_S| \quad (2.21)$$

where  $B = A / \rho a$ , and  $R = g A \Delta t \sin \alpha$ , and  $FF = f \Delta t / 2DA$ .

Fig. 2-1, which graphically represents Eq. (2.15) and (2.17), shows the characteristics in the  $x-t$  plane along which Eq. (2.14) and (2.16) are integrated.

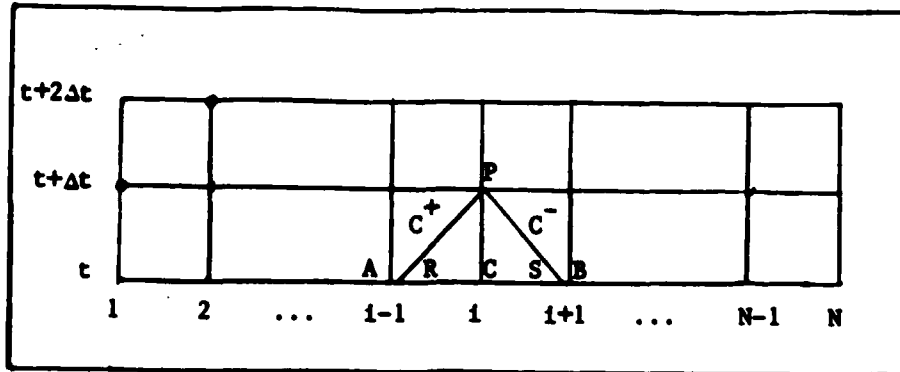


Fig. 2-1. x-t grid for a pipe divided into N reaches.

To determine the mesh of the grid the method of specified time intervals is used. In order to keep the solution numerically stable, the Courant condition (14:58) must be satisfied

$$\Delta t(V+a) \leq \Delta x \quad (2.22)$$

The method of specified time intervals assumes the conditions are known at A, B, and C (Fig. 2-1) either from the previous time step or from the steady solution. Following the usual approach, a linear interpolation is then made to find the pressure and the volume flow rate at points R and S. The stability criteria is necessary to insure that points R and S do not fall outside points A and B, thus maintaining the validity of the interpolation. From Fig. 2-1

$$(Q_R - Q_A) / (Q_C - Q_A) = (x_R - x_A) / (x_C - x_A) \quad (2.23)$$

which becomes,

$$Q_R = Q_C - \xi(Q_C - Q_A) \quad (2.24)$$

after approximating  $V+a$  by  $\underline{a}$  in Eq. (2.15). This approximation is valid where  $V \ll a$ , which holds for most transient problems in fluid pipelines (13:58).

By interpolations similar to Eq. (2.23)

$$Q_S = Q_C - \zeta(Q_C - Q_B) \quad (2.25)$$

$$P_R = P_C - \zeta(P_C - P_A) \quad (2.26)$$

$$P_S = P_C - \zeta(P_C - P_B) \quad (2.27)$$

where  $\zeta = a\Delta t / \Delta x$ .

To calculate the final solution for volume flow rate and pressure at P it is necessary to solve six equations. The six are Eqs. (2.23) through (2.27), and Eq. (2.20) and (2.21). The addition of Eq. (2.18) and (2.19), followed by the solution of the resulting equation for the flow,  $Q_p$ , gives:

$$Q_p = (C_M + C_p) / 2 \quad (2.28)$$

The flow,  $Q_p$ , may then be substituted into either Eq. (2.18) or (2.19) to obtain the pressure at that point.

### III. Boundary Conditions

The equations developed in the last section allow the calculation of pressure and volume flow rate at any point P within the pipe. However, by examining Fig. 2-1, the end points of the grid which correspond to the pipe under consideration, begin influencing the interior points after the first time step. Therefore, to have a complete solution for any time after the first time step, the appropriate boundary conditions become necessary.

For any one pipe, only one characteristic equation is available at either end, as seen in Fig. 3-1. Referring back to Fig. 2-1 and the discussion in the last section, Eq. (2.19) is valid at the upstream boundary, while Eq. (2.18) holds at the downstream end. With only the one characteristic equation available at either end, a second equation is required to complete the solution. Thus, to find the pressure and the volume flow rate at the end of a pipe, auxiliary equations are needed to be developed.

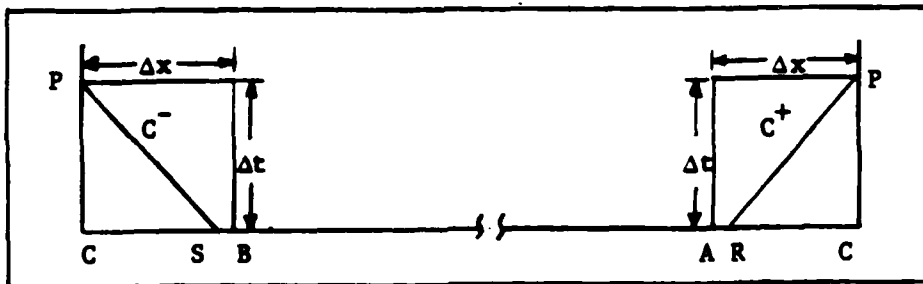


Fig. 3-1. Characteristic lines at the pipe ends

#### Known End Conditions

If either the pressure or volume flow rate at an end of the pipe is a known function of time,  $F(t)$ , this information can be combined with the appropriate characteristic equation to fix the end point conditions. For

example, if the pressure at the inlet of the pipe changes in a known manner, say as a sine wave, the boundary condition is

$$F(t) = P_p = P_o + \Delta P \sin \omega t \quad (3.1)$$

where  $\omega$  is the frequency and  $\Delta P$  is the amplitude of the wave. With the pressure known at any instant, the flow at the inlet is then determined by direct solution of Eq. (2.19).

### Series Connection

From Fig. 3-2, recalling Figs. 2-1 and 3-1, it can be inferred Eq. (2.18) is available for pipe 1, and Eq. (2.19) is available for pipe 2. However, an additional equation is required to solve each characteristic equation. The continuity expression provides one equation, while a second equation is obtained by equating the pressure on either side of the junction after the losses are assumed to be negligible (16:9.2).

$$Q_{P1} = Q_{P2} \quad (3.2)$$

$$P_{P1} = P_{P2} \quad (3.3)$$

Along with Eq. (2.18) and (2.19), Eq. (3.2) and (3.3) provide four equations and four unknowns which may then be solved for the pressure at the junction.

$$P_p = (C_p - C_M) / (B_1 + B_2) \quad (3.4)$$

The remaining unknowns are calculated directly from the appropriate equation.

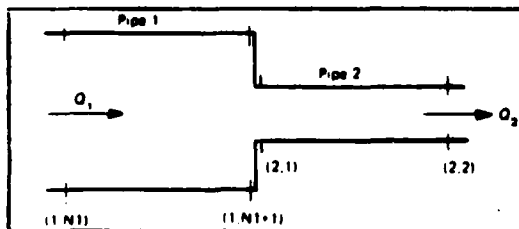


Fig. 3-2. Series Connection  
(16:9.3)

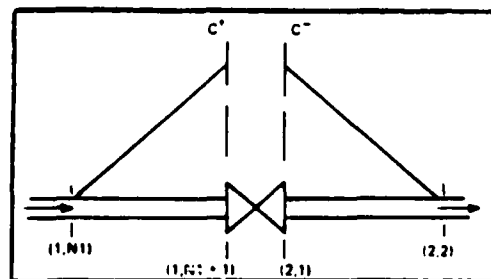


Fig. 3-3. Valve-in-line  
(16:9.5)

### Valve-in-line

When a valve or orifice is located between two pipes, the necessary equations are provided in much the same manner as in a series connection. Respectively, Eq. (2.18) and (2.19) are available where appropriate as before, and the continuity expression, Eq. (3.2), is still valid. However, the fourth equation is supplied by the valve pressure-discharge characteristic,  $\tau$  (13:695). For positive flow (Fig. 3-3)

$$\tau = (Q_p/Q_o) [P_o / (P_{p1} - P_{p2})]^{1/2} \quad (3.5)$$

where  $P_o$  is the drop in pressure across the fully open valve at the initial flow  $Q_o$ , and  $\Delta P_p$  is the drop in pressure across the partially closed valve at an instantaneous flow  $Q_p$ . By solving the above equations simultaneously, a quadratic in  $Q_p$  results which may be solved to yield:

$$Q_p = -C_v(1/B_1 + 1/B_2) + [C_v^2(1/B_1 + 1/B_2)^2 + 2C_v(C_p/B_1 - C_M/B_2)]^{1/2} \quad (3.6)$$

where  $C_v = Q_o^2 \tau^2 / 2P_o$ . If there is flow in the negative direction then Eq. (3.5) becomes

$$\tau = -(Q_p/Q_o) [P_o / (P_{p2} - P_{p1})]^{1/2} \quad (3.7)$$

which yields the solution

$$Q_p = C_v(1/B_1 + 1/B_2) + [C_v^2(1/B_1 + 1/B_2)^2 + 2C_v(C_p/B_1 - C_M/B_2)]^{1/2} \quad (3.8)$$

Upon examination of the equations, it is only possible to have negative flow if  $C_p/B_1 - C_M/B_2 < 0$ . Hence, Eq. (3.6) is valid when  $C_p/B_1 - C_M/B_2 > 0$ , and Eq. (3.8) is used when  $C_p/B_1 - C_M/B_2 < 0$ . With the flow now determined, Eq. (2.18) and (2.19) are used to find the pressure,  $P_p$ .

Valve at Downstream End of Pipe. A special case of the valve-in-line is a valve at the end of a pipeline discharging to ambient conditions. For this situation Eq. (3.5) may be written in the following manner (14:38)

$$\tau = (Q_p/Q_o) (P_o/P_{p1})^{1/2} \quad (3.9)$$



Thus, only Eq. (2.18), the downstream characteristic equation, is necessary for a complete solution. This simplification results in Eq. (3.6) reducing to

$$Q_p = -C_v/B + [(C_v/B)^2 + 2C_v C_p]^{1/2} \quad (3.10)$$

While the corresponding pressure is computed from either Eq. (2.18) or (3.9).

### Cavitation

During transient flows, the pressure may drop below the vapor pressure of the fluid. When this occurs the fluid undergoes vaporization, causing vapor bubbles to appear in the flow. The phenomena can be treated in two different manners. The first method is to assume the vapor bubbles are dispersed homogeneously throughout the liquid. The effective wave speed resulting from this two-phase flow is then treated as a function of pressure, temperature, and vapor volume (14:136). The alternate method, which is used in this study, lumps the free gas at the computing sections. The liquid in the reaches between the gas volumes is assumed to be pure liquid without free gas. This assumption allows the use of a constant wavespeed in the reaches between the cavities (17:49).

When the pressure falls below the vapor pressure, the cavity boundary condition becomes:

$$P_p = P_v \quad (3.11)$$

where  $P_v$  is the vapor pressure. The flow upstream of the cavity is then calculated from Eq. (2.19)

$$Q_{pu} = C_p - B P_p \quad (3.12)$$

and the flow downstream by Eq. (2.18)

$$Q_p = C_M + B P_p \quad (3.13)$$

The liquid mass conservation is maintained by applying the local continuity relation at each gas volume.

$$dV_g/dt=Q_d-Q_u \quad (3.14)$$

Integration of Eq. (3.14) gives

$$V_g'=V_g+\Delta t[(Q_p+Q)-(Q_{p_u}+Q_u)]/2 \quad (3.15)$$

where  $V_g'$  is the gas volume at the current time and  $V_g$  is the gas volume from the previous time step (14:137). As long as the cavity size is positive, vapor pressure persists. Once the volume becomes less than zero the gas cavity is declared to have collapsed and the flow calculations proceed as usual for an interior section (17:49).

However, in some instances the system to be analyzed may contain other gases dissolved in the fluid. This phenomenon is common in rocket propulsion where fuel and oxidizer tanks are often pressurized with high pressure helium or nitrogen. Due to the presence of this other gas in the fluid, the bubbles which occur during cavitation will contain both the vapor of the fluid and the gas evolved from the fluid. Wylie (17) developed a method for handling the additional gas release in the discrete bubble method. The equations in terms of the notation of this study are:

$$P_p = \frac{-B + 2(P_v + P_b) + [(B_I + 2(P_v + P_b))^2 + 8C_4]^{1/2}}{4} \quad (3.16)$$

where,

$$B_I = [\phi(C_M - C_P) + V_g/2\Delta t + (1-\phi)(OQ - OQ_u)]/\phi B$$

$$C_4 = C_1/2\Delta t B \phi$$

$$C_1 = P^* \alpha_0 V$$

In which  $\alpha_0$  is the void fraction at some reference pressure,  $P^*$ , while  $V$  is the volume of the adjacent reach. By choosing the void fraction to be

$10^{-7}$  or less, this method is also able to closely approximate the results obtained for a liquid containing no dissolved gases (17:50).

To find the gas volume, Eq. (3.14) is once again used, however, Wylie introduced a weighting factor in the time direction. Thus, when integrated

$$V_g' = V_g + 2\Delta t [\phi(Q_p - Q_{p_u}) + (1 - \phi)(OQ - OQ_u)] \quad (3.17)$$

where,

$$\phi = \Delta t' / 2\Delta t, \quad 0 < \phi < 1$$

In which  $V_g$ ,  $OQ$ , and  $OQ_u$  are values from  $2\Delta t$  earlier. By integrating in this manner, the calculation is spread over two time steps, thereby introducing numerical damping in the form of  $\phi$ .

#### Accumulator

In this study an accumulator is a pressure vessel connected to the main pipeline. The sealed vessel contains a layer of compressed gas overlaying the liquid inside. The conditions which exist at this location are reminiscent of those around a cavitation bubble. Thus, Eq. (3.14) is once again used to express the continuity relationship, and Eq. (2.18) and (2.19) are valid where appropriate. However, the accumulator pressure is greater than vapor pressure, so a fourth equation is needed to complete the solution. Dorsch et al. (10:8) obtained the necessary equation by introducing the compliance,  $a'$ , of the gas volume.

$$a' = dV_g / dP \quad (3.18)$$

Making use of the chain rule from calculus

$$dV_g / dt = (dV_g / dP)(dP / dt) = a' dP / dt \quad (3.19)$$

Therefore

$$dP/dt=(Q_d-Q_u)/a' \quad (3.20)$$

Finally, substituting Eq. (2.18) and (2.19) into Eq. (3.20) gives

$$dP/dt=(C_M+B_2P-C_P+B_1P)/a' \quad (3.21)$$

The pressure at the accumulator is now a known function of time. Eq. (3.21) can then be numerically integrated to find pressure at any time. In this analysis a first order integration is used to give

$$P_{t+\Delta t}=P_t+\Delta t(C_{M_{avg}}+B_2P_{avg}-C_{P_{avg}}+B_1P_{avg})/a' \quad (3.22)$$

The average values in Eq. (3.22) are determined by iteration (see Appendix A for a listing of the computer code). The pressure,  $P_p=P_{t+\Delta t}$ , so  $Q_p$  above and below the accumulator can be found from Eq. (2.18) and (2.19) respectively.

#### IV. Systems Analysis

In this section, the equations developed in section II by the method of characteristics and in section III for the various boundary conditions were used to model several pipe systems found in the literature. The systems examined began with a simple one-pipe system and moved on to systems of greater complexity. The results published about these systems were then used in section V to verify the accuracy of the digital computer program written for this study.

##### Single Pipe Models

As mentioned above, the first systems that were modeled center around a single pipe. The single horizontal pipe was combined with various upstream and downstream boundary conditions to verify the accuracy of the models used in this study and to examine the effect of such boundary conditions on a system. Note, in each case the system was assumed to have achieved steady flow before any changes in the boundary conditions were imposed.

Valve Closure. Wylie and Streeter (14:39) presented the simple pipe flow problem of a sudden valve closure at the end of a single pipe. In this case the system consisted of a single pipe with a reservoir of water at the upstream end and a valve at the downstream end. The flow in the pipe was steady until at some time,  $t=0$ , the valve began to close such that the valve pressure-discharge characteristic, Eq. (3.9), followed the exponential law

$$\tau = (1-t/t_c)^{Em} \quad (4.1)$$

where  $t_c$  is the time at which the valve is fully closed.

The input data taken from Wylie and Streeter for this system were:  $D = 0.5$  m,  $L = 600$  m,  $a = 1200$  m/s,  $f = 0.018$ ,  $P_0 = 1.4716$  MPa,  $Q_0 = 0.477$  m<sup>3</sup>/s,  $t_c = 2.1$  s, and  $E_m = 1.5$ . The upstream boundary condition was modeled as a constant pressure reservoir. With the pressure at the reservoir a known function of time, the volume flow rate was determined by Eq. (3.2). At the downstream end the flow was discharging through the valve to ambient conditions, so the flow through the valve was calculated by Eq. (3.11). Hence, the pressure at the downstream end could be computed with either Eq. (3.9) or Eq. (2.18).

In an attempt to discover the effect of several parameters on the severity of the fluid transients, variations were introduced into the input data. The variables varied appear in Table I, along with the par-

Table I. Input Variations for Single Pipe Closure

Run No.	$t_c$ (s)	$E_m$	$f$	$L$ (m)
1	2.1	2.0	0.018	600
2	2.1	1.0	0.018	600
3	2.1	0.5	0.018	600
4	1.5	1.5	0.018	600
5	2.5	1.5	0.018	600
6	2.1	1.5	0.036	600
7	2.1	1.5	0.072	600
8	2.1	1.5	0.0001	600
9	2.1	1.5	0.018	300
10	2.1	1.5	0.018	150
11	2.1	1.5	0.018	75
12	2.1	1.5	0.018	10

ticular values for each simulation. The remainder of the variables were kept the same as those presented above.

Vaporous Cavitation. To demonstrate the cavitation model, a simple system examined by Wylie (17:50) was analyzed. During his study Wylie worked with two systems having similar configurations. In each the pressure at both ends of the pipe was a known function of time. The downstream end of both systems was connected to a constant pressure reservoir. At the upstream end both pipes were connected to a pump, which Wylie represented by the pressure as a given function of time. However, the two systems differed as to the physical dimensions of the pipes, as well as to the properties and conditions of the fluids in the systems.

For the first of the two examples, the system parameters were:  $D = 0.61$  m,  $L = 3048$  m,  $f = 0.02$ ,  $Q_p = 0.89$  m<sup>3</sup>/s,  $a = 981$  m/s,  $\rho = 1000$  kg/m<sup>3</sup>, and  $P_v = -98.72$  kPa gage. The negative pressure resulted from the pressure being gage. The pressure at the upstream end of the pipe was dropped linearly from an initial value of 0.495 MPa gage to zero in 0.2 s, then held there for the remainder of the simulation (17:51). Thus, the pressure at both ends of the pipe was known for any time, allowing the volume flow rate to be calculated with either Eq. (2.18) or (2.19).

In the second of the two examples, the system data not included in Fig. 4-1 were:  $\rho = 1000$  kg/m<sup>3</sup>, and  $P_v = -99.11$  kPa gage. As in the first case, the downstream boundary condition was again a constant pressure reservoir. The upstream conditions however were of a more complex form as depicted in Fig. 4-1.

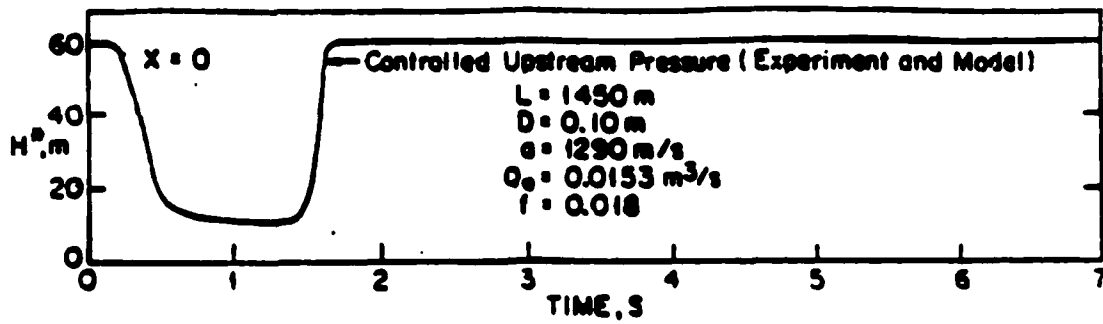


Fig. 4-1. Upstream pressure in simulation 2

In an effort to further verify the model used in study, two additional cases were constructed by altering the original input data given for the first simulation. The new hypothetical systems retained the same input values as before with the exception of the vapor pressure. In the one case the vapor pressure was set at  $H_v = -5.03 \text{ m}$ , while in the other case  $H_v = -100 \text{ m}$ .

#### Multipipe Models

Valve-in-line. The next system to be used for comparison was a system analyzed by Swaffield (13). In the Swaffield system a valve was closing in the middle of a series of pipes instead of at the end. For that investigation Swaffield used aviation kerosene as the working fluid not water. The pipeline itself was modeled as consisting of three pipes of the equal diameter in series, where both the upstream and the downstream ends of the system were connected to reservoirs. The valve in question was situated between the first and second pipe, and as in the previous valve problem, there was steady flow until time,  $t=0$ , when the valve began to close. The parameters which describe the system are given in Tables II and III.



Table II. Flow Parameters for Valve-in-line

Density,  $\rho=800 \text{ kg/m}^3$       Wave Speed,  $a=918 \text{ m/s}$

Run	$t_c$ (s)	Downstream Pres. (kPa)	Initial flow ( $\text{m}^3/\text{s}$ )
1	0.081	102	0.00355
2	0.160	222	0.00355
3	0.140	120	0.00541

Table III. Pipeline Parameters for Valve-in-line

Pipe	Length (m)	Diameter (m)	$f$
1	5.80	0.0508	0.02
2	3.17	0.0508	0.02
3	6.70	0.0508	0.02

Starting with the upstream end of the pipeline, there was once again a reservoir. The pressure was assumed to be constant, allowing the volume flow rate to be calculated from Eq. (2.19). Moving downstream, the next boundary condition encountered was the valve between pipes 1 and 2. Here, as shown in section III, the flow was given by Eq. (3.6), where the valve pressure-discharge characteristic was assumed to obey Eq. (4.1). The pressure on the upstream and downstream face of the valve could then be calculated from Eq. (2.18) and (2.19) respectively. At the junction of pipes 2 and 3, there was a simple series connection. The pressure was determined by Eq. (3.4) and the flow was then calculated once again using either Eq. (2.18) or (2.19). The final boundary condition was the constant pressure reservoir at the downstream end. The conditions here were evaluated by substituting the known pressure once more into Eq. (2.18).

Valve Closure. A second, more complex downstream valve closure problem was also presented by Wylie and Streeter (14:60). Like the first problem, water was once again flowing from a reservoir at the upstream end through a pipeline to a valve at the downstream end. In this example though, the pipeline consisted of three pipes of different diameter in series between the reservoir and the valve. Furthermore, the valve pressure-discharge characteristic, Eq. (3.9), did not follow an exponential law, instead,  $\tau$  follows the curve in Fig. 4-2.

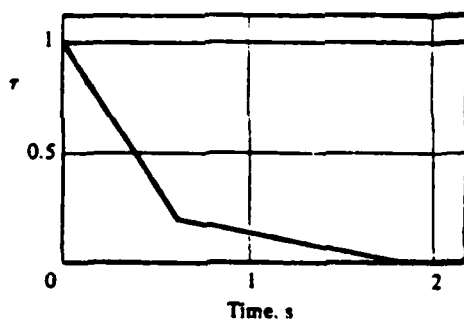


Fig. 4-2. Valve characteristic,  $\tau$

In this three pipe problem, the initial flow,  $Q_0$ , was  $0.2 \text{ m}^3/\text{s}$ , and the initial pressure at the valve equaled  $981.4 \text{ kPa}$  gage. The parameters for the pipes are given in Table IV.

Table IV. System Data for Series Closure

Pipe	Length (m)	Dia.(m)	f	Wave Speed (m/s)
1	351	0.30	0.019	1200
2	483	0.20	0.018	1200
3	115	0.15	0.018	1200

As in the single pipe problem, the reservoir was assumed to be constant pressure, which allowed the flow to be calculated at that point with Eq. (2.19). Also, the flow through the valve was again calculated

using Eq. (3.10). Therefore, the pressure at the valve could be calculated with either Eq. (2.18) or (3.9). However, in contrast to the original single pipe closure problem there were now two interior boundary conditions as well. At both of the locations, there were changes in area. The pressure at such junctions is calculated by Eq. (3.4). The flow through the junction could then be determined from either Eq. (2.18) or (2.19).

Since propellant feedline systems are rarely a single pipe or a constant diameter, this multipipe valve closure problem provided an excellent system to further examine the effect of certain parameters on the fluid transients. The system was simple enough to require relatively short run times on the computer, about 10 CPU seconds on the Cyber. Yet, at the same time, the system contained features that are present in the final model which is described later.

As before with the single pipe system, while keeping the other values the same as in the original system, the variations seen in Table V were introduced into the input data one at a time.

Table V. Input Variations for Series Closure

Run No.	Reservoir Pressure (m)	Closure
1	289	original
2	400	original
3	200	original
4	289	hard
5	289	soft

The closure designation indicates the rapidity of the closing of the valve. The original closure was the valve characteristic in Fig. 4-2.

During a hard closure, the value of  $\tau$  decreased from 1.0 to 0.1 in the first 0.6 s, then went to zero in the next 0.6 s. And lastly, in the soft closure,  $\tau$  dropped from 1.0 to 0.4 during the first 0.6 s, went from 0.4 to 0.15 in the next 0.6 s, then fell to zero during the final 0.6 s. Thus, the characteristic curve for the hard closure not only had a steeper slope, but also a cut-off time that was 0.6 s shorter than the other two curves.

In addition to running each case with water as the working fluid, runs were also made with rocket fuels RP-1, a fuel very similar to the aviation kerosene used by Swaffield, and liquid hydrogen. However, in order to have a complete set of input data for these addition fluids, several assumptions were made. The first of the assumptions was associated with the wave speeds. When a wave speed is not explicitly stated in the input list, the program calculates the wave speed as follows (14:58)

$$a^2 = K/\rho(1 + DK + Ee) \quad (4.2)$$

where the bulk modulus,  $K$  and the density,  $\rho$ , are fluid properties, while the Young's modulus,  $E$ , the pipe diameter,  $D$ , and the pipe thickness,  $e$ , are properties of the pipe.

The wave speed for water was given, along with the diameter of the pipes for the series closure by Wylie and Streeter (14:60), but nothing else. Therefore, the water was assumed to have a density of  $1000 \text{ kg/m}^3$  as in the single pipe cavitation problems. Given this density, a bulk modulus of  $2.016 \times 10^9 \text{ N/m}^2$  was obtained from Appendix B of Dehoff (2). Also, the pipes were assumed to have a Young's modulus of  $7.24 \times 10^{10} \text{ N/m}^2$ , the value reported by Swaffield (13:698) for his system. With everything but one variable now known in Eq. (4.2), it was possible to determine a

thickness for each pipe. Substituting the appropriate values into the equation gave  $e_1=0.021$  m,  $e_2=0.014$  m, and  $e_3=0.01$  m, where  $e_x$  is the thickness of pipe x. Thus, a complete description of the pipe system was produced. As for the fluid properties, they are listed below:

	<u>RP-1</u>	<u>LH<sub>2</sub></u>
Temperature (°F)	89.10	-423.2
Density (kg/m <sup>3</sup> )	800.00	72.1
Bulk Modulus (10 <sup>8</sup> Pa)	12.34	0.1
Vapor Pressure (Pa)	700.00	127,000

The second set of assumptions centered around the friction factor. In equation form the friction factor is given by

$$f=2\Delta P_f D/\rho LV^2 \quad (4.3)$$

where  $\Delta P_f$  = pressure loss due to friction,  $V$  = mean flow velocity, and  $L$ =pipe length. For the simulations where the RP-1 and LH<sub>2</sub> replaced water everything in Eq. (4.3) but the density remained constant. Thus, a friction factor for the other two fluids was obtained by multiplying the friction factor of water by a ratio of the density of the water to the density of the other fluid. However, this process produced a very high friction factor for LH<sub>2</sub>, so a second run with LH<sub>2</sub> as the fluid was included for each case of the simulation. In this second run LH<sub>2</sub> was given the same friction factor as water to determine how strongly the friction was affecting the transients in the LH<sub>2</sub>.

Saturn V Feedline. The final system analyzed was chosen in order to test the routines developed in this investigation on a real aerospace system. The system chosen was one that was reported on by Brod (18). During the Apollo program, Boeing constructed a test installation to

simulate the LOX suction duct of the Saturn V's F-1 engine. In the course of the testing performed with this apparatus, some experiments were conducted which consisted of closing the main drain valve and observing the fluid transients (18:15). Unfortunately, the results from these experiments were no longer available from Boeing. Thus, the results of this study for this simulation were of a more qualitative nature.

Table VI. Feedline Configuration Data

Pipe	Length (m)	Dia. (m)	Wave Speed (m/s)
1	0.25	0.508	770.7
2	7.50	0.508	770.7
3	5.17	0.508	770.7
4	0.32	0.457	862.1
5	0.20	0.500	658.4
6	0.80	0.457	862.1
7	0.49	0.457	1165.3
8	0.49	0.457	1165.3
9	0.23	0.457	862.1
10	0.41	0.462	207.8
11	0.43	0.640	177.5
12	0.41	0.462	207.8
13	0.43	0.457	800.2
14	0.13	0.457	1330.0
15	1.19	0.457	1330.0

In general, this problem was related to the multipipe example taken from Wylie and Streeter (14). In both, there was a reservoir, a series of pipes, and a valve at the downstream end. In addition, both were modeled as horizontal pipelines for this study, however, the similarities end there. The F-1 feedline was comprised of 15 pipes in all. The data for the pipes was given in Table VI. Furthermore, in addition to more pipes in the system, there were a few additional interior boundary conditions. In the junction between pipes 7 and 8 was a device called the prevalve. Initially the prevalve was a simple visor valve. But, as part of the experiments at the test installation, the valve cavity was evacuated and pressurized with helium. In this way the engineers hoped to control the fluid transients by essentially creating an accumulator at that point. Therefore, for the purposes of this analysis the prevalve was modeled as an accumulator when there was a volume of gas present.

The second new boundary condition was the pulser valve between pipes 13 and 14. To model this component an additional boundary condition was developed. Recalling similar circumstances in Figs. 3-2 and 3-3, it was apparent from Fig. 4-3 that Eq. (2.18) and (2.19) were again available. The continuity equation for this junction is of the form

$$Q_{PU} = Q + Q_p \quad (4.4)$$

where the flow out of the pulser valve was assumed to be of the form

$$Q = Q_v |\sin \omega t| \quad (4.5)$$

The final relationship required to form a closed solution was taken from a work by Thorley (16:9.3). In that paper, he proposed that in a branching connection such as this a common pressure could be assigned at the junction, as long as any losses were neglected as minor. Thus, Eqs. (2.18), (2.19), and (4.5) were substituted into the continuity equation

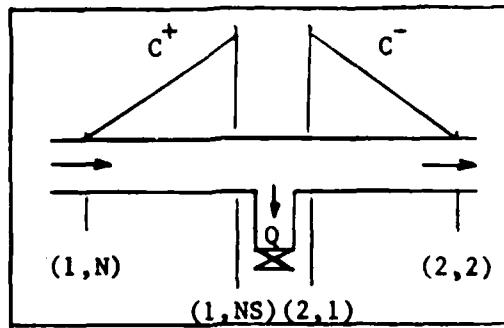


Fig. 4-3. Pulsar Valve

and solved for the pressure to give

$$P_p = (C_p - C_M - Q_v |\sin \omega t|) / (B_1 + B_2) \quad (4.6)$$

The pressure was then substituted back into Eq. (2.18) and (2.19) to find the flow at those sections.

The remaining interior boundary located between pipes 14 and 15 also had a boundary condition other than a series connection. In order to complete the simulation of the LOX suction duct, a second accumulator was included to approximate cavitation at the inlet of the turbopump.

In this system, the parameters reported by Dehoff (2) and Brod (18) were as follows:  $Q_0 = 1.7 \text{ m}^3/\text{s}$ ,  $P_0$  at the valve = 621 and 896 kPa,  $\rho = 1000 \text{ kg/m}^3$ ,  $\omega = 0$  to 27 Hz,  $Q_v = 0.071 \text{ m}^3/\text{s}$ ,  $V_g$  of the pre valve accumulator = 0, 30, 60, and 90 percent of the total accumulator volume, valve cut-off times = 1.25 to 4.0 s, and  $V_g = 0.0129 \text{ m}^3$  at the pump inlet when cavitation was included. The specific values arbitrarily chosen for each parameter which had a range of values is shown in Table VII.



Table VII. Input Parameters for F-1 Feedline

Run no.	Valve(kPa)	$t_c$ (s)	$E_m$	(Hz)	Vol.(m <sup>3</sup> )	cav.
1	621	1.5	1.2	0.0	0.000	no
2	621	3.0	1.2	0.0	0.000	no
3	621	1.5	1.0	0.0	0.000	no
4	621	1.5	1.5	0.0	0.000	no
5	896	1.5	1.2	0.0	0.000	no
6	621	1.5	1.2	2.5	0.000	no
7	621	1.5	1.2	10.0	0.000	no
8	621	1.5	1.2	25.0	0.000	no
9	621	1.5	1.0	2.5	0.000	no
10	896	1.5	1.2	2.5	0.000	no
11	896	1.5	1.0	10.0	0.000	no
12	621	1.5	1.0	0.0	0.000	yes
13	621	1.5	1.0	0.0	0.018	yes
14	621	1.5	1.0	0.0	0.036	yes
15	621	1.5	1.0	0.0	0.072	yes
16	896	1.5	1.0	0.0	0.000	yes
17	896	1.5	1.0	0.0	0.054	yes
18	621	1.5	1.0	2.5	0.054	yes

## V. Results

### Single Pipe Verification for Valve Closure

Some of the published results used for verification were in terms of piezometric head instead of pressure. Since the program uses equations in terms of pressure, a conversion was required. To obtain the conversion the equation,  $P = \rho g(H - z)$ , was solved for  $H$ . Thus, when necessary, the resulting conversion was incorporated into the output statement of the program, making use of FORTRAN's ability to perform mathematical operations on the variable to be output.

Simple Valve Closure. The first system to be analyzed was the single pipe valve closure presented by Wylie and Streeter (14). The results published by Wylie and Streeter for this problem appear in Fig. 5-1. The agreement between the published results and the results predicted by the program, which appear in Fig. 5-2, was very close. For the pressure, both results depicted the piezometric head increasing to a peak of about 285 m at the valve as the decreasing area generated compression waves which traveled upstream. The compression waves reflected from the constant pressure boundary at the reservoir, becoming expansion waves which propagated back toward the valve. Since vapor pressure was not reached, the expansion waves which returned to the valve in  $2L/a = 1.0$  s were stronger than the compression waves being generated at the valve, dropping the head pressure at that point. Here, the strength of a wave was equated with the pressure difference across a wave. Once the valve was fully closed, the waves in the pipe simply reflected between the free boundary at the reservoir and a wall at the valve with a period of  $4L/a = 2.0$  s.

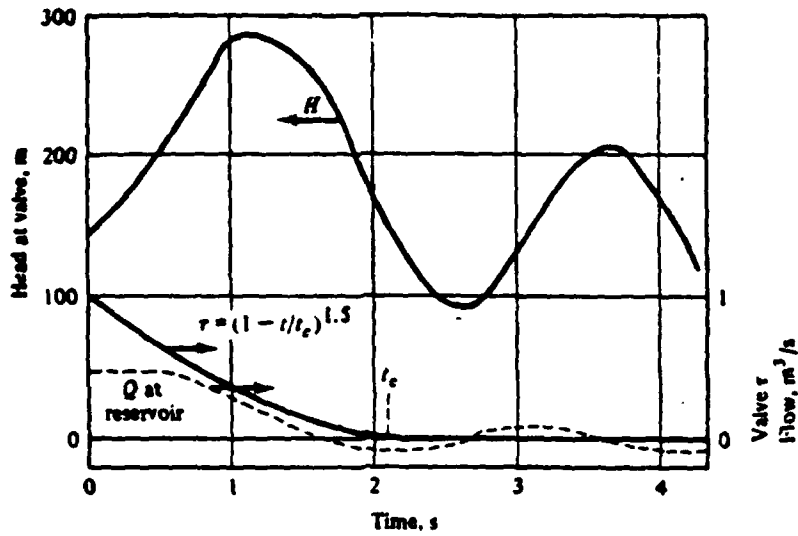


Fig. 5-1. Results of Wylie and Streeter ( $L=600$  m,  $a=1200$  m/s,  $D=0.5$  m,  $t_c=2.1$  s,  $E_m=1.5$ ,  $f=0.018$ )

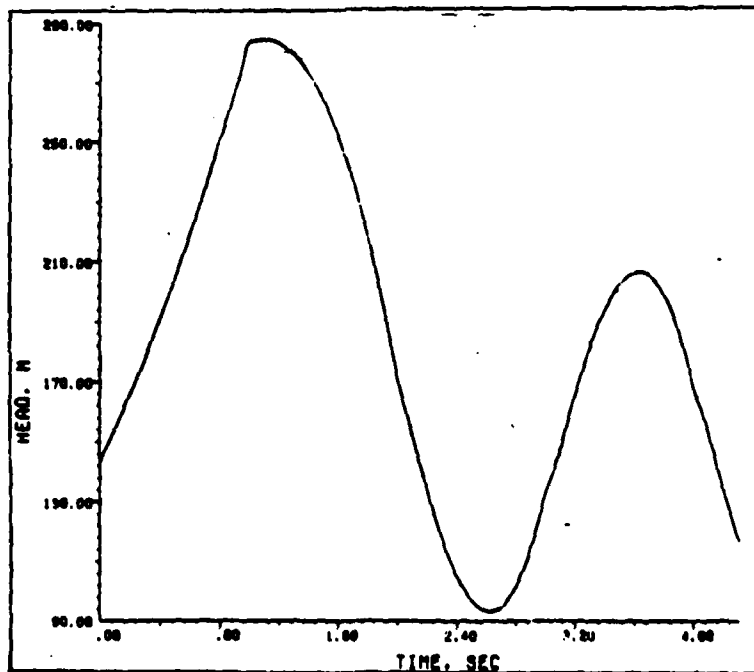


Fig. 5-2. Program results for single pipe closure ( $L=600$  m,  $a=1200$  m/s,  $D=0.5$  m,  $t_c=2.1$  s,  $E_m=1.5$ ,  $f=0.018$ )

The predictions of the pressure matched very closely when compared point by point. So, in order to further explore the effect of certain system parameters on the resulting fluid transients, the variations listed in Table I were introduced into the system. The plots of the results predicted for the various changes appear in Figs. 5-3 through 5-6.

Effects of Closure Curve. The first of the parameters examined was the valve closure characteristic,  $\tau$ . In Fig. 5-3, appear the results produced by varying the exponent,  $E_m$ , from Eq. (4.1), the equation used to represent the valve closure. Not only did the magnitude of the first peak change with changes in  $E_m$ , but the slope of the curve as the peak was approached changed with  $E_m$  as well, this was as expected though. The timing of the reflections should have been and was the same as seen in Fig. 5-2. The change during these runs was expected in the strength of the waves at a particular time during the closure. It was anticipated that when the closure was initially rapid then slowed, that the pressure would peak more quickly than when the closure was initially slow then became increasingly quicker. Further, it was anticipated that the peak magnitude would increase as  $E_m$  became larger or smaller, since in either case the closure was approaching an instantaneous cut-off.

Starting with an  $E_m$  greater than one, the valve closed rapidly at first but slowed as the cut-off time approached. Consequently, the strongest compression waves were generated during the start of the closure, while the weakest occurred at the end. This meant that when the waves returned from the reservoir at  $2L/a=1.0$  s, the reflected expansion waves were stronger than the compression waves currently being generated by the closing valve. So, the pressure began to drop. At  $4L/a=2.0$  s the

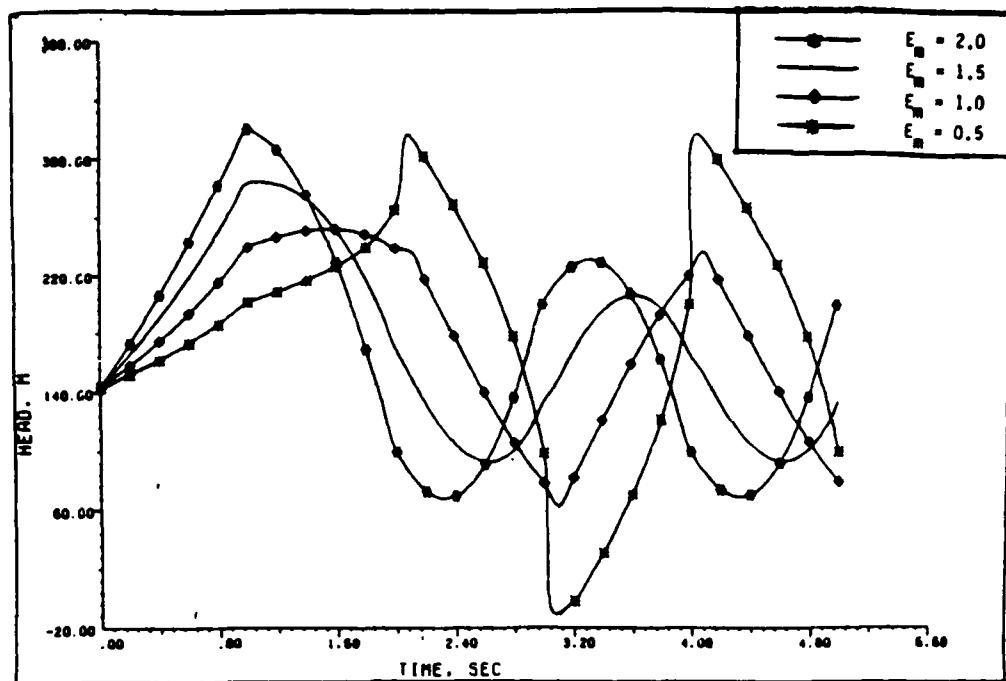


Fig. 5-3. Program results for changes in  $E_m$  ( $L=600$  m,  $a=1200$  m/s,  $D=0.5$  m,  $t_c=2.1$  s,  $f=0.018$ )

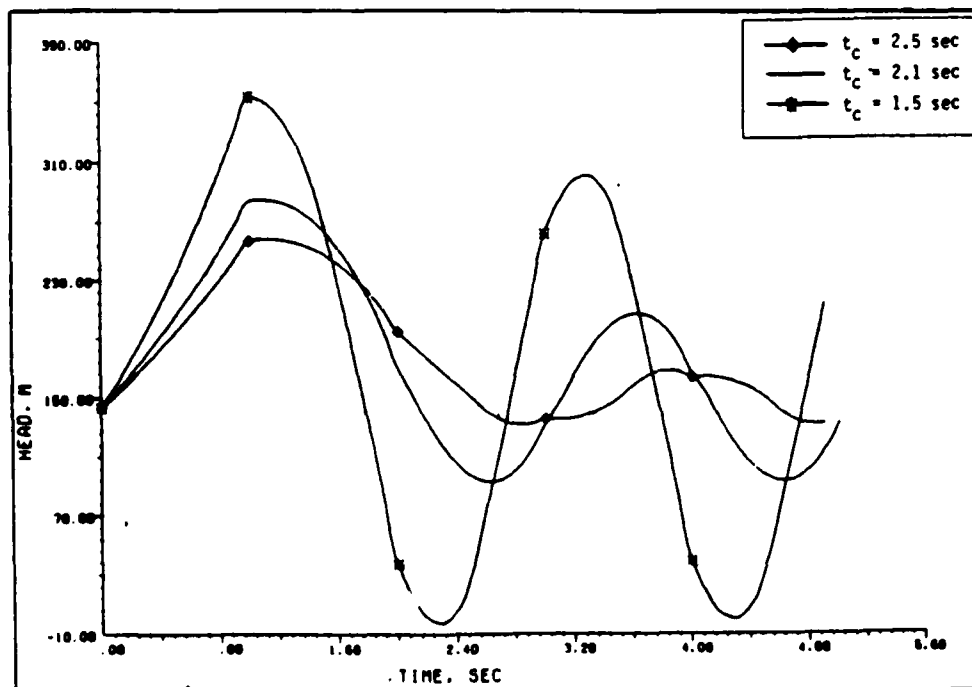


Fig. 5-4. Program results for changes in  $t_c$  ( $L=600$  m,  $a=1200$  m/s,  $D=0.5$  m,  $E_m=1.5$ ,  $f=0.018$ )

compression waves which resulted from a second reflection at the reservoir began to arrive. This third set of waves combined with the wave trains already at the valve to decrease the rate at which the pressure decreased. Then, at  $t=2.1$  s, the valve was totally closed and all that remained was the interaction of the reflecting wave trains as they travel back and forth.

When  $E_m$  was one, the valve closed at a constant rate, generating compression waves which diminished slightly in strength as the flow went to zero. Therefore, when the expansion waves began to arrive after the first reflection, there was essentially a cancellation between them and the compression waves being generated at that time. This cancellation resulted in the relatively flat portion of the curve observed between 1.0 and 2.0 s. Then at  $t=2.0$  s the second reflection from the reservoir arrived, reducing the rate of the pressure drop. But at  $t=2.1$  s, the valve was completely closed, thus compression waves were no longer being generated. And so, the expansion waves, which had not been as greatly attenuated by friction as the compression waves, produced a pressure drop that continued until  $t=3.1$  s, when the last of the wave train from the first reflection finally passed. Then once more all that remained was the wave train reflecting back and forth.

Finally, for  $E_m$  less than one, the valve shut slowly at first then closed with increasing rapidity as the cut-off time approached. Consequently, the strength of the compression waves generated at the valve increased with time. Thus, when the wavefront returned from the first reflection at 1.0 s, the expansion waves were not as strong as the compression waves, and the pressure continued to rise, but at a slower rate. However, at 2.0 s the compression waves from the second reflection

arrived, further increasing the rate of the pressure rise. But, once more the valve was totally closed at 2.1 s, allowing the expansion waves from the first reflection to dominate, resulting in a steep pressure drop. And once more, all that remained after this time was the wave train repeatedly reflecting within the pipe.

Effects of Valve Cut-off Time. Moving now to the second parameter, the length of time required for the valve to totally close was examined for its effect on the transient. In Fig. 5-4, the result of the original simulation with a cut-off time of 2.1 s was compared with the results of a simulation where the cut-off time had been reduced to 1.5 s, as well as a simulation where the cut-off time was increased to 2.5 s. For the case of the shorter cut-off time, the valve closed more suddenly than in the original case. This more sudden closure generated stronger compression waves, hence produced a steeper pressure rise during the first second, as seen in Fig. 5-4. Since  $E_m$  was greater than one, at  $2L/a=1.0$  s, the expansion waves from the first reflection arrived causing a drop in pressure. However, in this case the valve was fully closed by 1.5 s, so, the expansion waves did not encounter any other waves until  $t=2.0$  s when the compression waves from the second reflection of the wave train arrived. This period of pure expansion dropped the pressure near vapor pressure before the arrival of the second reflection could reverse the trend. But ultimately, this case settled into the same pattern as before with pressure oscillations occurring with a period of  $4L/a=2.0$  s.

In the case of a cut-off time longer than  $t_c=2.1$  s, the closure was more gradual than the original, generating weaker compression waves as a result. As seen in Fig. 5-4, these weaker waves produced a slower pressure rise which lasted until the expansion waves from the first

reflection arrived at 1.0 s. When the compression waves from the second reflection arrived at 2.0 s the valve was still closing, thus the two sets of weaker compression waves combined to reduce the rate of the pressure decrease produced by the expansion waves. Then at 2.5 s the valve was totally closed. But, even though compression waves were no longer generated at the valve, the pressure began to rise due to the difference in wave strengths caused by the relative difference in times during the closure at which the waves currently at the valve were generated. Then, at 3.0 s expansion waves from the third reflection began to arrive, decreasing the rate at which the pressure increased towards the second peak. With the valve closed, all that remained after this time were the waves reflecting between the valve and the reservoir.

Effects of Friction Factor. The next parameter investigated for its effect on the pressure at the valve during the fluid transient was the friction factor of the pipe. The results of changing the friction factor are plotted in Fig. 5-5. As the friction factor increased, the attenuation due to the friction increased. This attenuation was apparent in several ways. First, the initial pressure at the valve decreased with increasing values of the friction factor. Second, the rate at which the pressure oscillations damped out increased as the friction factor increased. And third, despite an increasing difference between the initial pressure and the peak pressure, the peak magnitude of the transient decreased as the friction factor increased.

Structurally, the peak magnitude is the most important factor. However, in this study the initial valve pressure was of more interest due to its relationship with the timing of the peak magnitude as well as the timing and magnitude of the secondary peaks. When the friction fac-



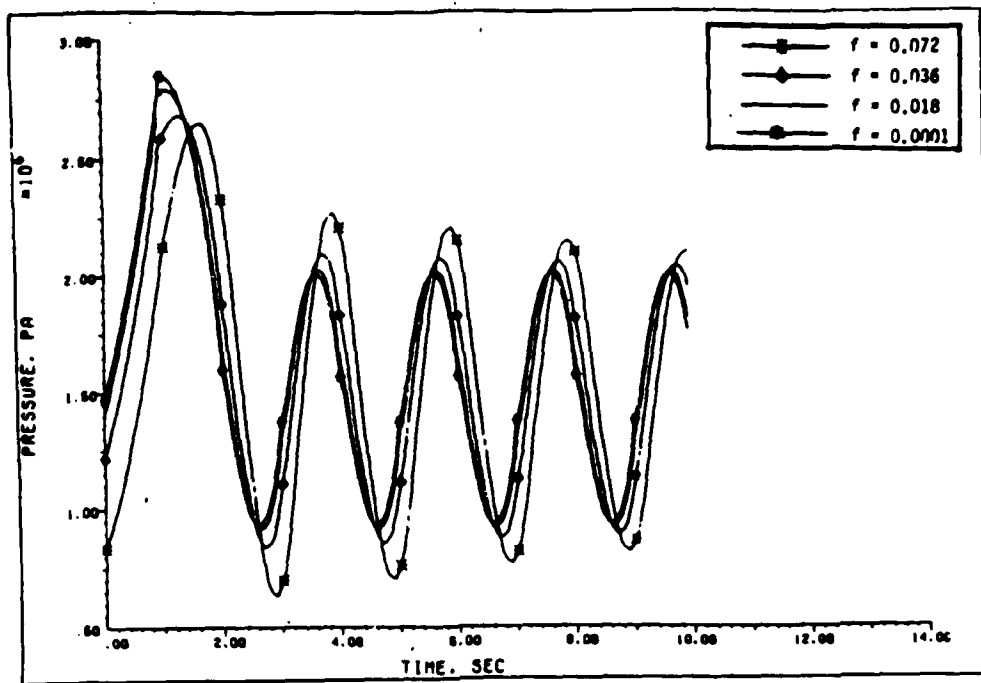


Fig. 5-5. Program results for changes in friction factor ( $L=600$  m,  $a=1200$  m/s,  $D=0.5$  m,  $t_c=2.1$  s,  $E_m=1.5$ )

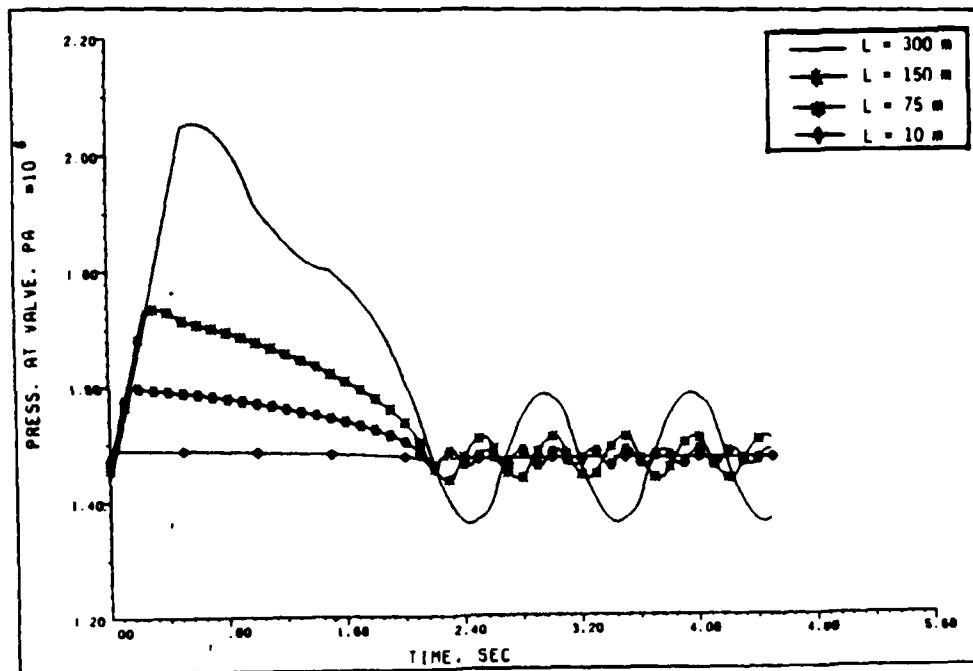


Fig. 5-6. Program results for changes in pipe length ( $a=1200$  m/s,  $D=0.5$  m,  $t_c=2.1$  s,  $E_m=1.5$ ,  $f=0.018$ )

tor was small there was little attenuation of the flow, so the pressure gradient between the reservoir and the valve was very slight. Thus, once the valve began to close, the pressure at the valve rose until the first reflection arrived at 1.0 s. At this time the returning expansion waves began to reduce the volume flow rate almost immediately since the pressure gradient was small. Afterwards, the wave interactions were like those described in the original case, with waves reflecting back and forth between the valve and the reservoir.

But, as the friction factor and the attenuation increased, the initial pressure at the valve decreased, creating a steeper pressure gradient. As the gradient steepened, the strength of the compression at the valve increased. Hence, the pressure at the valve rose faster initially. Also, once the reflection returned, the expansion waves took longer to reverse the flow, causing what appears as a displacement in time of the pressure peaks. For the case of  $f=0.072$ , the gradient was such that despite the arrival of the expansion waves, the pressure continued to rise significantly before the flow was finally reversed and the pressure began to drop. Further, since the compression strengthened as the friction factor increased, the subsequent reflections of the wave train were stronger as well. This meant that even though the peak magnitude decreased with increasing friction factor, the increasing  $\Delta P$  caused the the magnitude of the secondary peaks to be greater initially, but damp out at a higher rate due to the increased friction.

Effects of Pipe Length. The final parameter examined for its effect on the transient was the actual length of the pipe under consideration. The results produced by altering the length of the pipe appear in Fig. 5-6. As the pipe becomes shorter, the time required for the waves to

traverse the length of the pipe decreases. Consequently when  $L=300$  m, the first reflection arrived at the valve in 0.5 s, while the system had a period of 1.0 s. For  $L=150$  m, the reflection arrived in 0.25 s, while the system period was 0.5 s, and so on as the pipe length decreased. Moreover, since the expansion waves returned to the valve with increasing quickness, the pressure had increasingly less time to be influenced by the compression due to the closure. Thus, the magnitude of the peak pressure decreased as the pipe length decreased.

Aside from the effects already mentioned, the reduced travel time had two other effects. First, the relative strength of any two waves was dependent on the points in time during the closure at which each of the waves was generated, since the closure characteristic was nonlinear. Again, strength was equated to the pressure difference across a wave. Therefore, the shorter the travel time, the closer the compression waves currently generated at the valve were in strength to the reflected expansion waves returning from the reservoir. Second, as the travel time decreased, the time interval between reflections decreased as well. This meant the number of reflections occurring before the valve was totally closed increased.

The significance of these two effects was that the combination of the two produced the differing responses observed in the time interval between the arrival of the first reflection and the complete closure of the valve. When the pipe length was such that  $2L/a$  was a significant percentage of the closure time, only a few reflections occurred during closure and the relative strengths of the current and the reflected waves were very different. Hence, as was seen in Fig. 5-6, for  $L=300$  m the pressure dropped rather rapidly once the reflection arrived at 0.5 s. In

addition, it was easy to distinguish the additional reflections every 0.5 s after that point. However, as the pipe became shorter, more reflections of about the same relative strength began interacting at the valve more quickly. The result was essentially a cancellation among all of the reflections, which left the relative difference between the strengths of the primary compression and the first reflection as the main driving force of the pressure changes observed during the valve closure.

#### Single Pipe Verification for Cavitation

First Simulation. In the first of the cavitation simulations the upstream pressure was dropped from 495 kPa to zero and held there. The results published by Wylie for this system are shown in Fig. 5-7, while Fig. 5-8 and 5-9 show the results of the program developed in this study. In general, all the curves agreed with the expected results. That was, the pressure downstream of the "pump" dropped to vapor pressure as the

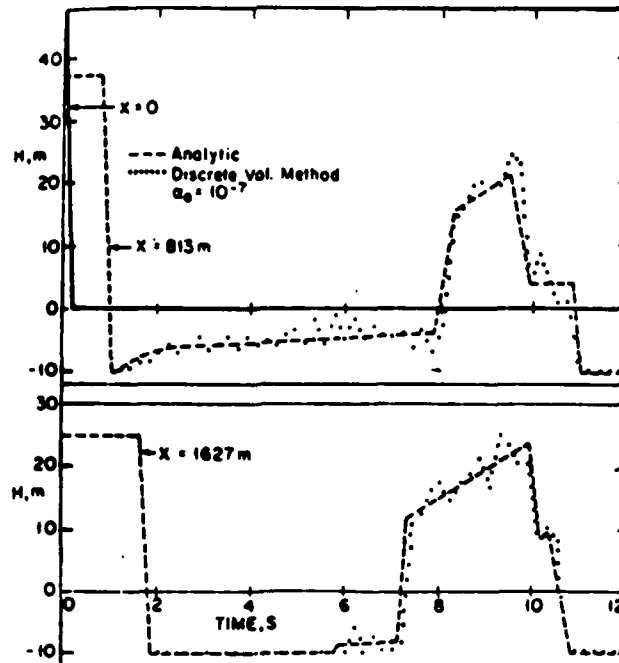


Fig. 5-7. Wylie's results for two locations ( $L=3048$  m,  $a=981$  m/s,  $D=0.61$  m,  $Q_0=0.89$  s,  $H_v=-10.06$  m)

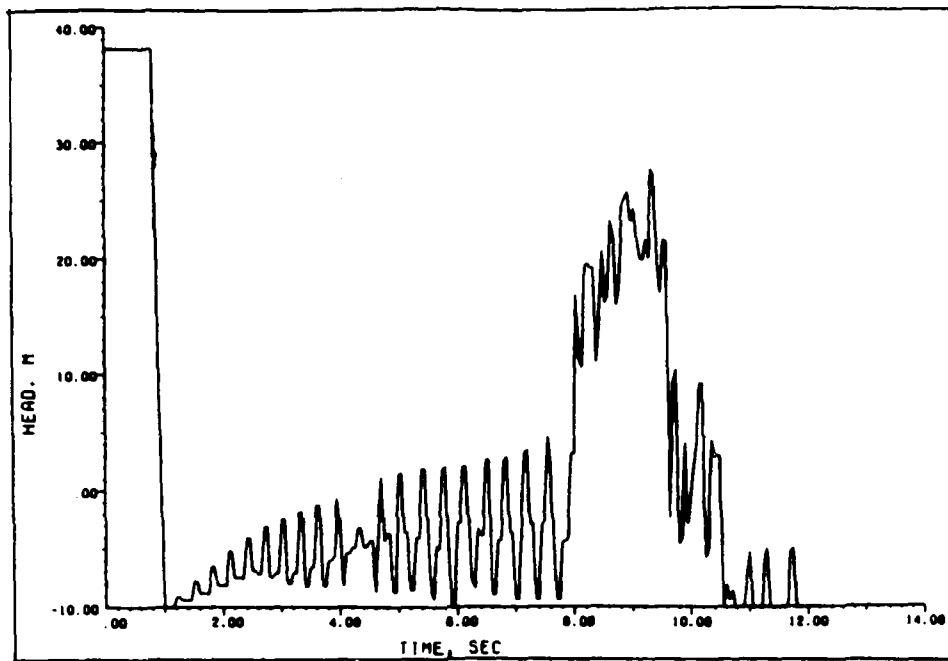


Fig. 5-8. Program results for first cavitation simulation ( $x=813$  m,  $L=3048$  m,  $a=981$  m/s,  $D=0.61$  m,  $Q_0=0.89$  s,  $H_v=-10.06$  m)

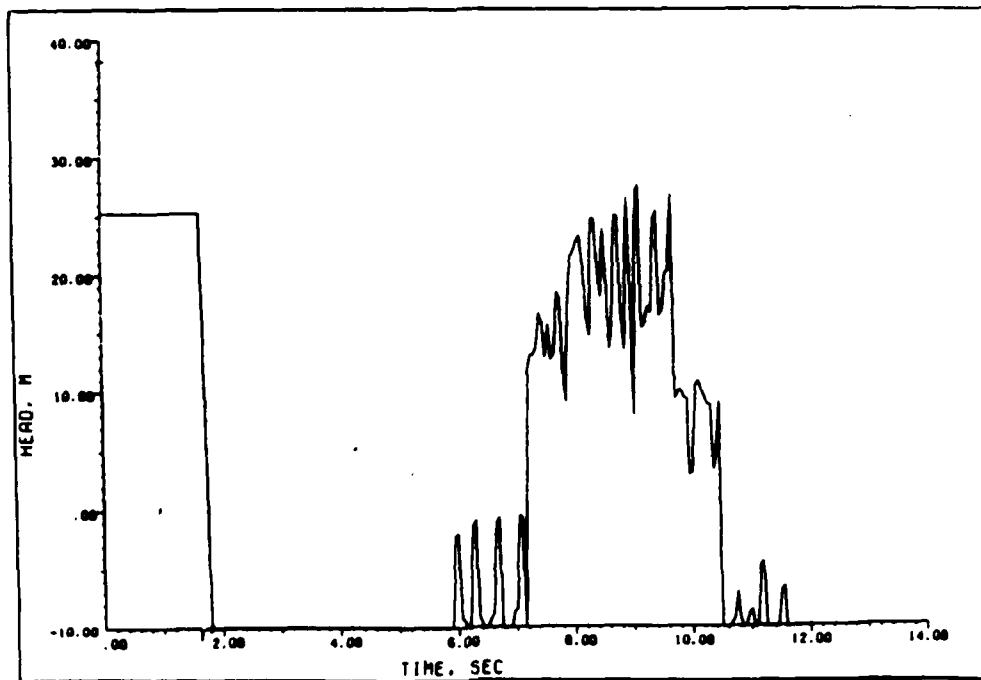


Fig. 5-9. Program results for first cavitation simulation ( $x=1627$  m,  $L=3048$  m,  $a=981$  m/s,  $D=0.61$  m,  $Q_0=0.89$  s,  $H_v=-10.06$  m)

expansion waves generated by the change in upstream conditions traveled down the pipe. Further, as was expected, the reflection of those waves returned at some time greater than  $2L/a=4.56$  s as indicated by the location of the major pressure surge. The surge itself was due to the expansion waves reflecting as compression waves from the constant pressure boundary at the reservoir, then propagating back upstream. The delay in the return of the waves seen in the results was introduced by the formation of vapor within the pipe system. As discussed by Wylie (14, 17), the effective wave speed is inversely related to the mass of the vapor present. Thus, as vapor was released the effective wave speed decreased, creating the delay in the occurrence of the pressure surge at the station indicated.

Figs. 5-7, 5-8, and 5-9 agreed very closely as to the time and approximate magnitude of the major events. Unexpectedly, the exact magnitude of the program results was obscured by numerous pressure spikes in the solution. The period of the spikes was related to the distance between the downstream end of the cavitation bubble and the end of the pipe. The cause of those spikes however, will be discussed later.

Second Simulation. For the second of the cavitation simulations, the upstream conditions became those seen in the bottom curve in Fig. 5-10. The results Wylie published for this slightly more complex interaction appear in Fig. 5-10 as the upper two curves. The results of this study follow in Fig. 5-11 and 5-12. In this case the change in the upstream boundary condition generated both expansion and compression waves. The comparison of the curves was quite good, considering the approximation of the upstream pressure that was used for the program results. Both sets of results agreed that the first peak was delayed due

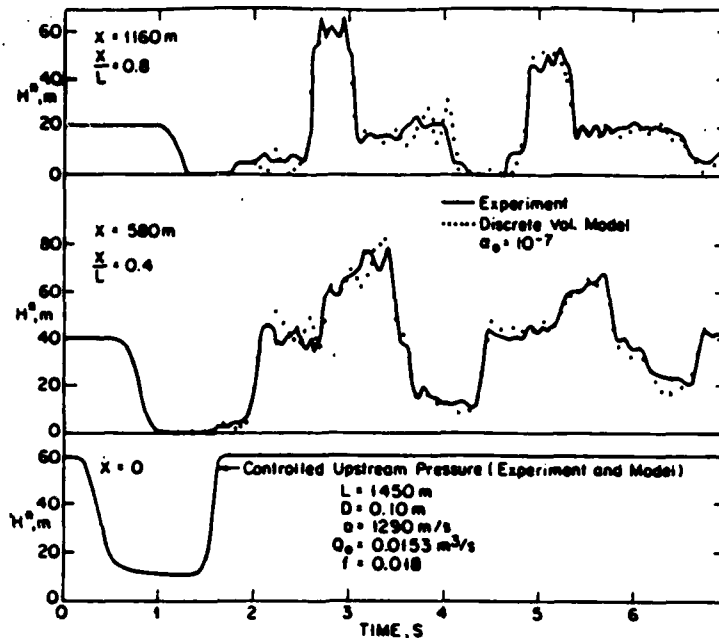


Fig. 5-10. Wylie's results for simulation 2 ( $H_v = -10.1 m$ )

to the pressure falling to vapor pressure. Also, both sets indicated the system had a period of 2.25 s once the cavities had collapsed, a period which was half of the expected  $4L/a = 4.5 s$ . This anomaly was explainable by realizing both the expansion and the compression which occurred at the upstream end were of approximately the same magnitude and were separated in time by almost exactly  $L/a = 1.1 s$ . Thus, the expansion and the compression separated by this time interval caused the system to act as if the pipe was only half of its actual length. But, even though the magnitude of the peaks agreed well, there were still minor discrepancies in the exact shape and magnitude.

Further Verification. To verify that the discrete vapor model was indeed working correctly in light of the unrealistic pressure spikes, the first cavitation simulation was repeated, but with two different vapor pressures. Theoretically, if two fluids with different vapor pressures were exposed to the same drop in pressure, the fluid with the higher

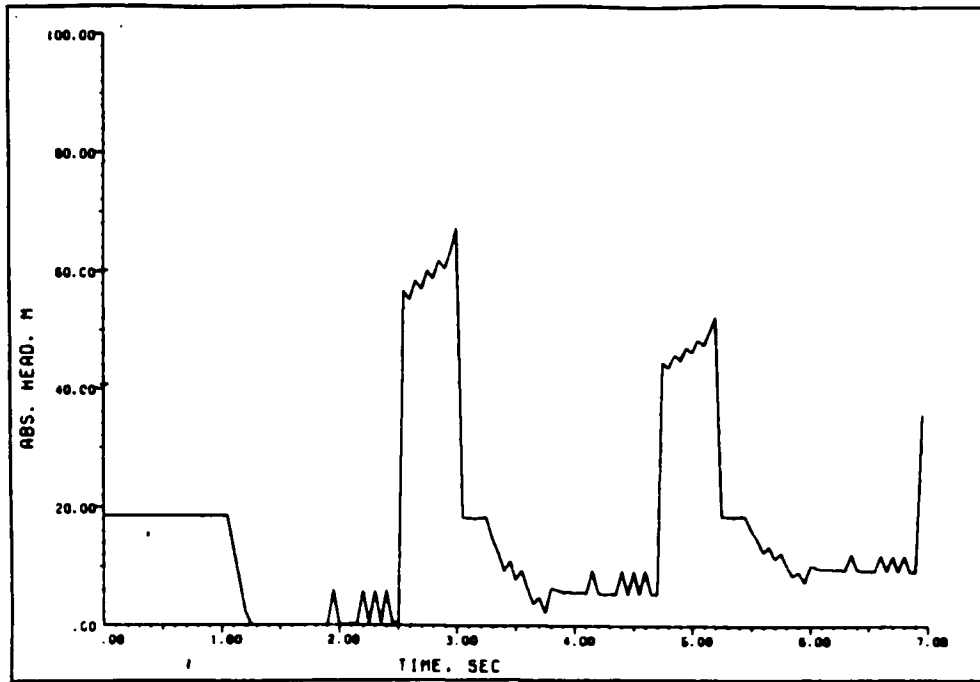


Fig. 5-11. Program results for simulation 2 ( $x=1160$  m,  $L=1450$  m,  $D=0.1$  m,  $a=1290$  m/s,  $Q_0=0.0158$  m<sup>3</sup>/s,  $H_v=-10.1$  m)

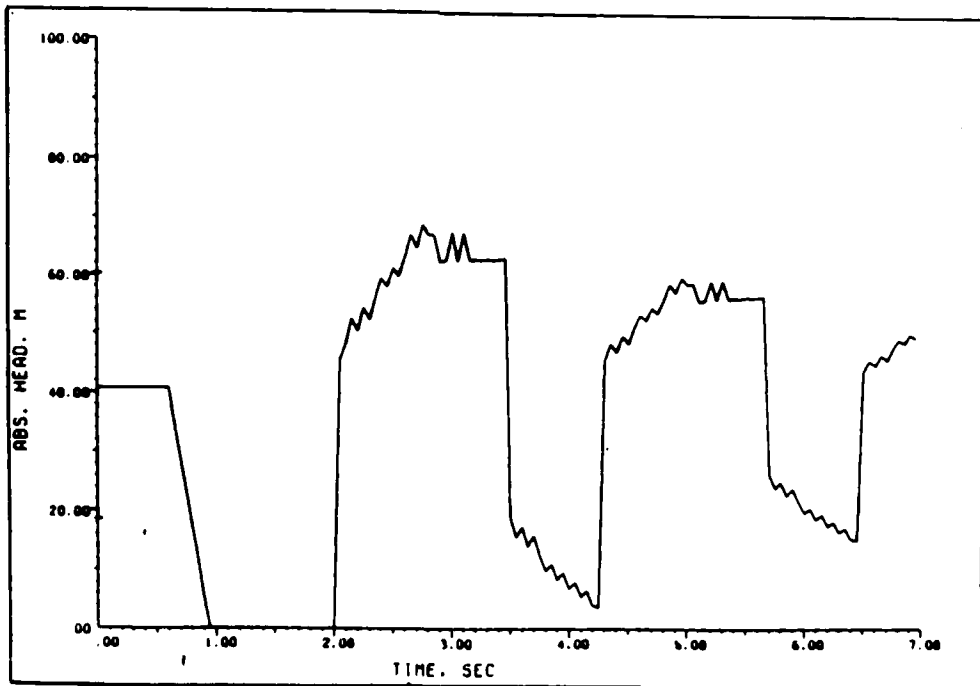


Fig. 5-12. Program results for simulation 2 ( $x=580$  m,  $L=1450$  m,  $D=0.1$  m,  $a=1290$  m/s,  $Q_0=0.0158$  m<sup>3</sup>/s,  $H_v=-10.1$  m)



vapor pressure would release a greater amount of vapor. Further, the larger mass of vapor would produce a larger decrease in the effective wave speed, given the same initial wave speed in both fluids. A vapor pressure of  $-100$  m was first chosen to insure that the fluid remained a liquid throughout the simulation. This choice of vapor pressure made it possible to verify that the model was correctly handling the wave propagation and attenuation. For example, the pressure surge at  $x=813$  m downstream from the inlet should occur  $2L/a=4.56$  s after the first expansion wave passes that point. That is the time required for a wave traveling  $981$  m/s to propagate downstream and return. For the results in Fig. 5-13, the initial wave passed  $x=813$  m at about  $0.8$  s, the surge began at  $5.4$  s. This made a difference of  $4.6$  s, which is within one percent of the predicted value. As for the attenuation of the waves, the decrease in the strength of the waves could be seen by the manner in which the curves converged towards zero.

For the case of a vapor pressure higher than the original case, the previous argument was still true. That is to say, the higher the vapor pressure, the greater the amount of vapor released, and the lower the wave speed must be for a given pressure drop. Thus, when the vapor pressure was raised to  $-5.03$  m gage in the cavitation simulation, the pressure surge was expected to occur at some later time. A comparison of Fig. 5-8, the results for  $H_v=-10.06$  m, and Fig. 5-14, the results for  $H_v=-5.03$  m, indicated that the pressure surge was indeed delayed, verifying that much of the model. However, the results were again plagued by the nonphysical pressure fluctuations.

Pressure Spikes. These fluctuations and spikes were attributed to the method by which the vapor was accounted for in the flow. By lumping

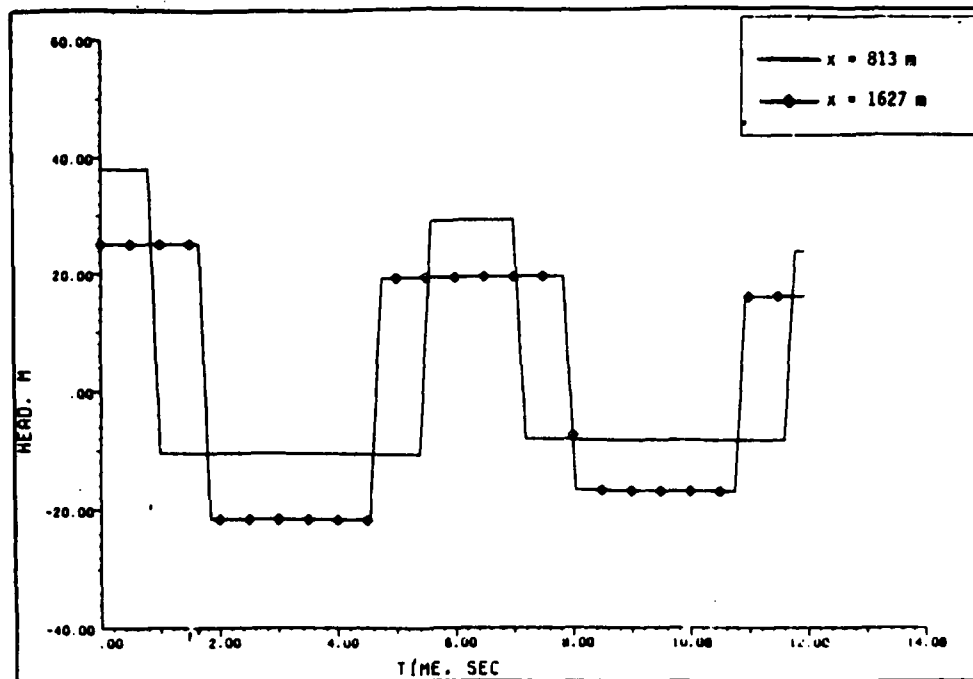


Fig. 5-13. Program results for simulation 1 ( $L=3048$  m,  $a=981$  m/s,  $D=0.61$  m,  $Q_0=0.89$  s,  $H_v=-100$  m)

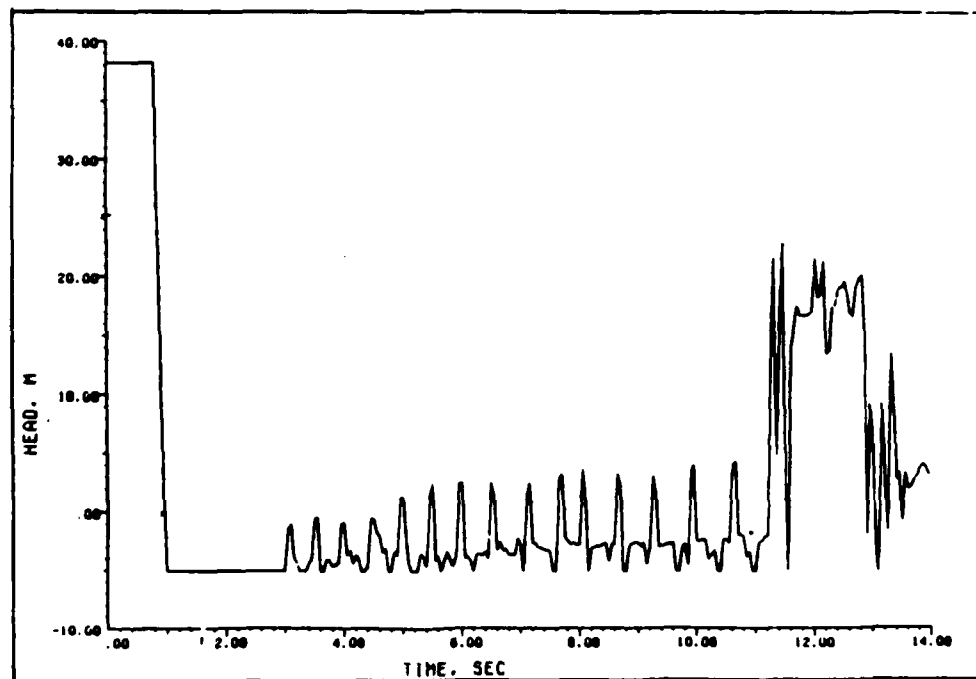


Fig. 5-14. Program results for simulation 1 ( $x=813$  m,  $L=3048$  m,  $a=981$  m/s,  $D=0.61$  m,  $Q_0=0.89$  s,  $H_v=-5.03$  m)

the gas bubbles at the computing sections, numerical oscillations in the magnitude of the pressure occurred. These nonphysical pressure oscillations arose for several reasons. First when the gas volume was lumped at a computing section, it effectively produced an internal constant pressure boundary. Hence, when multiple cavities occurred, there were multiple reflections of the waves traveling in the pipe. Second, when multiple cavities were predicted, they did not always physically exist. Thus, as these nonphysical cavities opened and closed, additional fluctuations were introduced into the solution. And third, mathematical instabilities could occur when the gas bubbles underwent very large volume changes during the course of a single time step. So, some caution is required for the choice of time steps.

In an effort to eliminate the nonphysical oscillations, several possible solutions were attempted. The first "fix" was drawn from a paper by Simpson and Wylie (19). They showed that the integration method used when computing the cavity volumes could introduce some of the error associated with nonphysical cavities. In the study Simpson and Wylie demonstrated three different methods by which Eq. (3.14) could be integrated. The first was Euler's one-step method. This gave  $\Delta V_g = \Delta t(Q - Q_u)$ , where  $Q$  and  $Q_u$  were the flow upstream and downstream of the cavity during the previous time step. The next method was the improved Euler's method, which was used in this study to obtain Eq. (3.15). Here, the difference in the flows at the previous and current time steps was averaged to find the change in volume. The third and last was the forward integration method, which gave  $\Delta V_g = \Delta t(Q_p - Q_{pu})$ , where  $Q_p$  and  $Q_{pu}$  were the flows at the current time step.

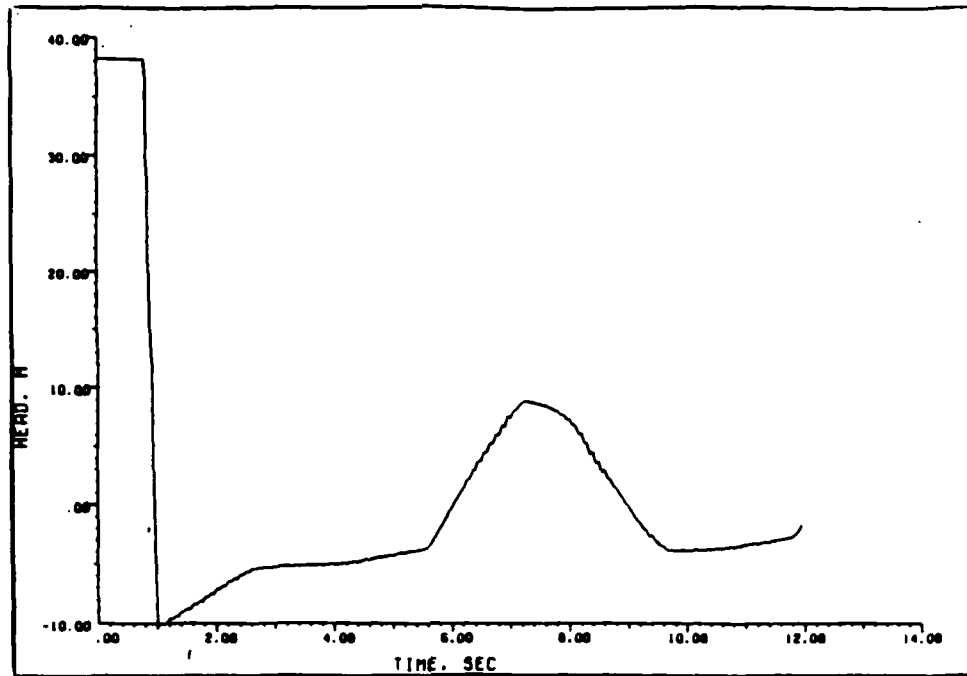


Fig. 5-15. Program results using Euler's method ( $x=813$  m,  $L=3048$  m,  $a=981$  m/s,  $D=0.61$  m,  $Q_0=0.89$  s,  $H_v=-10.06$  m)

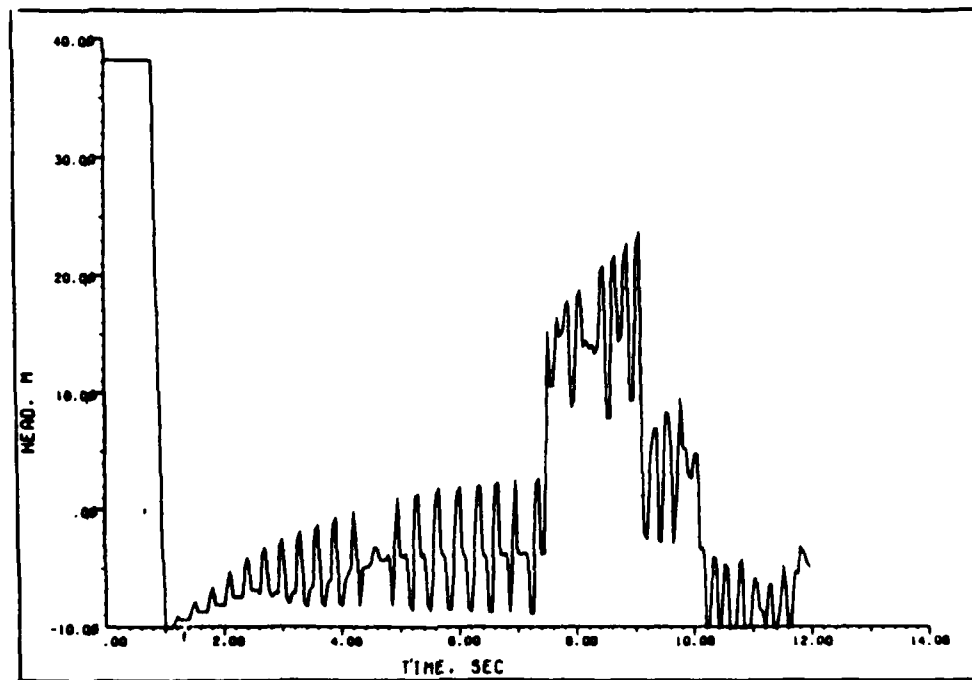


Fig. 5-16. Program results using forward integration ( $x=813$  m,  $L=3048$  m,  $a=981$  m/s,  $D=0.61$  m,  $Q_0=0.89$  s,  $H_v=-10.06$  m)

The results produced by using the improved Euler's method have already been presented in Figs. 5-8 and 5-9. Plots of the results obtained by the other two integration methods appear in Figs. 5-15 and 5-16. A comparison of the results in Figs. 5-8, 5-15, and 5-16 with Fig. 5-7 showed that for this case the improved Euler's method best reproduced the timing of the main surge when only vapor was accounted for. Both of the other methods underestimated the cavity volumes, so that the higher effective wave speeds caused the surge to occur sooner than expected. The Euler's method did succeed in eliminating the fluctuations, but sacrificed any claim to accuracy concerning the timing or the magnitude of the pressure surge.

Wylie (17) developed another method to reduce the nonphysical spikes, an air release model, which was presented under Cavitation in section III, Boundary Conditions. After incorporating Wylie's air release model into the program developed in this study, the first simulation was repeated. The results of this experiment, at  $x=813$  m only, are shown in Fig. 5-17. Upon comparison of Figs. 5-8 and 5-17, it was seen that the air release model did reduce the magnitude of the oscillations to a small degree, but did not eliminate them. Further, the air release model predicted the pressure surge would occur later than indicated in Fig. 5-7. The small delay came because the air release model slightly overestimated the amount of gas released. The additional gas was due to the inclusion of a very small amount of air release from the fluid along with the usual vapor formation.

The last approach in the attempt to eliminate the numerical oscillations was to reduce the size of the time step. During all the previous simulations a time step of 0.05 s was used. For the results seen in Fig.

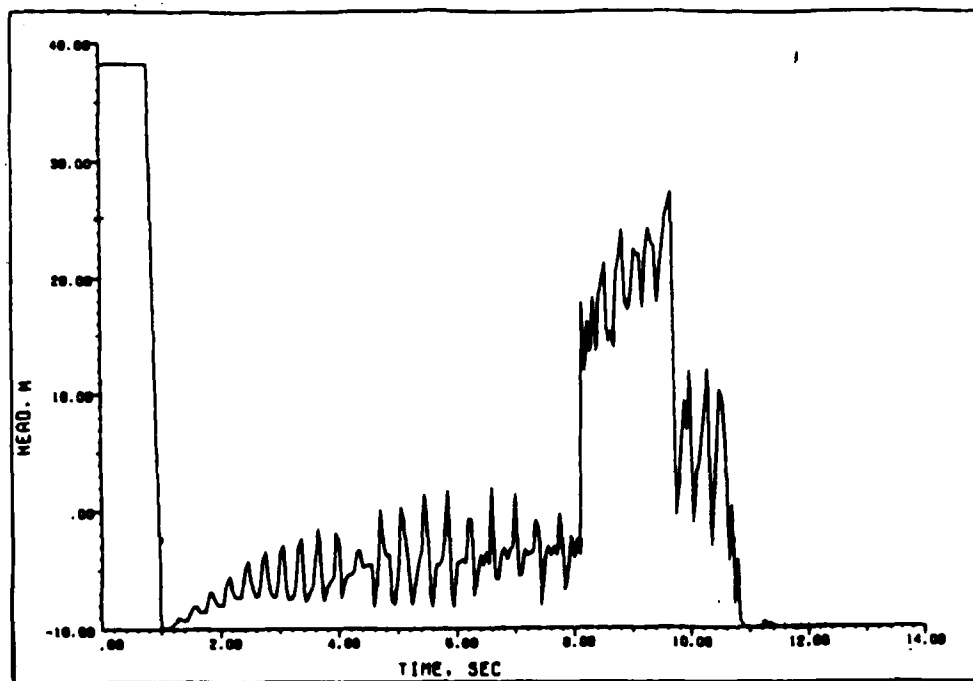


Fig. 5-17. Program results with air release ( $x=813$  m,  $L=3048$  m,  $a=981$  m/s,  $D=0.61$  m,  $Q_0=0.89$  s,  $H_v=-10.06$  m)

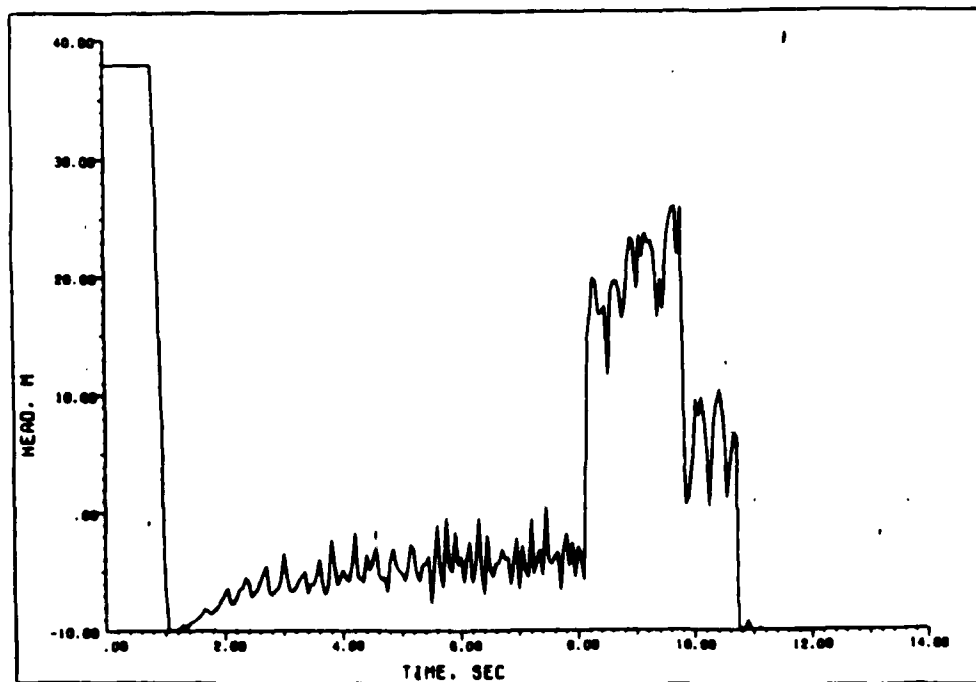


Fig. 5-18. Results for air release and reduced time step ( $x=813$  m,  $L=3048$  m,  $a=981$  m/s,  $D=0.61$  m,  $Q_0=0.89$  s,  $H_v=-10.06$  m)

5-18, the time step was decreased to 0.01 s. Unfortunately, it was not possible to further reduce the time step significantly. The number of large arrays required to complete the computation with a smaller time step overflowed the available memory in the computer. However, the trend observed by comparing Figs. 5-17 and 5-18, indicated that the magnitude of the oscillations was decreased by reducing the step size. It must be remembered though, that by reducing the step size, the run time and the memory required were increased, so a tradeoff between accuracy and cost must be made.

#### Multiple Pipe Verification of Valve-in-line

The first of the multiple pipe simulations was taken from a study by Swaffield (13), who was interested in the flow downstream of a valve. In essence, since the pipes of Swaffield's system all had the same diameter, the region downstream of the valve was analogous to the system in the first cavitation simulation. The disturbance at the valve was propagated downstream, where it was reflected in the opposite sense from the constant pressure reservoir at the end. The reflection traveled back upstream to the closed valve, where it was reflected in the same sense, propagating once more downstream.

First Simulation. As seen in section IV, the initial conditions for the first of the three cases were:  $P_d=102 \text{ kN/m}^2 \text{ abs}$ ,  $Q_0=0.00355 \text{ m}^3/\text{s}$ , and the valve cut-off time was 0.081 s. The results published by Swaffield for this case appear in Fig. 5-19, while the results produced by the program can be seen in Fig. 5-20. The program accurately predicted the magnitude of the first peak, but predicted magnitudes which were higher than expected for the second and third peaks. Furthermore, the pulses predicted by the program, Fig. 5-20, occurred between the

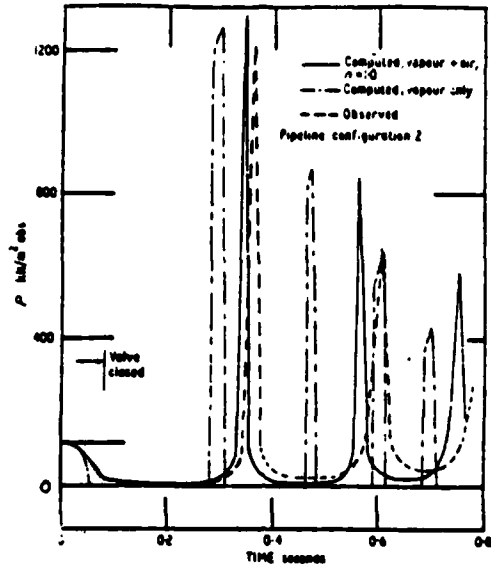


Fig. 5-19. Swaffield's results at the valve for case 1 ( $L_{2,3}=9.87$  m,  $a=918$  m/s,  $D=0.0508$  m,  $P_V=700$  Pa,  $t_c=0.081$  s)

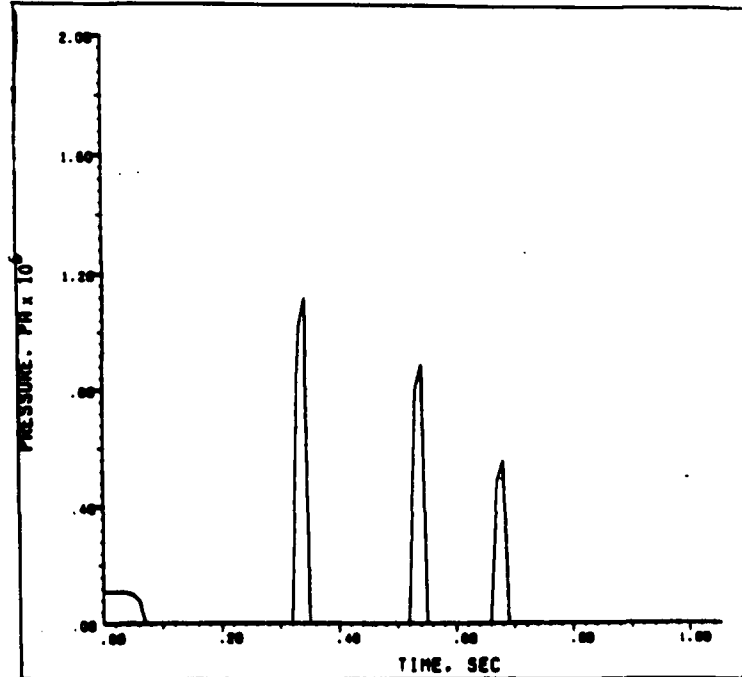


Fig. 5-20. Program results at the valve for case 1 ( $L_{2,3}=9.87$  m,  $a=918$  m/s,  $D=0.0508$  m,  $P_V=700$  Pa,  $t_c=0.081$  s)



pulses predicted in the two sets of Swaffield's results in Fig. 5-19.

All the results agreed that as the valve closed, a cavity formed on the downstream side of the valve. The discrepancies past the first peak resulted from different estimates of the amount of gas generated during the formation of the initial cavity. The disagreement about the cavity volume was inferred from the differences in the periods of the oscillations. The amount of gas predicted by the program was less than the observed amount, but greater than the amount predicted for pure vapor. Therefore, the effective wave speed fell in between the two predictions by Swaffield, causing the pulses also to fall in between the times predicted in Fig. 5-19. In addition, since the cavity implied by the program's results was smaller than the cavity implied from the observed results, the smaller cavity did not provide sufficient damping for the later pulses. Consequently, there was a digression in magnitude as well as period.

Second Simulation. For the second of the valve-in-line simulations, the downstream pressure was raised to 222 kN/m<sup>2</sup> abs and the valve cut-off time was 0.16 s. A comparison of the published results, Fig. 5-21, with the program results seen in Fig. 5-22 and 5-23, showed favorable agreement as far as the general shapes and magnitudes of the curves were concerned. However, the characteristic closure curve used in the program simulation was not completely accurate. The approximate curve had a more sudden closure, creating a slightly stronger expansion. The difference in the closure curves was seen in the rate at which the pressure initially dropped to vapor pressure. As a result of this closure the program predicted the peak pressure to occur at 0.24 s, about 0.1 s after the observed peak occurred. This delay implied a slight

overestimate of the gas released, causing a lower effective wave speed. Also, it was possible to determine that the gas release was restricted to the region immediately downstream of the valve. This observation stemmed from a comparison of the results at 4.04 m downstream of the valve with the results at 50.8 mm downstream of the valve. First, the pressure 4.04 m downstream of the valve never reached vapor pressure during the time preceding the first pressure peak. And second, the pressure oscillations between the first and second large peak in the results at 4.04 m had a period of 0.02 s, very nearly  $2L/a$  for the combined length of the second and third pipes of the system, even though vapor pressure was indicated at the valve during this same time interval.

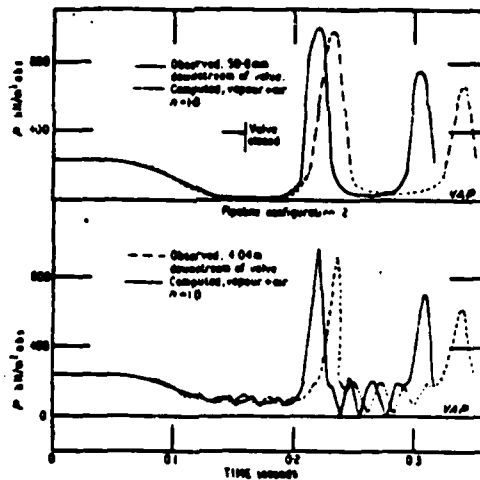


Fig. 5-21. Swaffield's results for case 2 ( $L_{2,3}=9.87$  m,  $a=918$  m/s,  $D=0.0508$  m,  $P_v=700$  Pa,  $t_c=0.16$  s)

Third Simulation. For the third case, the initial conditions were:  $P_d=120$  kN/m<sup>2</sup> abs,  $Q_0=0.00541$  m<sup>3</sup>/s, and the valve cut-off time was 0.14 s. Once again, the agreement between the published results in Fig. 5-24 and the program results in Fig. 5-25 was good. At 50.8 mm downstream of the valve, the program predicted a peak pressure of approximately 1600 kPa at 0.49 s, which was very close to the results observed by Swaffield. However, in this simulation only the results up until the first peak

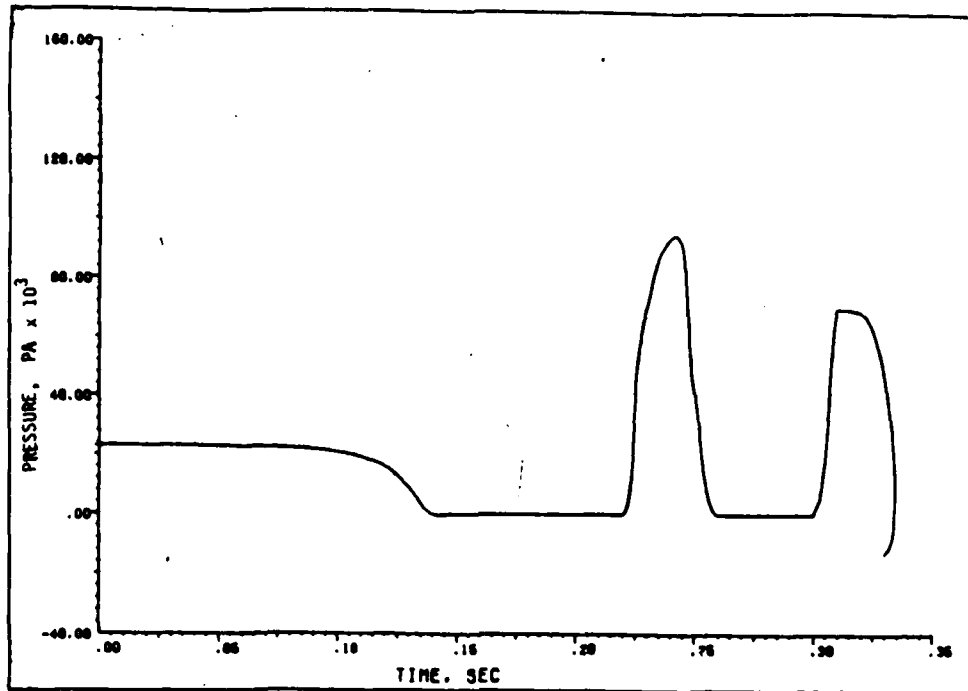


Fig. 5-22. Program results for case 2, 50.8 mm from valve ( $L_{2,3}=9.87$  m,  $a=918$  m/s,  $D=0.0508$  m,  $P_v=700$  Pa,  $t_c=0.16$  s)

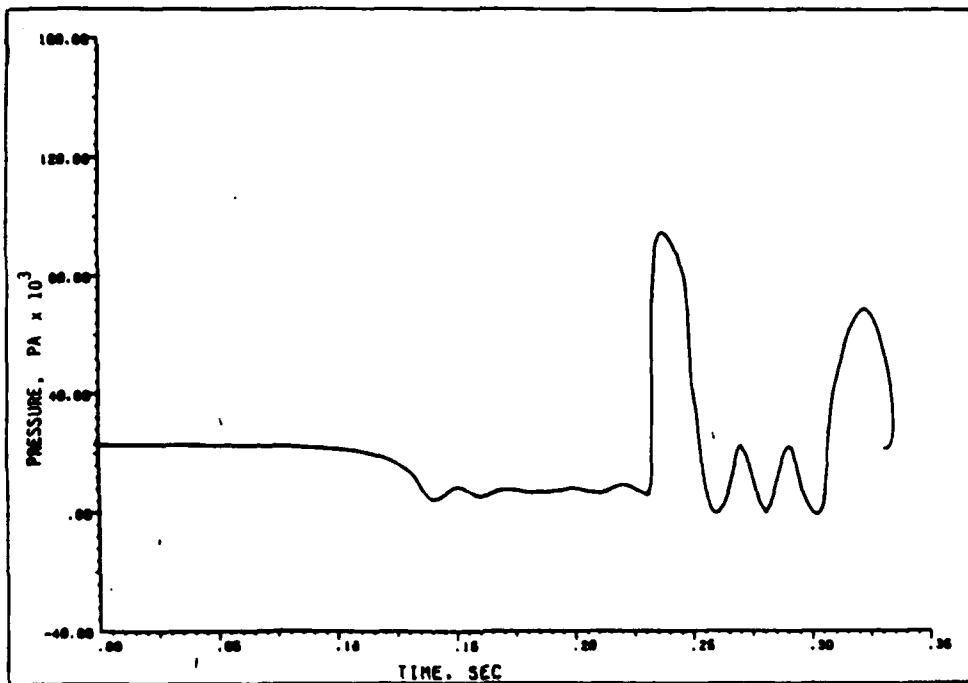


Fig. 5-23. Program results for case 2, 4.04 m from valve ( $L_{2,3}=9.87$  m,  $a=918$  m/s,  $D=0.0508$  m,  $P_v=700$  Pa,  $t_c=0.16$  s)

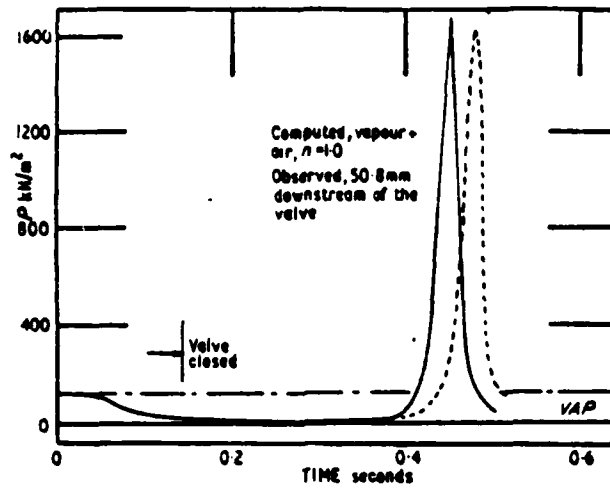


Fig. 5-24. Swaffield's results for case 3 ( $L_{2,3}=9.87$  m,  $a=918$  m/s,  $D=0.0508$  m,  $P_v=700$  Pa,  $t_c=0.14$  s)

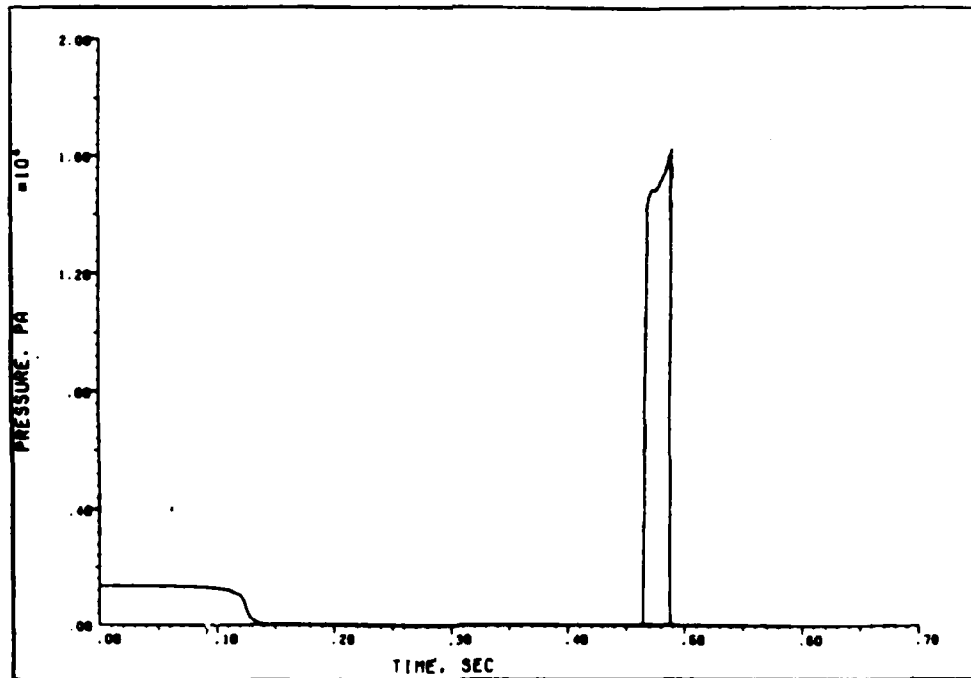


Fig. 5-25. Program results for case 3, 50.8 mm from valve ( $L_{2,3}=9.87$  m,  $a=918$  m/s,  $D=0.0508$  m,  $P_v=700$  Pa,  $t_c=0.14$  s)

were presented by Swaffield. As in the previous simulations the agreement was good up to that first peak. Unfortunately, none of the subsequent peaks were presented for this case. So, it was impossible to determine if the program results for this case were any better than the previous cases for agreement after the first peak.

#### Verification of Multiple Pipe Valve Closure

The second of the multiple pipe simulations was also the second of the two valve closure problems taken from Wylie and Streeter (14:60). Like the previous multipipe simulations, this system was composed of three pipes in series. For convenience the pipes were labelled as pipes 1, 2, and 3 starting at the upstream end of the system. Unlike the other multipipe system, this one by Wylie and Streeter also contained area changes at each of the internal junctions. Their results for the pressure at the valve were tabulated along with the results obtained from the program and presented in Table VIII. A point by point comparison of the two sets of results showed a variation of less than 0.1 percent for the duration of the simulation. However, looking down the columns of Table VIII or at the appropriate curve in Fig. 5-26, one does not observe the smooth rise and fall in the pressure seen in the single pipe results, Fig. 5-1, despite a basic similarity between the two systems. As expected, in Fig. 5-26, the area changes and the different closure curve superimposed irregularities over results approaching those in Fig. 5-1.

For the first 0.6 s, the valve closed rather rapidly as the valve characteristic,  $\tau$ , dropped from 1.0 to 0.2. In turn the hard closure during this time generated increasingly stronger compression waves, since the greater diameter columns of water in pipes 1 and 2 had greater inertia

Table VIII. Head at the Valve for Multiple Pipe Closure

<u>Time (s)</u>	<u>Wylie' s Calc. Head (m)</u>	<u>Program Calc. Head (m)</u>
0.0	100.00	99.99
0.1	127.65	127.64
0.2	167.51	167.50
0.3	224.67	224.64
0.4	311.71	311.64
0.5	448.71	448.57
0.6	668.70	668.39
0.7	673.58	673.24
0.8	651.84	651.50
0.9	690.25	689.89
1.0	736.11	735.72
1.1	764.86	764.43
1.2	790.15	789.68
1.3	805.23	804.72
1.4	805.76	805.21
1.5	773.19	772.64
1.6	684.02	683.51
1.7	683.85	683.32
1.8	686.38	685.81
1.9	570.22	569.71
2.0	407.59	407.18

than the column in pipe 3. Aside from affecting the compression, the differences in cross sectional area had a second effect. At each junction where a pipe was joined to a second pipe of different diameter, a traveling wave was both transmitted with the same sign and reflected with an opposite sign. This created multiple wave fronts within the system. Thus, at junction two between pipes 2 and 3, the compression waves traveling upstream from the valve were transmitted without changing sign and reflected as expansion waves. This first reflection, referred to as the first wave front, arrived back at the valve in about 0.2 s, but was only strong enough to reduce the rate of the pressure rise. The compression waves generated at the valve were stronger than the reflected expansion waves due to attenuation from friction and to the relative difference in time at which each wave was generated.

Starting at 0.4 s, compression waves due to the reflection of the first wave front from junction two arrived at the valve. Accordingly, the pressure began to rise more quickly. At 0.6 s the slope of the valve characteristic decreased such that it took the next 1.2 s for the valve to completely close. This softer closure generated weaker compression waves at the valve. Thus, the combination of the expansion waves from the first wave front with those from the second reflection of the first wave front was stronger than the combination of the current compression waves with those of the first reflection of the first wave front. So, the pressure began to drop as the flow began to reverse. However, around 0.8 s, the third reflection of the first wave front arrived about the time the expansion waves resulting from the hard closure in the first wave front came to an end. Therefore, the compression

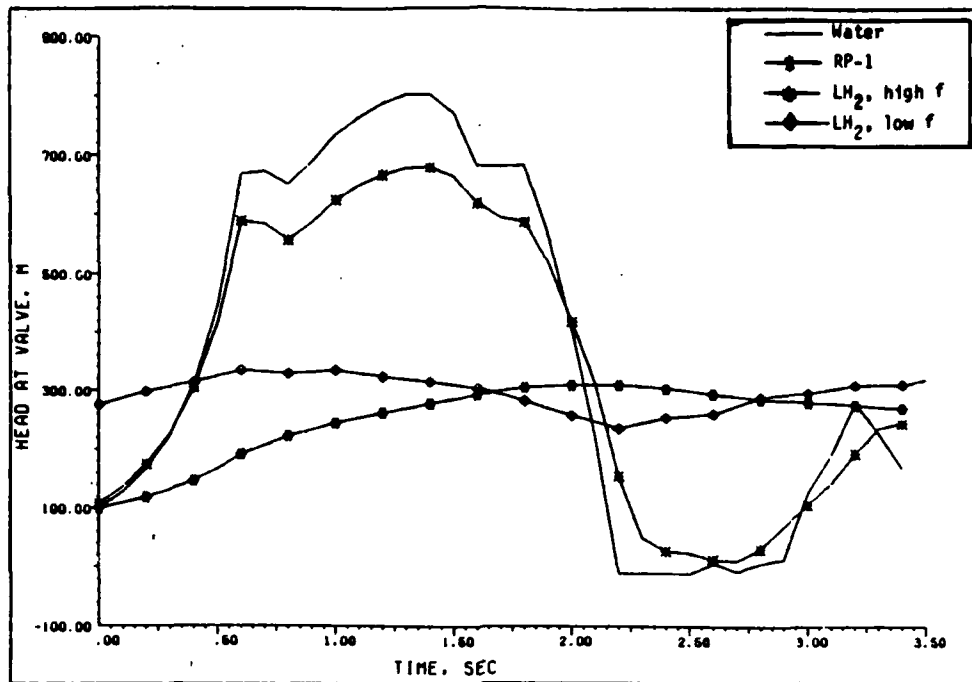


Fig. 5-26. Program results for case 1 of multipipe closure ( $L_1=351$  m,  $L_2=483$  m,  $L_3=115$  m,  $a=1200$  m/s,  $H_0=289$  m)

waves dominated once more and the pressure began to rise again.

Beginning at 1.0 s a new factor entered the picture as a second wave front, consisting of expansion waves due to the reflection of the original compression waves from the junction 1 between pipes 1 and 2, arrived at the valve. The arrival of these waves initially caused the rate of the pressure to slow. As the strength of the expansion waves increased, the rate of the pressure rise decreased even further. But, before the pressure could start to drop, compression waves due to the first reflection from junction 2 of the second wave front arrived at the valve around the 1.2 s point. These new waves acted to partially negate the expansion waves, slowing the reversal of the flow. However, at 1.4 s, expansion waves produced by the second reflection of the second wave front from junction two appeared at the valve causing the pressure to finally begin decreasing.



It was at 1.6 s that the third wave front, created by the original compression waves reflecting from the reservoir, reached the valve. At this same time two other events occurred. First, the expansion waves in the first reflection of the second wave front due to the hard closure came to an end. And second, compression waves due to the third reflection of the second wave front arrived at the valve. These three events interacted with the other waves at the valve to produce the nearly constant pressure seen between 1.6 and 1.8 s.

Another complex interaction occurred at 1.8 s. First, at this time the valve was completely closed, so no new compression waves were being generated. Second, the compression waves from the hard closure in the first reflection of the second wave front ended, leaving the weaker waves from the soft closure. Third, compression waves due to the first reflection of the third wave front reached the valve. And fourth, expansion waves due to the fourth reflection of the second wave front arrived at the valve. The end result of all these events was a steep pressure drop.

Fig. 5-26 includes a plot of the results from Table VIII as well as the results obtained for the simulation adapted as described in section IV for RP-1 and LH<sub>2</sub>. For all three fluids the timing of the waves was very similar since the average of the adjusted wave speed for all three were nearly equal. The wave speeds for water and for LH<sub>2</sub> were both calculated as having an average wave speed of 1175 m/s, while RP-1 was found to have a wave speed of 1125 m/s. Therefore, since even the wave speed stayed about the same despite changes in the fluids, the differences observed in the transients in Fig. 5-26 were due to the only remaining variables which could change, either the density or the friction factor.

In the single pipe closure problem, the peak pressure decreased by about 7 percent when the friction factor was doubled. In the results for the multipipe closure, the peak pressure for RP-1 was 14 percent lower than that of water, even though the friction increased by a factor of 1.25. It would be very easy at this point to reason that the change in density was the major driver for the significant change in peak pressure. Unfortunately, it was not that clear cut. The multipipe system was longer and narrower than the single pipe system, increasing the frictional effects. So, it was difficult to determine the true contribution of either the friction factor or the density.

When the results using LH<sub>2</sub> were compared with those for water, a much clearer indication of the effects of density and friction factor was attained. For the very high friction factor case for LH<sub>2</sub>, the attenuation of the reflected expansion waves was very great. Thus, the compression produced by the valve dominated until the valve was almost completely closed, only then did the pressure peak. The situation was very different for the low friction factor case. The pressure peaked relatively quickly due to the strong influence of the reflected waves on the pressure at the valve. But even though the time of the peak pressure was very different, the magnitudes of the peak pressures differed by less than 10 percent. This small change was in contrast to the difference of over 100 percent between the peak pressure experienced for water and the peak pressure for the low friction LH<sub>2</sub>. This significant effect of density was as expected when the relationship of density and inertia was considered. As the density increased, the mass of fluid within the pipe at any specified time increased, which in turn increased the inertia of the fluid. Thus, as the inertia increased, the force

required to bring that mass to rest increased, thereby increasing the force per area which can be defined as pressure.

Effects of Reservoir Pressure. The discussion above illustrated the influence of density on the severity of the transients by a comparison of the results for the different fluids in Fig. 5-26. In a similar manner, a comparison of the results for the same fluid in Figs. 5-26, 5-27, and 5-28 provided insight into the effect of different reservoir pressures on the transient pressures in a multipipe system.

The first and most obvious effect of changing the reservoir pressure was the corresponding change in the initial pressure at the valve. Given that the friction remained constant for any particular fluid in these simulations, the loss in pressure between the reservoir and the valve was always a constant for a particular flow rate. So, as the initial upstream pressure changed, the initial valve pressure also changed.

A second effect of changing the reservoir pressure appeared to be a change in the strength of the reflections. It was expected that the strength of the waves generated during the different closures would vary as a function of the reservoir pressure. However, a comparison of the results seen in Figs. 5-26, 5-27, and 5-28 indicated that the strength of the reflections was also a function of reservoir pressure. The results for the different fluids retained the same relationship with respect to the results for water as seen in the original case for this simulation. Therefore, the discussion of the second effect will be restricted only to the results obtained for water.

For the reservoir pressure of the original simulation, the results contained essentially three peaks, as seen in Fig. 5-26. The first peak

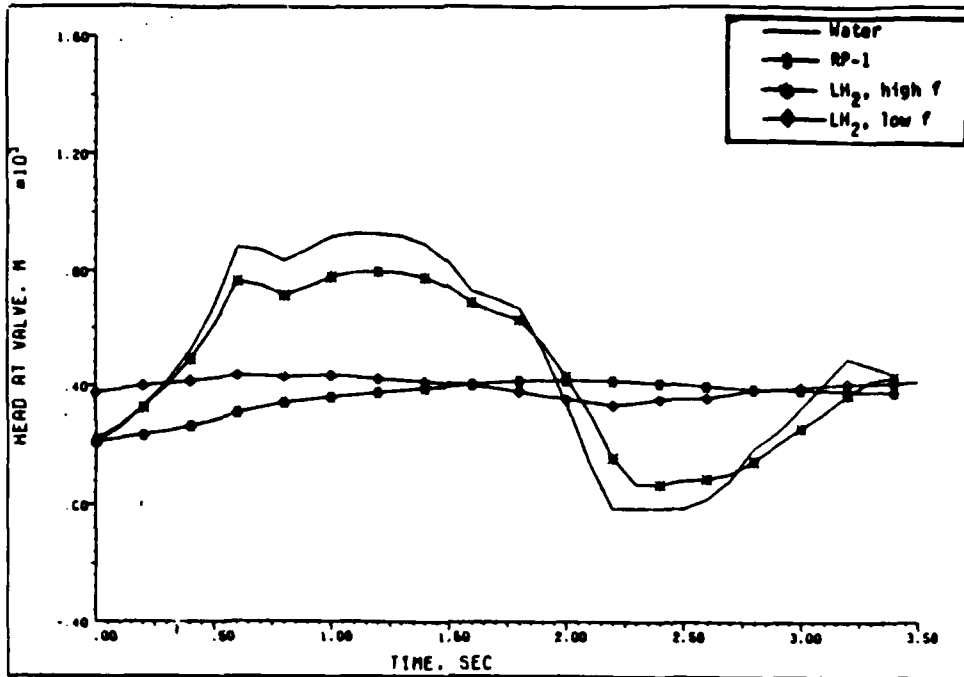


Fig. 5-27. Program results for case 2 of multipipe closure ( $L_1=351$  m,  $L_2=483$  m,  $L_3=115$  m,  $a=1200$  m/s,  $H_0=400$  m)

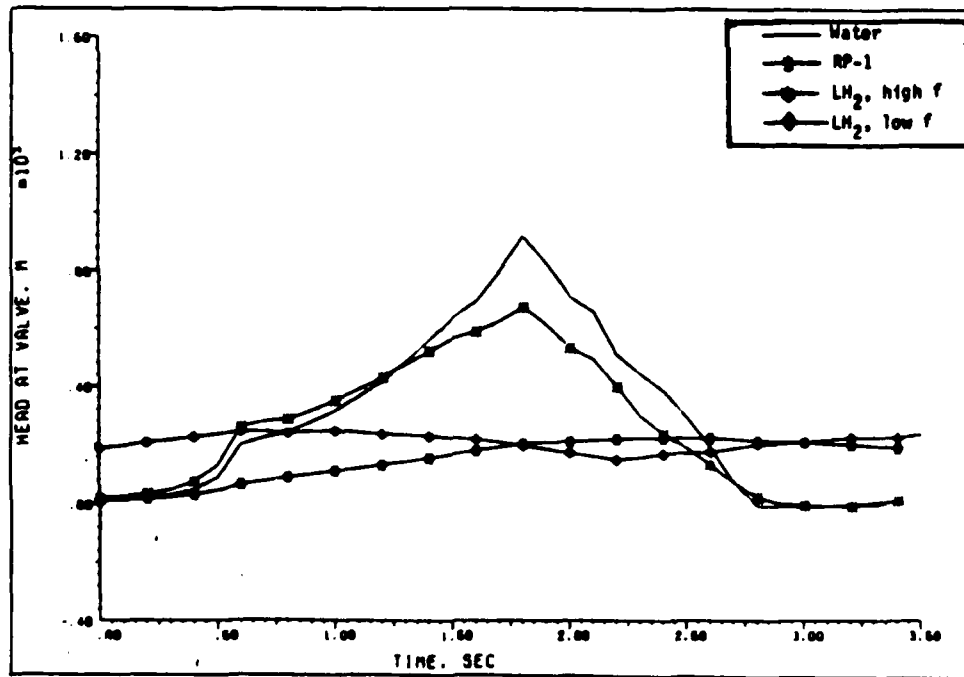


Fig. 5-28. Program results for case 3 of multipipe closure ( $L_1=351$  m,  $L_2=483$  m,  $L_3=115$  m,  $a=1200$  m/s,  $H_0=200$  m)

occurred when the closure changed from hard to soft. A second peak, also the highest, occurred just prior to the arrival of the third wave front. Lastly, a third peak that occurred about the time the valve finished closing. In the case of the higher reservoir pressure, Fig. 5-27, the first peak occurred much the same as in the original case. However, the second and third peaks were not simply higher magnitude versions of the peaks in Fig. 5-26. The second peak reached its maximum as soon as the second wave front arrived, an indication that the strength of the reflected expansion waves was enhanced. A further demonstration of the increased strength of the reflections was that the third peak did not truly exist. There was a leveling of the curve around the point where the third peak should have been, but the results were so dominated by the reflected expansion waves that there was only this change in the slope, not a real peak. In the case of the lower reservoir pressure, there was only one true peak remaining in the results in Fig. 5-28. Unlike the high pressure case, the absence of three distinct peaks was due to the weakness of the reflected expansion waves, they were unable to significantly affect the compression at the valve. Thus, when each of the first two wave fronts arrived at the valve, there were only changes in the slope. The only true peak did not occur until the valve was completely closed. At this time compression waves were no longer generated at the valve, so the expansion waves were now sufficient to cause a drop in the pressure.

Effects of Valve Characteristic Curve. Moving now to the results seen in Fig. 5-29 and 5-30, the effect obtained by changing the shape of the closure curve was examined for the multipipe closure. As before, the comparison of the results concentrated on the results for water.

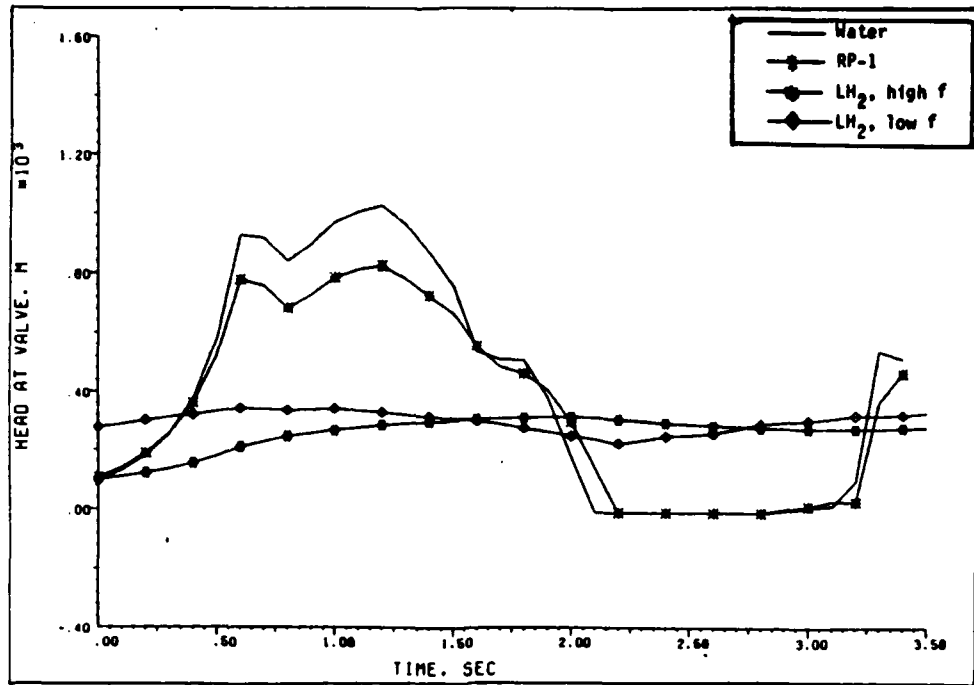


Fig. 5-29. Program results for case 4 of multipipe closure ( $L_1=351$  m,  $L_2=483$  m,  $L_3=115$  m,  $a=1200$  m/s,  $H_0=289$  m, hard closure)

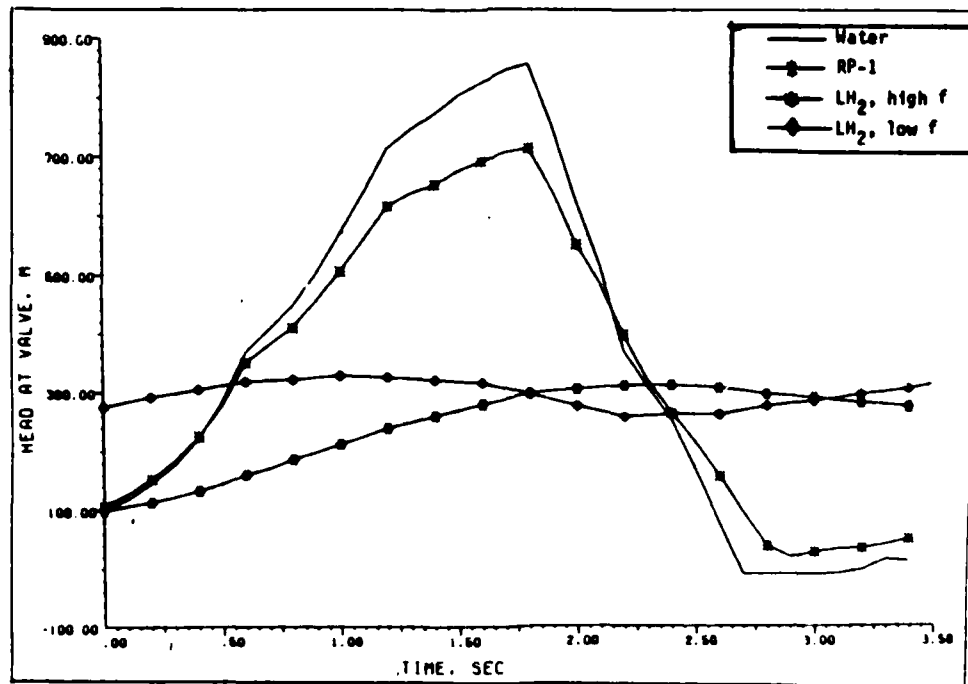


Fig. 5-30. Program results for case 5 of multipipe closure ( $L_1=351$  m,  $L_2=483$  m,  $L_3=115$  m,  $a=1200$  m/s,  $H_0=289$  m, soft closure)

Starting with the harder closure, a comparison of Fig. 5-26 and 5-29 indicated two major differences between the results for the hard closure and those for the original closure. First, since the compression waves were stronger during the more sudden closure, the first two peaks seen in the results in Fig. 5-29 were higher in magnitude than the corresponding peaks in Fig. 5-26. This result paralleled the findings of Fig. 5-4 which was a comparison of different cut-off times for the single pipe closure. And second, since the valve was completely closed 0.6 s earlier in the hard closure case, a greater pressure drop occurred after the second peak than seen in the original closure. In addition, the change in slope at the break point of the closure curve was more severe for the hard closure. Therefore, when the expansion waves of the third wave front arrived at 1.6 s, the relative strengths of the waves were such that a third peak still occurred, despite the absence of compression waves generated by the valve.

As for the soft closure case, Fig. 5-30, the changes in the slope of  $\tau$  were more gradual. During the first 0.6 s, the pressure rose in a manner similar to that seen in Fig. 5-26. At the 0.6 s point was the first change in the slope of the closure curve. Since the changes in slope were more gradual in the soft closure, the actual slope of the closure curve was much steeper than the corresponding portion of the curve in the original closure. Hence, the portion of the closure curve between 0.6 and 1.2 s was steeper than the original curve, and so, the compression waves generated at the valve were stronger for this period of time. Thus, the pressure continued to rise at a rate which was reflective of the closure curve. Finally, as in the low reservoir pressure case, the pressure peaked only after the valve completely

closed, ending the generation of new compression waves at the valve, and thereby allowing the expansion waves to finally dominate the solution.

#### Saturn V Feedline

In this final system an in-depth wave by wave description of the interactions was not included, as it would quickly become too complex to follow. Instead, a number of runs were made with only the pipes of the system in order to establish a baseline. These runs included variations on the input parameters in much the same manner as were previously incorporated in the single and multiple valve closure simulations. The results for the F-1 feedline were then analyzed by a comparison with the trends established by earlier simulations with the simpler systems. Once the baseline was determined, additional components were added and analyzed, until finally all the components were included in the final run.

Baseline Simulations. Beginning the baseline portion of the F-1 feedline analysis, the results from the first run on Table VII appear in Fig. 5-31. The shape of the curve was surprising until the system was looked at in terms of the findings of the earlier simulations. First, in comparison to the earlier simulations, the feedline was a low pressure system. Furthermore, the changes of diameter at the junctions were small compared to those in the multipipe closure. The combination of these two factors meant that any reflections from the internal junctions would be extremely weak, and hence the system would tend to act as if it was a single pipe. And second, the overall pipe length was such that the cut-off time for the valve was much greater than the oscillatory period of the system. So, the system would be expected to behave in a



manner reminiscent of the short pipe results seen in Fig. 5-6.

The expected results extrapolated from the findings of the earlier simulations agreed well with the results in Fig. 5-31. The oscillations once the valve was closed were a smooth sinusoid with a period of 0.182 s, about the same as would be observed in a single pipe having the same period as the feedline. And, as in the short pipe results for the single pipe, the pressure at the valve was dominated by the relative strengths of the compression generated by the valve and the expansion due to the reflection from the reservoir, creating the large first peak. Also, as per the description of the single pipe valve closure, the exponential law of the closure curve was reflected in the shape of the first peak, specifically, in the slope of the curve as the pressure decreased just after passing the peak magnitude. This lasted up until the time when the valve was fully closed, at which time the pressure became dominated by the reflections, significantly dropping the pressure.

For the results of the second run which appear in Fig. 5-32, the only change from the first run was that the cut-off time had been increased to 3.0 s. As was expected due to Fig. 5-4, the magnitudes of both the primary and the secondary peaks decreased as a result of the softer closure produced by an extended cut-off time. Once the valve was closed the period of the pressure oscillations was still 0.182 s. And finally, the changes in the slope of the closure curve were more gradual for the longer cut-off time. Consequently, the time was longer until the reflected expansion waves were strong enough, relative to the compression waves at the valve, to begin decelerating the flow and thereby dropping the pressure. Thus, the pressure rose gradually to a peak and then gradually decreased, as the relative strengths of the waves slowly

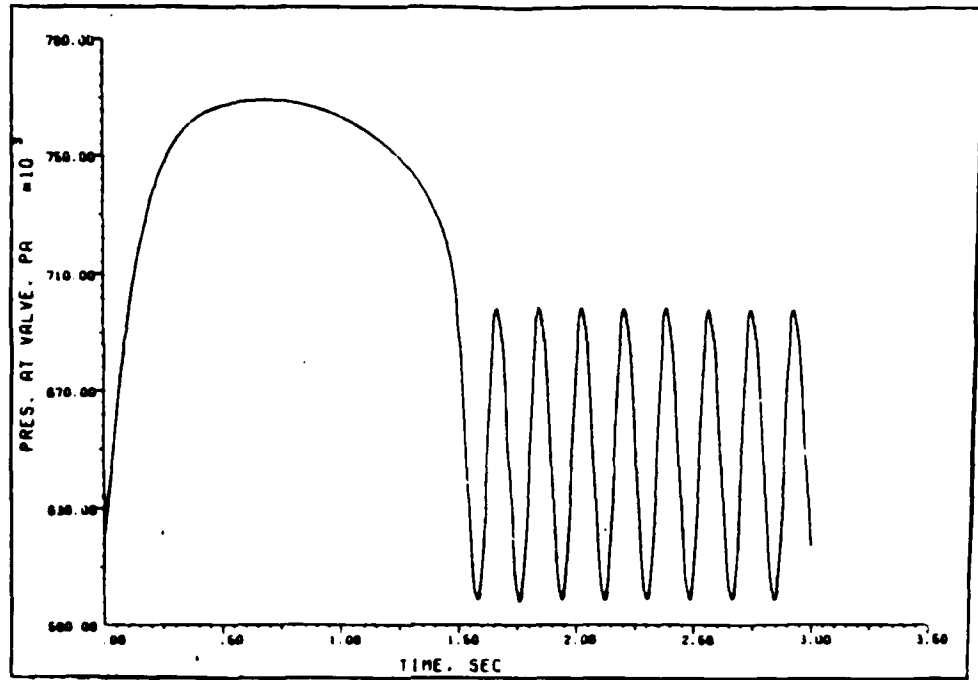


Fig. 5-31. Results of run 1 for Saturn V feedline ( $P_0=621$  kPa,  $t_c=1.5$  s,  $E_m=1.2$ )

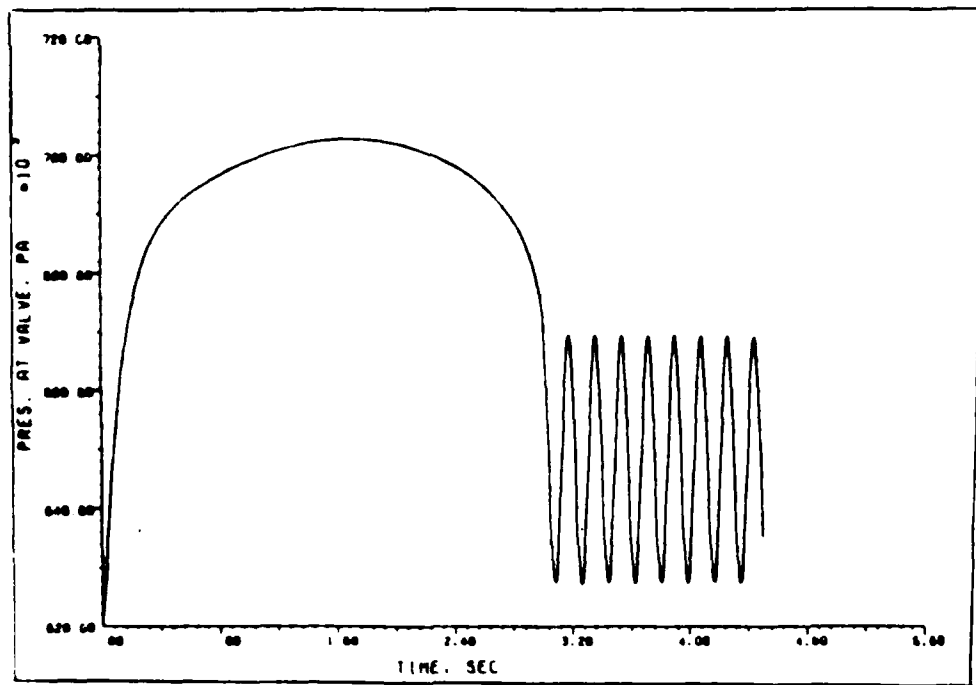


Fig. 5-32. Results of run 2 for Saturn V feedline ( $P_0=621$  kPa,  $t_c=3.0$  s,  $E_m=1.2$ )

reversed from the compression being stronger to the expansion being stronger during the first peak.

In the third run, Fig. 5-33, the cut-off time was once more 1.5 s, but  $E_m$  from Eq. (4.1) was changed to 1.0. This implied that the closure curve was now linear. Therefore, once the initial reflection returned from the reservoir, the rate of increase in pressure was reduced since the compression waves and their reflections were nearly equal in magnitude. However, because the closure curve was linear, the closure did not soften as the cut-off time approached as in the first two runs. Instead, the flow ended abruptly as indicated by the sharp drop in pressure seen in Fig. 5-33 at  $t_c=1.5$  s. Further, this sharp cut-off also affected the pressure oscillations after the valve closure. Even though the oscillations had the same period, the peak magnitudes were nearly equal to the magnitude of the initial peak. And lastly, when  $E_m$  was 1.2, Fig. 5-31, the slope of the closure curve started off steeper than the linear closure, then gradually decreased until the slope was less than that for  $E_m=1$ . Thus, when Fig. 5-31 and 5-33 are compared, the pressure in Fig. 5-31 increased quicker due to the steeper slope of the closure curve. As the first reflection arrived the pressure rise slowed in each case. However, in Fig. 5-31, the strength of the compression decreased as the slope of the closure decreased, causing the peak and gradual decline in pressure. While in Fig. 5-33, the slope did not change, so the strength of the compression remained the same. Therefore, since the reflections had been attenuated by friction, they were not as strong as the compression and the pressure continued to rise, albeit slowly. This rise continued until  $t_c=1.5$  s, when the valve closed, ending the generation of compression waves at the valve. Due to

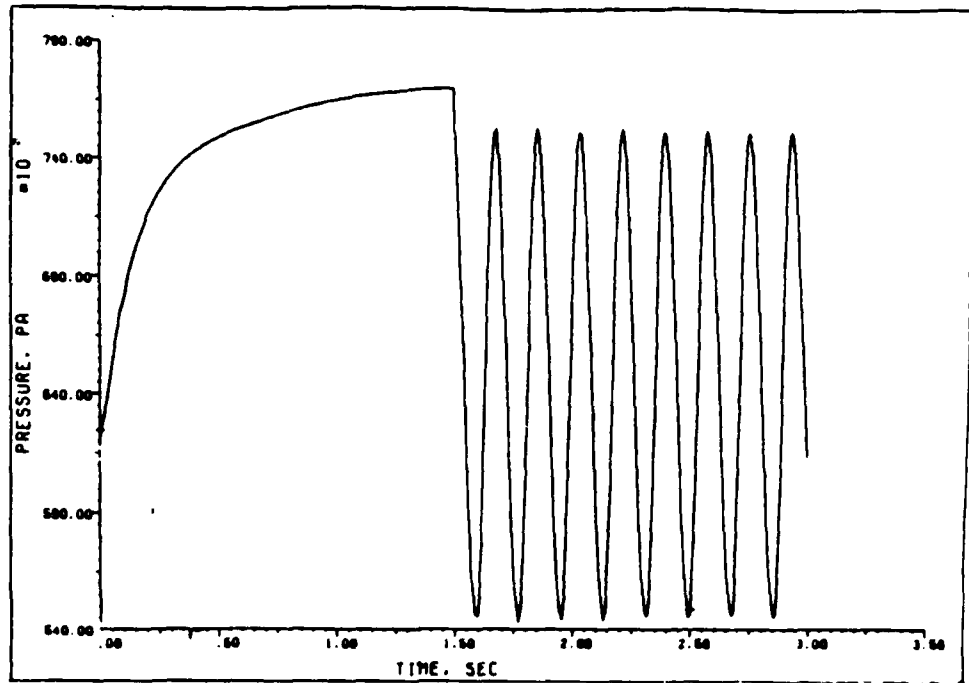


Fig. 5-33. Results of run 3 for Saturn V feedline ( $P_0=621$  kPa,  $t_c=1.5$  s,  $E_m=1.0$ )

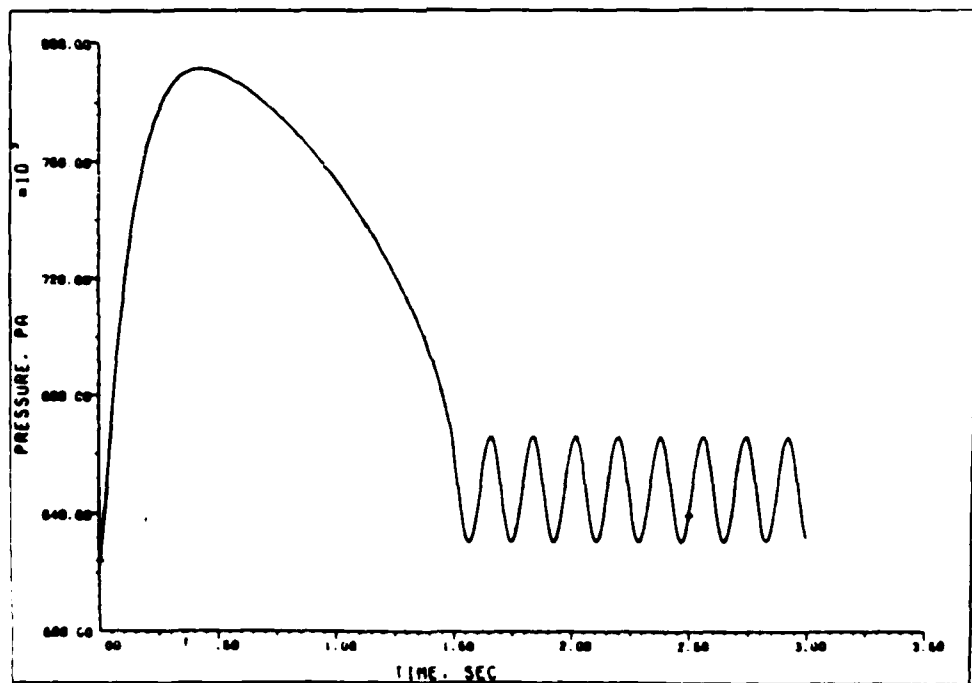


Fig. 5-34. Results of run 4 for Saturn V feedline ( $P_0=621$  kPa,  $t_c=1.5$  s,  $E_m=1.5$ )

this continual pressure rise in the results in Fig. 5-33, the peak pressure was slightly higher than that seen in the results in Fig. 5-31.

The results which appeared in Fig. 5-34 were those for run 4, where  $E_m=1.5$ . In this case the closure was initially harder, but ended softer than the closure experienced in Fig. 5-31, producing several effects. First, the slope of the initial closure was steeper than the previous runs, hence the peak pressure was higher. Second, in Fig. 5-34, due to the more radical difference in the slopes of the closure at the beginning and at the end, the relative strengths of the compression and its reflections caused the pressure to decrease more rapidly than in Fig. 5-31. And third, during the final moments of the closure, the slope of the closure curve more closely approached zero when  $E_m=1.5$  than in the earlier cases. For this reason the magnitude of the pressure oscillations was small, though the period still remained the same. This was expected due to the results seen in Fig. 5-3 and 5-6 for the single pipe. From Fig. 5-3 it was determined that the pressure rose more quickly and peaked higher as  $E_m$  increased. And, except for the fact that the cut-off time was decreased to 1.5 s, Fig. 5-34 could almost be one of the curves in Fig. 5-6, the results agree that well.

Run 5 was the last of the baseline cases. For this case the inputs had been returned to the original values, except for the initial valve pressure, which was increased by 40 psi,  $2.76 \times 10^5$  Pa in metric units. The results, which appear in Fig. 5-35, were almost an exact duplicate of those in Fig. 5-31. The only observable differences were the increases in magnitude of the primary and secondary peak pressures. The shape of the first peak and the frequency of the pressure oscillations in Fig. 5-35 remained the same as in Fig. 5-31.

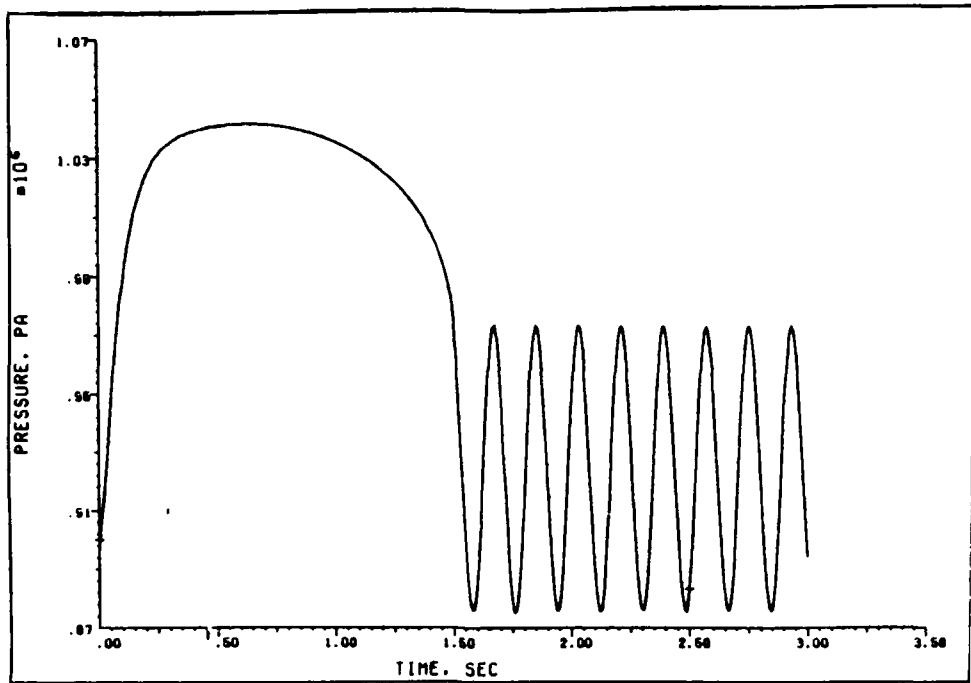


Fig. 5-35. Results of run 5 for Saturn V feedline ( $P_0=896$  kPa,  $t_c=1.5$  s,  $E_m=1.2$ )

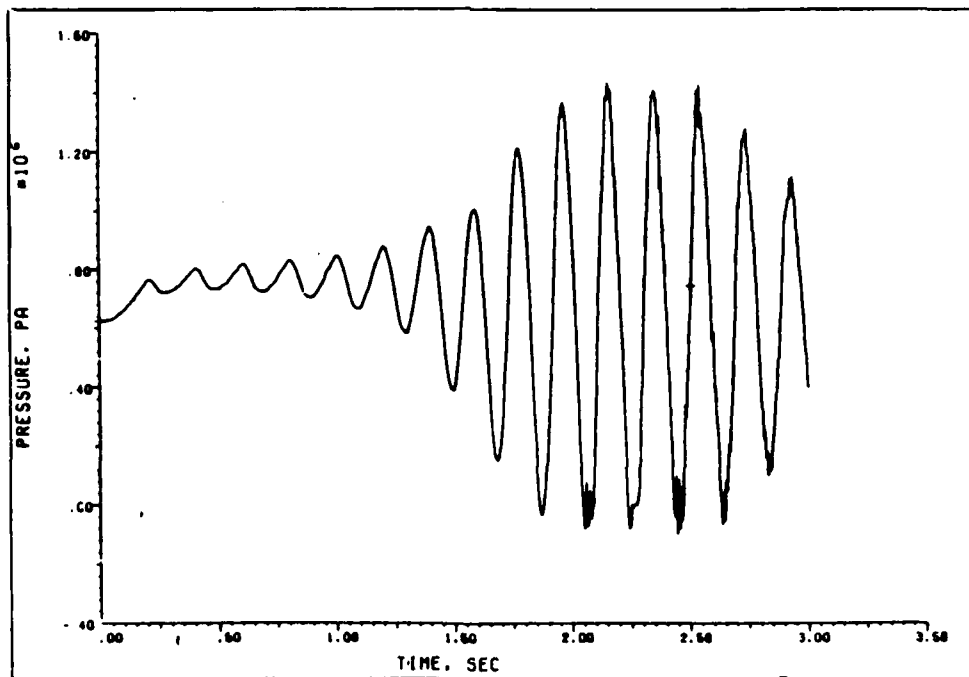


Fig. 5-36. Results of run 6 for Saturn V feedline ( $P_0=621$  kPa,  $t_c=1.5$  s,  $E_m=1.2$ ,  $\omega=2.5$  Hz)

Pulser Valve Simulations. The next six runs began the inclusion of other components into the simulations. For these runs a pulser valve was included, operating at frequencies of 2.5, 10, and 25 Hz. The first and third frequencies were chosen to test the frequency response of the models in use, the frequencies were arbitrarily chosen near two resonant frequencies reported for this system by Dehoff (2). The last frequency was chosen as a control to provide a median value which was not identified as a resonant frequency.

The results for the first of these runs appeared in Fig. 5-36. In this run the frequency of the pulser was 2.5 Hz. The results seem to indicate a resonant condition due to the large oscillations that built up and finally masked the expected response. It should be noted, that due to the choice of the function to represent the flow out of the pulser valve, Eq. (4.5), the frequency of the sinusoid was effectively doubled due to the absolute value being used. Hence, the frequency of 2.5 Hz became 5 Hz for all practical purposes, and very nearly the natural frequency observed in the previous runs. Thus, the system was near resonance, and the magnitude of the pressure oscillations became so large that the system began to reach vapor pressure. Consequently, as with the cavitation simulations, pressure spikes were introduced into the solution. More important though, the oscillations remained bounded and finally decreased because the gas released by the column separation changed the effective wave speed, thereby changing the natural frequency of the pipeline.

When the frequency of the pulser was increased to 10 Hz as in Fig. 5-37, the results were not as dramatic as those seen in Fig. 5-36. In this case the results resembled Fig. 5-31 with a small magnitude

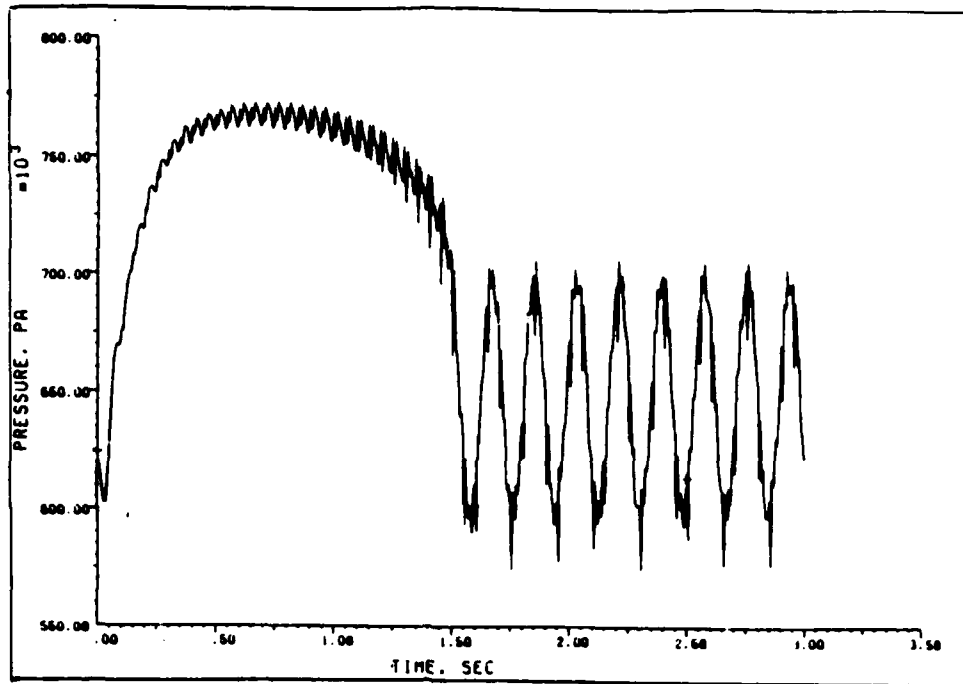


Fig. 5-37. Results of run 7 for Saturn V feedline ( $P_0=621$  kPa,  $t_c=1.5$  s,  $E_m=1.2$ ,  $\omega=10$  Hz)

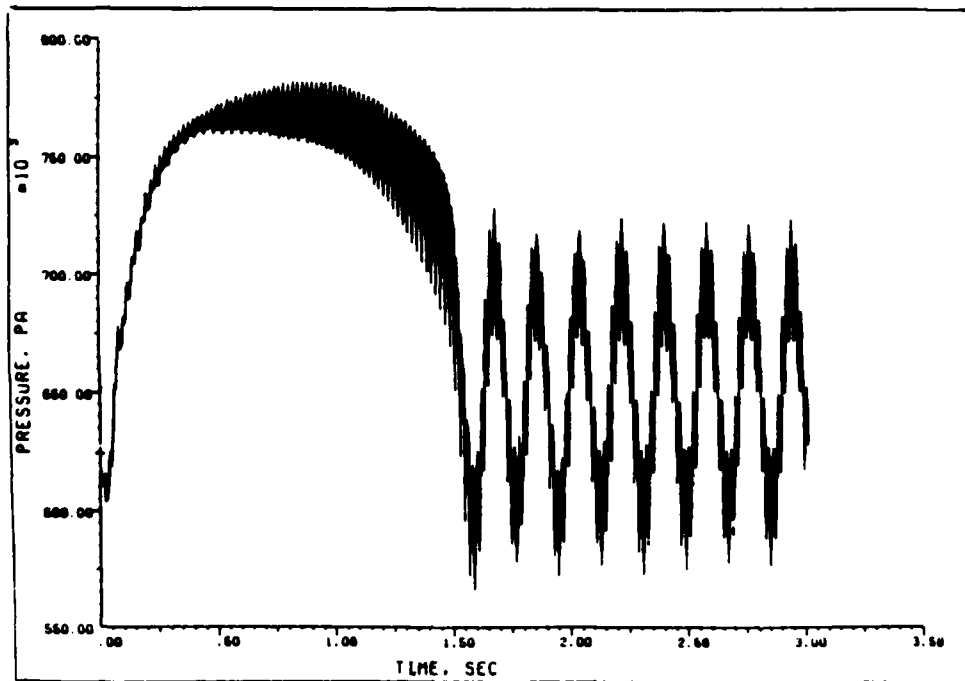


Fig. 5-38. Results of run 8 for Saturn V feedline ( $P_0=621$  kPa,  $t_c=1.5$  s,  $E_m=1.2$ ,  $\omega=25$  Hz)



oscillation superimposed on top of them. At this frequency the oscillations at the valve started small and built up to a magnitude that was only a fraction of the magnitude of the oscillations following the valve closure. Increasing the frequency further to 25 Hz produced the results seen in Fig. 5-38. Once again, the oscillations were simply superimposed over the results of Fig. 5-31. The pulser's effective frequency of 50 Hz was nearly a harmonic. This was indicated in the results by the magnitude of the oscillations growing more quickly and to a larger value than those seen in Fig. 5-37.

The last three runs of this set examined the effect of changes in some of the system parameters while the pulser was present. In run 9,  $E_m$  was changed to 1.0 to see if a change in the closure curve affected the resonance condition exhibited in Fig. 5-36. As seen by the results in Fig. 5-39, the change had no significant impact. Jumping from the case with the largest oscillations to the one with the smallest, for run 10, run 7 was repeated with the initial valve pressure increased to 130 psi which is  $8.96 \times 10^5$  Pa. Examining the results of run 10 in Fig. 5-40, the curve was little more than a translation in the y-direction of Fig. 5-37. However, as seen by Fig. 5-41, when the system pressure was increased while keeping  $E_m=1.0$ , the resonant condition was not as dominant. While still very sizable, in this case the pressure oscillations after the valve closed were out of phase with the oscillations due to the pulser. Hence, the erratic pressure response after the valve was fully closed.

Accumulators and Cavitation Simulations. The next six runs incorporated the other system components, the "pump inlet cavitation" and the prevalue accumulator. Run 12 started things off with cavitation only.

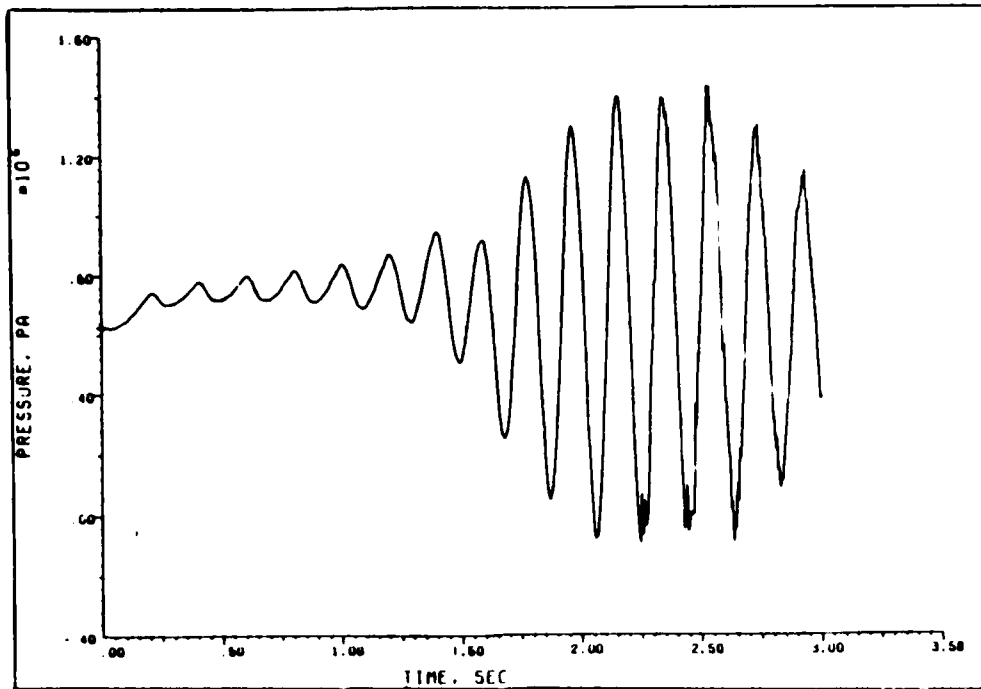


Fig. 5-39. Results of run 9 for Saturn V feedline ( $P_0=621$  kPa,  $t_c=1.5$  s,  $E_m=1.0$ ,  $\omega=2.5$  Hz)

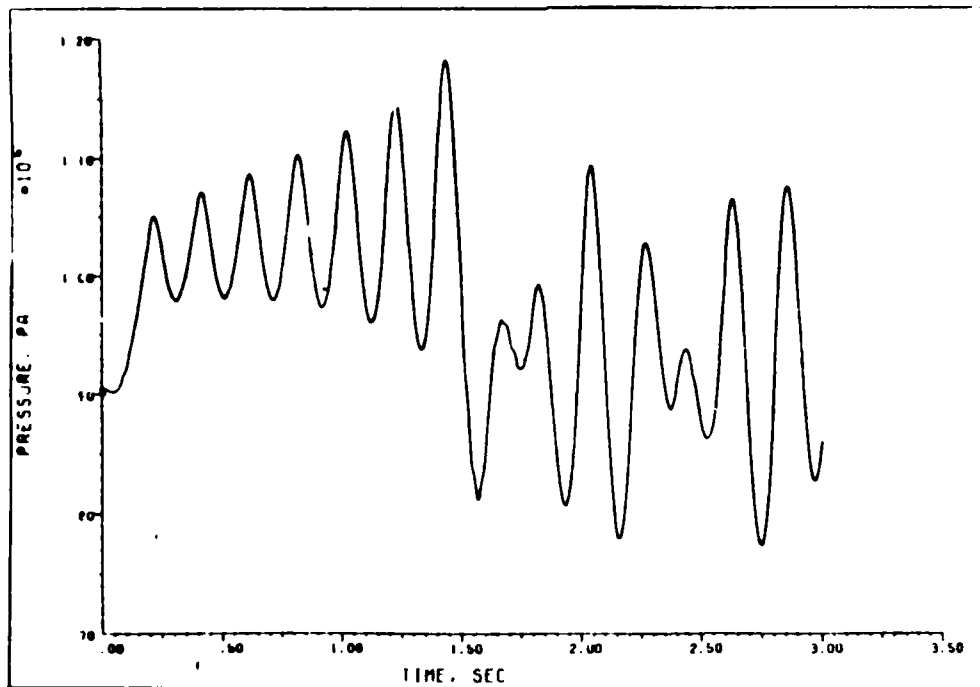


Fig. 5-40. Results of run 10 for Saturn V feedline ( $P_0=896$  kPa,  $t_c=1.5$  s,  $E_m=1.2$ ,  $\omega=2.5$  Hz)

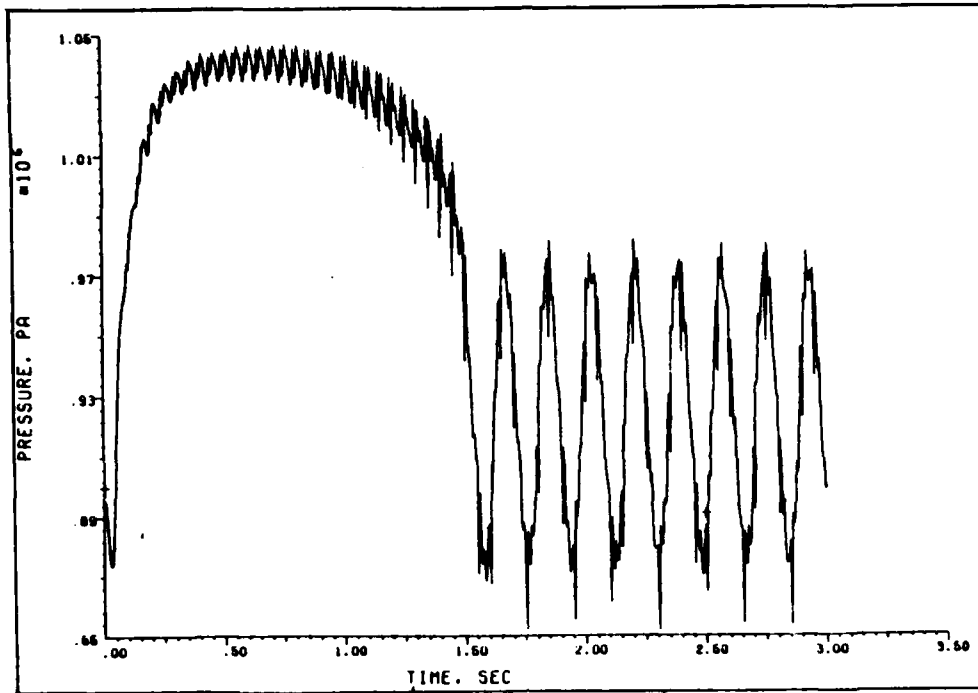


Fig. 5-41. Results of run 11 for Saturn V feedline ( $P_0=896$  kPa,  $t_c=1.5$  s,  $E_m=1.0$ ,  $\omega=10$  Hz)

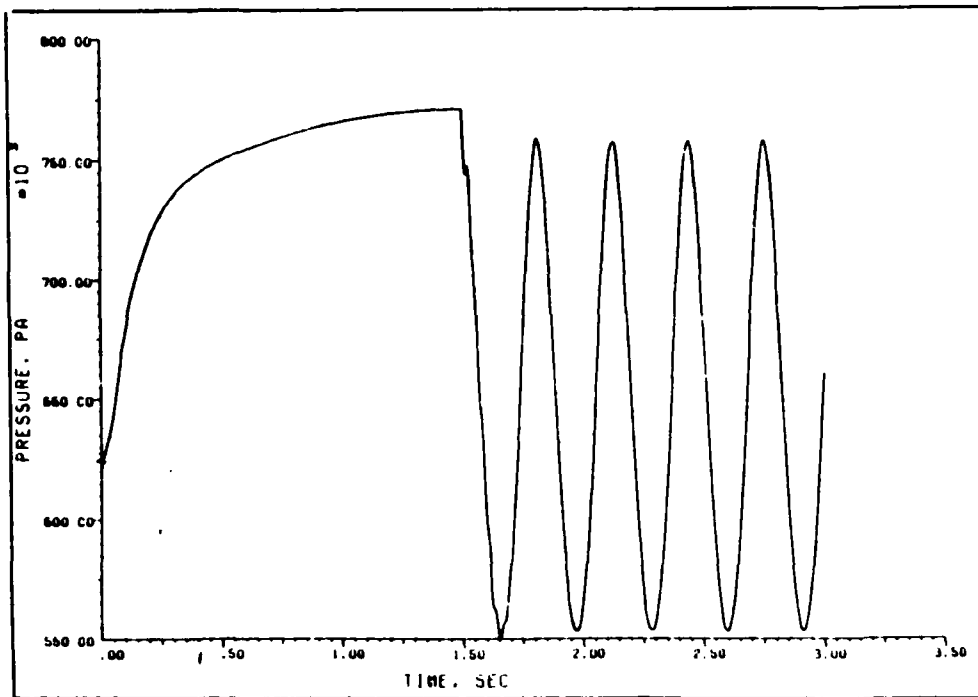


Fig. 5-42. Results of run 12 for Saturn V feedline ( $P_0=621$  kPa,  $t_c=1.5$  s,  $E_m=1.0$ ,  $vol.=0.0$  m<sup>3</sup>)

Upon comparison of the run 12 results, Fig. 5-42, with the results in Fig. 5-33, one major change could be noted. Once the valve was closed, the results in Fig. 5-42 showed a decrease in the frequency from 5.5 Hz to 3.2 Hz. This decrease in frequency was to be expected however. In run 12 there was now vapor present in the form of the turbopump inlet cavitation which produced a reduction of the effective wave speed in that region, thereby increasing the travel time of the waves.

In runs 13, 14, and 15 the cavitation was still present, however, the pre valve accumulator had been included with volumes as seen in Table VII. Comparing Fig. 5-42 with Figs. 5-43, 5-44, and 5-45 delineated several trends. The most notable trend was the increase in the period of the pressure oscillations as the gas volume in the accumulator increased. Also, the strength of the reflections from an internal boundary condition increased with increasing gas volume. This aspect was best demonstrated by the increase in the rippling of the pressure trace as the accumulator gas volume increased. And finally, there was no significant decrease in the peak magnitudes as the accumulator volume increased. Taken together, these trends indicated a problem in the modeling of an accumulator. Instead of acting as a surge suppressor, the model developed for this study acted in a manner very similar to a vapor cavity in the discrete bubble model of cavitation.

This supposition concerning the accumulator model was further demonstrated by the results of runs 16 and 17. In run 16 the initial valve pressure was again increased to 896 kPa. In comparison to the results in Fig. 5-42 the results were as expected. The pressure trace was essentially the same curve translated in the y-direction. The frequency of the pressure oscillations even stayed the same. However, com-

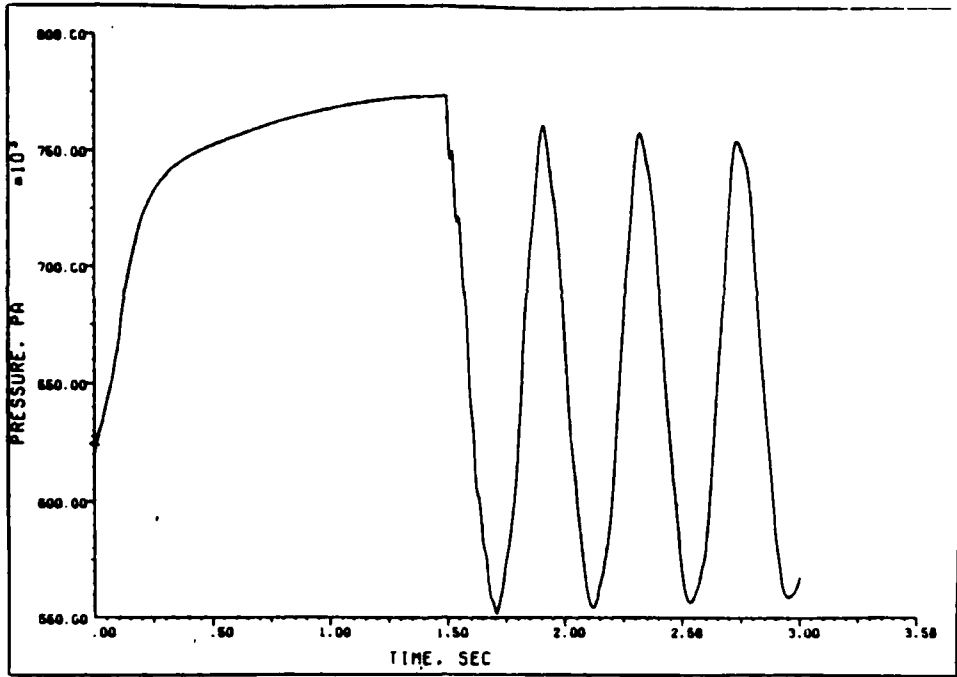


Fig. 5-43. Results of run 13 for Saturn V feedline ( $P_0=621$  kPa,  $t_c=1.5$  s,  $E_m=1.0$ , vol.= $0.018$  m<sup>3</sup>)

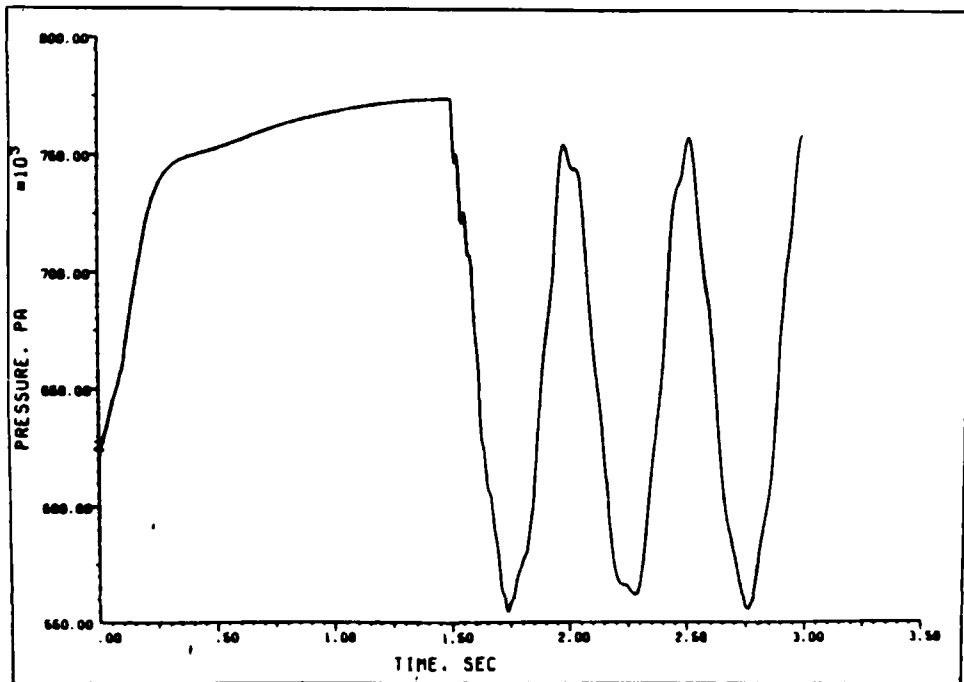


Fig. 5-44. Results of run 14 for Saturn V feedline ( $P_0=621$  kPa,  $t_c=1.5$  s,  $E_m=1.0$ , vol.= $0.036$  m<sup>3</sup>)

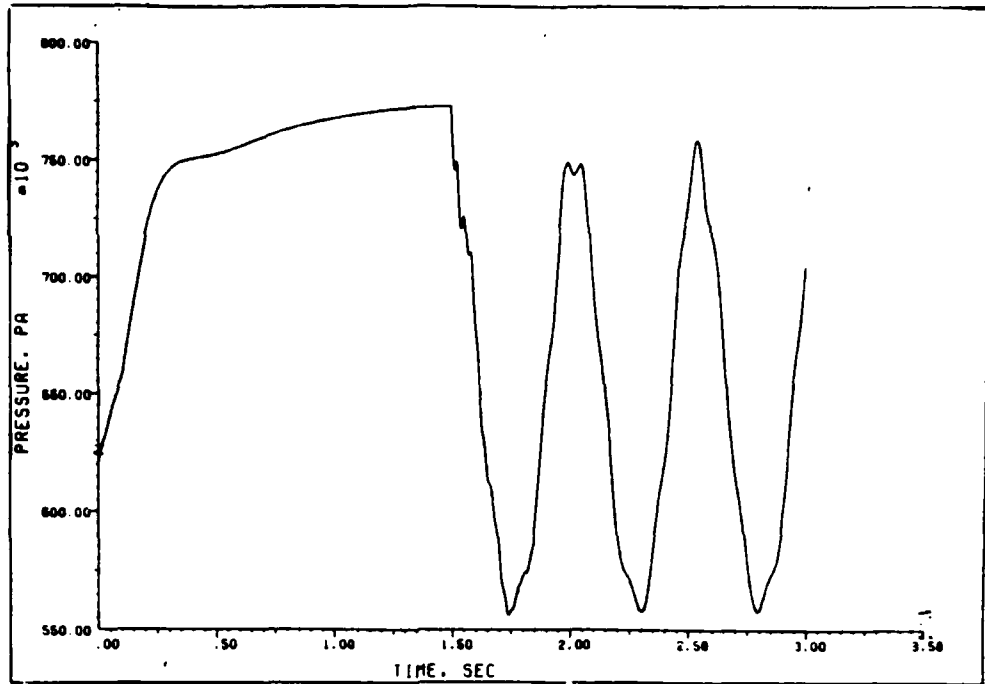


Fig. 5-45. Results of run 15 for Saturn V feedline ( $P_0=621$  kPa,  $t_c=1.5$  s,  $E_m=1.0$ , vol.= $0.054$  m<sup>3</sup>)

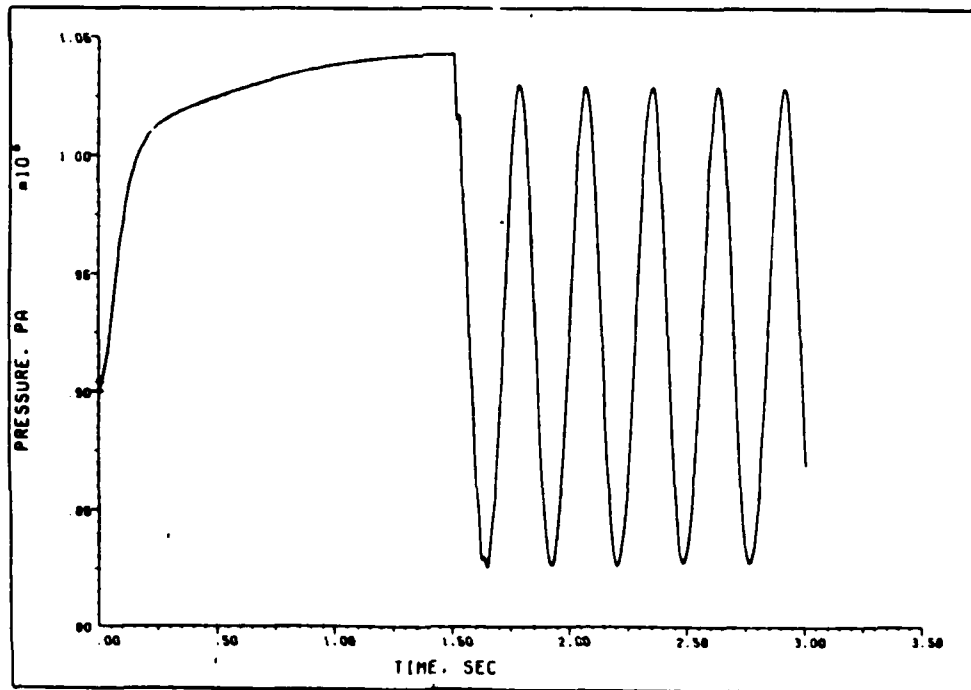


Fig. 5-46. Results of run 16 for Saturn V feedline ( $P_0=896$  kPa,  $t_c=1.5$  s,  $E_m=1.0$ , vol.= $0.0$  m<sup>3</sup>)

paring between the results of run 16 in Fig. 5-46 and those of run 17 in Fig. 5-47, the period of the oscillation increased significantly when the accumulator with an initial volume of  $0.054 \text{ m}^3$  was included. Furthermore, the existence of relatively strong internal reflections was once again readily apparent. And, there was still no surge suppression demonstrated by the accumulator model. Thus, when all the components were included for run 18, the massive pressure oscillations seen in Figs. 5-36 and 5-39 were not eliminated from the results seen in Fig. 5-48 by surge suppression. Rather, the inclusion of the accumulator suppressed the surges by changing the natural frequency of the system such that pressure oscillations caused by the pulser took longer to build up to the larger magnitudes.

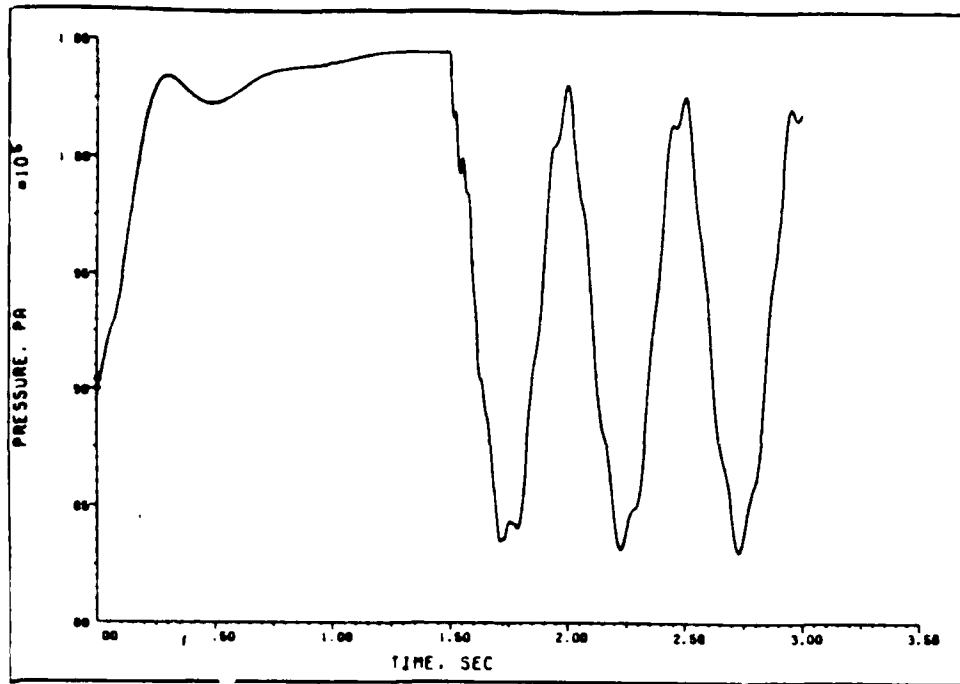


Fig. 5-47. Results of run 17 for Saturn V feedline ( $P_0=896$  kPa,  $t_c=1.5$  s,  $E_m=1.0$ , vol.= $0.054$  m<sup>3</sup>)

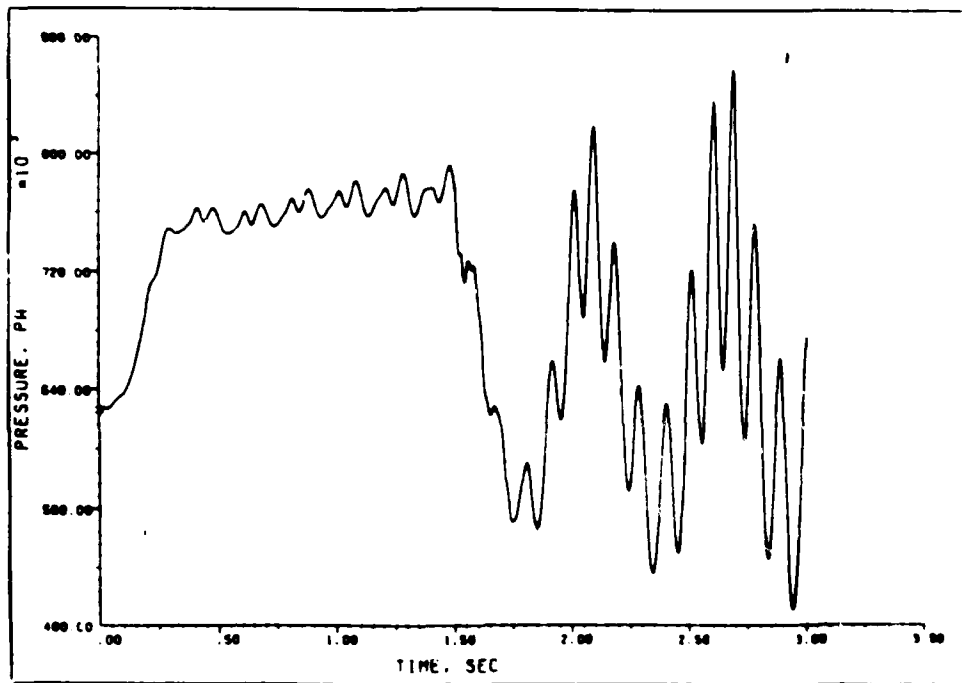


Fig. 5-48. Results of run 18 for Saturn V feedline ( $P_0=621$  kPa,  $t_c=1.5$  s,  $E_m=1.0$ ,  $\omega=2.5$  Hz, vol.= $0.054$  m<sup>3</sup>)



## VI. Conclusions

In this study a simple but flexible computer program was developed and used to analyze fluid transients in pipelines. The derivation of the equations of motion used in the numerical analysis was based on the method of characteristics. Boundary conditions were obtained from either published sources or developed mathematically to allow for conditions which commonly occur in propellant feedline systems.

The results of the program were quite good when compared against published data. Further, a number of trends were observed in the results:

- 1) The integration method, the inclusion of air release, and the size of the time step all affected the numerical stability of the discrete bubble method.
- 2) The valve characteristic,  $\tau$ , the cut-off time, the friction factor, and the pipe length strongly influenced the peak magnitude of the pressure transient.
- 3) The density strongly influenced the peak magnitude of the transient pressure through inertial effects. And
- 4) The pressure of the system affected the strength of the reflections from the internal boundary conditions.

It is recommended that a new accumulator model be found or created to replace the one currently included in this study. Also, even though the results obtained through the use of this program were good, there is still room for additional improvements in the modeling and procedures. One specific area that might be improved is that section of the code which provides the initial solution for the numerical analysis.

## Bibliography

1. Wood, Don J. et al. Digital Distributed Parameter Model for Analysis of Unsteady Flow in Liquid-filled Lines. NASA TN D-2812. National Aeronautics and Space Administration, Washington, D. C., 1965.
2. Dehoff, Capt. Bryan S. Application of the Hydraulic System Frequency Response Program to Propellant Feedline Systems. MS Thesis. School of Engineering, Air Force Institute of Technology, Wright-Patterson AFB, OH, December 1984.
3. Rosenberg, 2Lt David A. A Closed Loop Analysis of Pogo Instability. MS Thesis. School of Engineering, Air Force Institute of Technology, Wright-Patterson AFB, OH, December 1984.
4. Rubin, Sheldon. "Longitudinal Instability of Liquid Rockets Due to Propulsion Feedback (POGO)", Journal of Spacecraft and Rockets, 3: 1188-1195 (August 1966).
5. Ryan, R. S. et al. "Simulation of Saturn V S-II Stage Propellant Feedline Dynamics", Journal of Spacecraft and Rockets, 7: 1407-1412 (December 1970).
6. Johnson, R. W. Longitudinal Propulsion Coupling System, Volume 2: Digital Computer Solution to Equations of Motion. NASA-CR-103101. Martin Marietta Corp., March 1971 (N71-23666).
7. Holster, J. L. and J. Astleford. "Analytical Model for Liquid Propellant Feedline Dynamics", Journal of Spacecraft and Rockets, 11: 180-187 (March 1974).
8. D'Souza, A. F. and R. Oldenberger. "Dynamic Response of Fluid Lines", Journal of Basic Engineering, Trans. ASME, 87: 589-598 (September 1964).
9. Woods, W. A. "Method of Calculating Liquid Flow Fluctuations in Rocket Motor Supply Pipes", Journal of American Rocket Scientists, 31: 1560-1567 (November 1961).
10. Dorsch, Robert G. et al. Distributed Parameter Analysis of Pressure and Flow Disturbances in Rocket Propellant Feed Systems. NASA TN D-3529. National Aeronautics and Space Administration, Washington, D. C., August 1966.
11. Fashbaugh, R. H. and V. L. Streeter. "Resonance in Liquid Rocket Engine Systems", Journal of Basic Engineering, 87D: 1011-1017 (December 1965).
12. DeGarcia, H. et al. Advanced Fluid System Simulation. Final Report AFWAL-TR-80-2039. Aero Propulsion Laboratory, Wright-Patterson AFB, OH, April 1980.

13. Swaffield, J. A. "A Study of the Influence of Air Release on Column Separation in an Aviation Kerosene", Proceedings of the Institute of Mechanical Engineers, 186: 693-703 (1972).
14. Wylie, E. B. and V. L. Streeter. Fluid Transients. New York: McGraw-Hill Book Company, 1978.
15. Watters, Gary Z. Analysis and Control of Unsteady Flow in Pipelines (Second Edition). Boston, MA: Butterworth Publishers, 1984.
16. Thorley, A. R. D. "Complex Systems: Common Boundary Conditions for Unsteady Liquid Flow", Unsteady 1-D Flows in Complex Networks and Pressurized Vessels. 9.1-15. Von Karman Institute for Fluid Dynamics, 1980.
17. Wylie, E. B. "Simulation of Vaporous and Gaseous Cavitation", Applied Mechanics, Bioengineering, and Fluids Engineering Conference. 47-52. ASME, New York, 1983.
18. Brod, E. J. et al. LOX Suction Duct Dynamic Evaluation, D13339, Summary of Test Results. The Boeing Company Report D5-14061, May 1970.
19. Simpson, A. R. and E. B. Wylie. "Problems Encountered in Modeling Vapor Column Separation", Proceedings of 1985 ASME Winter Meeting. 103-107. ASME, New York, 1985.
20. Tullis, J. P. et al. "Waterhammer Analysis with Air Release", BHRA 2nd International Conference on Pressure Surges. C3.35-47. BHRA Fluid Engineering, Cranfield, Bedford, England, 1976.
21. Streeter, V. L. "Unsteady Flow Calculations by Numerical Methods", Journal of Basic Engineering, 105: 457 (June 1972).
22. Streeter, V. L. and E. B. Wylie. Hydraulic Transients. New York: McGraw-Hill Book Company, 1967.
23. Lawler, W. H. Shuttle POGO Stability Program, Volume 1: Theory Manual. NASA-CR-135721. Boeing Co., Huntsville, Ala. September 1973.

## Appendix A. A User's Guide

### Computational Requirements

The program developed during this investigation was written in FORTRAN 77 and implemented on the ASD CDC-Cyber mainframe computer. The routine which is detailed later in this Appendix did not require a great deal of computational power. In the case of the single pipe models, run times averaged up to 20 CPU's. The Saturn V model usually required around 200 CPU's due to the small time step required to achieve an integer number of reaches in the very short pipes.

### Program Explanation

Fig. A-1 is a general flow diagram of the routine developed in this study. The program begins by dimensioning all of the arrays that are found in the program. Since FORTRAN cannot dimension arrays after reading in any data, the user must be sure the arrays are large enough at the start. The next part of the program is the reading of the input data. The user must pay close attention to the sequence of Read statements in this program (see program listing). The first three Read statements are used only once, the remaining three Reads are repeated within separate loops. Thus, the input deck must contain sufficient data to satisfy the full range of any one Read statement for the length of its loop before trying to input data for the next Read.

After all the data has been input, if the wave speed has been set to zero, the program will then calculate a value by Eq. (4.2). Once the wave speed is known each pipe must be subdivided into reaches for computational purposes. The routine the program uses to make this calculation is taken from Wylie and Streeter (14:45). In each pipe of the

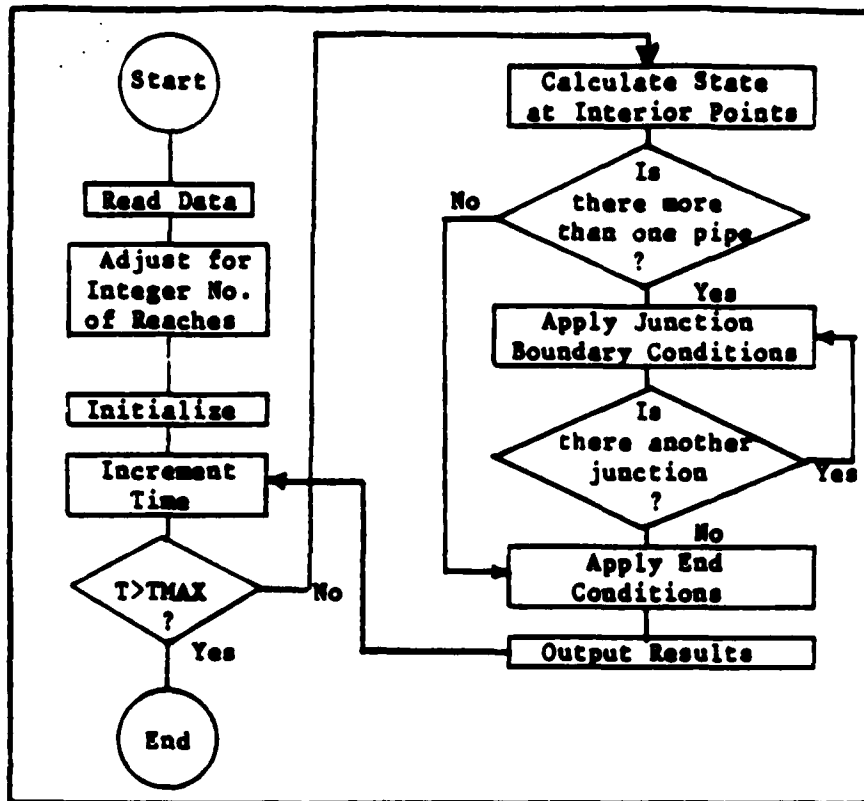


Fig. A-1. Program Flow Chart

system it is required that

$$\Delta t = L/aN \quad (A.1)$$

in which  $N$  is an integer. However, for computational purposes the time step must remain constant for all the pipes in the system. Wylie and Streeter argued that the wave speed does not need to be known exactly, thus may be adjusted slightly to arrive at an integer number of reaches in every pipe. In equation form

$$\Delta t = L/a(1+c)N \quad (A.2)$$

where  $c$  is a constant equal to the permissible variation in the wave speed, which is always less than 0.15.

With the pipes now subdivided for computation, the finite difference routine needs an initial condition from which to start. In this

program the steady state pressure at either the upstream or the downstream end must be known. If the upstream pressure is input, the program will then use the steady state form of the finite difference equations to relate the upstream pressure to the pressure at any point in the flow. However, if the downstream pressure is input, the program must first work backwards through the steady state solution to find the pressure at the upstream end. Once the pressure is known at the upstream end, the pressure may be calculated at any point as before. In the program listing the loop to work backwards through the solution is DO 22 etc., so the user must be careful to eliminate this loop if the upstream pressure is input as an initial condition.

Once the program has the initial condition from which to start, the transient loop begins. The first part of this loop is the calculation of the pressure and the volume flow rate at all the interior points of the pipes. After the values at the interior points have been calculated, a loop to apply the boundary conditions to any internal junctions begins. First, the flag, M, is checked to see if there is more than one pipe. As shown in Fig. A-1, if there is only one pipe the program skips down to the exterior boundary conditions. However, if there is more than one pipe, the various flags are then checked to determine which of the boundary conditions exist at that particular junction. If no other boundary condition is specified the default boundary condition is a series connection.

The last section of the program before the next time increment begins is the exterior boundary conditions of the system being analyzed. These boundary conditions are not actually exterior to the pipe system, simply the conditions at the upstream end of the first pipe and the

downstream end of the last one. The user must make sure the correct end conditions are being used since a number of different end conditions have been left in the program as Comment statements.

#### Program Variables

A	wave speed
AR	pipe area
B, FF, R	pipeline constants, Eq. (2.20) and (2.21)
B0, B1, B2, B3	pump constants, Eq. (B.8)
CM, CP	constants from Eq. (2.18) and (2.19)
CM1	CM for pipe 2 of a branch
CV	constant from Eq. (3.6) and (3.8)
CVP	initial value of CV
D	pipe diameter
DP	pressure rise due to pump
DPPO, PPO	pump constants
DT	time step
E	Young's modulus
EM	exponent from Eq. (4.1)
F	friction factor
G	gravitational acceleration
I	counter to indicate which reach within a pipe
ICAV	indicator for the existence of cavitation bubbles
IPR	constant governing amount of output
J	counter to indicate which pipe
JMAX, IMAX	location of maximum pressure
J2	counter for branches

K	counter used with IPR
KL	bulk modulus
L, LB	flags for branches (see top of program listing)
M	number of pipes in main line
MB	M + NB
N	number of reaches in a pipe
NA	accumulator flag
NB	number of branches
NP	pump flag
NPLS	pulser flag
NS	last computation point in a pipe
NTA	number of points if TAU is not exponential
NV	valve flag
OLDCM, OLDCP	CM and CP from previous time step
P	pressure from previous times step
PAO	initial pressure of an accumulator
PB	barometric pressure
PMAX	maximum pressure
PO	initial pressure
POR	initial pressure at the upstream end
PP	pressure for current time increment
PSI	adjustment factor for wave speed
PV	vapor pressure
Q	volume flow rate at previous time step
QP	volume flow rate at current time increment
QPO	initial volume flow rate of a pump
QPU, QU	volume flow rate on upstream side of computing location



QV	volume flow rate through pulser valve
RHO	density
T	time
TAU	closure characteristic, Eq. (3.5)
TC	cut-off time for valve at end of the system
TCUT	cut-off time for internal valve
TH	interpolation factor for nonexponential TAU
TMAX	time limit
TMX	time of maximum pressure
TOL	tolerance for accumulator iteration
TT	pipe wall thickness
TX	exponent of Eq. (4.1) for valve at end of system
VAO	initial volume of accumulator
VCAV	volume of a vapor cavity
W	frequency of pulser valve
XL	pipe length
ZETA	interpolation factor from Eq. (2.24)



```

      IF (N(J).EQ.0) GOTO 16
      A(J)=XL(J)/(N(J)*DT)
15     NS(J)=N(J)+1
      WRITE(8,8)'J= ',J,' SECTIONS= ',NS(J)
16     IF (N(J).EQ.0) THEN
          WRITE(8,8)'DT TOO BIG FOR PIPE ',J
          GOTO 99
      ENDIF

```

```

C
C
C     CALCULATION OF SYSTEM CONSTANTS

```

```

      AR(J)=.7854*D(J)**2
      RL(J)=XL(J)/N(J)
      V(J)=RL(J)*AR(J)
      POST=PO+PB
      C1(J)=POST*AO*V(J)
      ZETA(J)=N(J)*DT*SA(J)/XL(J)
      B(J)=AR(J)/(RHO*SA(J))
      R(J)=G*AR(J)*DT*SIN(ALPH(J))
      FF(J)=F(J)*DT/(D(J)*AR(J)**2)
      NN=NS(J)
      DO 20 I=1,NN
          VCAV(J,I)=0.
          ICAV(J,I)=0
20     CONTINUE
      DO 22 J=1,M
          POR=POR+FF(J)*N(J)*SO*PO**2/B(J)
22     CONTINUE
      WRITE(6,8)G,POR,PO,GO,DT,THAX,IPR

```

```

C
C
C     INITIAL CONDITIONS

```

```

      P(1,1)=POR
      PRINT 8,P(1,1)
      DO 25 J=1,MB
          NN=NS(J)
          IF (J.GT.1) THEN
              P(J,1)=P(J-1,NS(J-1))
              IF (NV(J).EQ.1) THEN
                  P(J,1)=.998*P(J,1)
              ENDIF
          ENDIF
          IF (NA(J).EQ.1) THEN
              PAO(J)=P(J,1)
          ENDIF
          DO 25 I=1,NN
              Q(J,I)=QPO
              QU(J,I)=QPO
              OQ(J,I)=QPO
              OQU(J,I)=QPO
              IF (J.EQ.NP.AND.I.EQ.1) THEN
                  CALL DELP(J,A,Q,P,NS,DP)
                  P(J,1)=P(J-1,NS(J-1))+DP
              ENDIF
              P(J,I)=P(J,1)-(I-1)*FF(J)*Q(J,I)**2/B(J)

```

```

25  CONTINUE
    M1=M+1
    IF (MB.NE.M) THEN
    DO 30 J=1,MB
      P(J,1)=P(LB(J),NS(LB(J)))
      NN=NS(J)
      DO 30 I=1,NN
        Q(J,I)=0.
        QU(J,I)=0.
        P(J,I)=P(J,1)
30  CONTINUE
    ENDIF
    TAU(M,2)=TA(1)
    CVP(M,2)=QPOS*2/(2*P(M,NS(M)))
    T=0
    K=0
    DO 35 J=1,MB
      CVP(J,1)=QPOS*2/(0.01*P(J,1))
      WRITE(6,8)J,A(J),F(J),ZETA(J)
35  CONTINUE
    WRITE(6,8)'DESIG= ',DESIG
40  WRITE(6,8)T,P(M,NS(M)),P(14,1),P(8,1),Q(1,1),P(1,1)
    C  WRITE(6,8)'MAX AT ',TMX,JMAX,IMAX,PMAX
    DO 45 J=1,MB
    C  WRITE(6,8)'J= ',J,P(J,1),Q(J,1),P(J,NS(J)),Q(J,NS(J))
    C  WRITE(6,8)Q(J,1),Q(J,NS(J))
    C  WRITE(6,8)'J= ',J,(P(J,I),I=1,NS(J))
    C  WRITE(6,8)(Q(J,I),I=1,NS(J))
    C  WRITE(6,8)
45  CONTINUE
    C
    C  TRANSIENT LOOP
    C
50  T=T+DT
    IF (T.GT.TMAX) GOTO 99
    K=K+1
    C
    C  INTERIOR POINTS
    C
    DO 61 J=1,MB
      IF (T.GE.TCUT(J)) GOTO 51
      TAU(J,1)=(1-T/TCUT(J))*EM(J)
      GOTO 52
51  TAU(J,1)=0.
52  CV(J,1)=CVP(J,1)*TAU(J,1)**2
      NN=N(J)
      IF (NN.EQ.1) GOTO 61
      DO 60 I=2,NN
        CALL FCH(I,J,Q,QU,P,B,R,FF,ZETA,CH)
        CALL FCP(I,J,Q,QU,P,B,R,FF,ZETA,CP)
        IF (ICAV(J,I).EQ.1)GOTO 55
        QP(J,I)=(CP+CH)/2
        PP(J,I)=(CP-QP(J,I))/B(J)
        IF (PP(J,I)+PB.LT.PV) GOTO 55
      GOTO 59

```

```

55      CONTINUE
C      WRITE(*,*) 'CAVITATION IN SECTION ',I,' OF PIPE ',J
      BI=(PHI*(CH-CP)*VCAV(J,I)/(2*DT)+(1-PHI)*(OQ(J,I)
*      -OQU(J,I)))/(PHI*B(J))
      C4=C1(J)/(2*DT*PHI*B(J))
      PP(J,I)=(-BI+2*(PV-PB)+SQRT((BI+2*(PV-PB))*2+8*C4))/4
C      PP(J,I)=-PB+PV
      ICAV(J,I)=1
57      QPU(J,I)=CP-PP(J,I)*B(J)
      QP(J,I)=CH+PP(J,I)*B(J)
C      VCAV(J,I)=VCAV(J,I)+DT*(PHI*(QP(J,I)-QPU(J,I))
C      *      +(1-PHI)*(Q(J,I)-OQ(J,I)))
      *      VCAV(J,I)=VCAV(J,I)+2*DT*(PHI*(QP(J,I)-QPU(J,I))
      *      +(1-PHI)*(OQ(J,I)-OQU(J,I)))
      IF (VCAV(J,I).GT.0.) GOTO 60
      ICAV(J,I)=0
      VCAV(J,I)=0.
      QP(J,I)=(CP+CH)/2
59      PP(J,I)=(CP-QP(J,I))/B(J)
      QPU(J,I)=QP(J,I)
60      CONTINUE
61      CONTINUE
C      C
C      C
C      PIPE JUNCTIONS
      IF (M.EQ.1) GOTO 75
      J2=M
      DO 70 J=2,M
      IF (L(J-1).NE.0) THEN
          J2=J2+1
      ELSE
          J2=J2
      ENDIF
      I=1
      CALL FCM(I,J,Q,QU,P,B,R,FF,ZETA,CH)
      CH1=CH
      CALL FCM(I,J2,Q,QU,P,B,R,FF,ZETA,CH)
      J1=J-1
      I=NS(J1)
      CALL FCP(I,J1,Q,QU,P,B,R,FF,ZETA,CP)
      IF (T.EQ.DT) THEN
          OLDCP(J1)=CP
          OLDCN(J)=CH1
      ENDIF
      IF (NV(J).EQ.1) GOTO 63
      IF (NA(J).EQ.1) GOTO 64
      IF (L(J-1).EQ.1) GOTO 65
      IF (J.EQ.NP) GOTO 67
      IF (J.EQ.NPLS) GOTO 69
      PP(J,1)=(CP-CH1)/(B(J)+B(J-1))
      QP(J,1)=CH1+B(J)*PP(J,1)
      QPU(J,1)=QP(J,1)
      QP(J-1,1)=QP(J,1)
      QPU(J-1,1)=QP(J,1)
      PP(J-1,1)=PP(J,1)

```

```

63      GOTO 70
C      CALL VALUE(J,B,NS,CP,CH1,CV,OP,PP,OPU)
      WRITE(8,8)'VALUE CALLED'
      GOTO 70
64      CALL ACCUM(J,B,P,Q,CP,CH1,DT,NS,PAO,VAO,TOL,PP,OP,OPU)
      GOTO 70
65      CALL BRANCH(J,J2,B,NS,CP,CH,CH1,OP,PP,OPU)
C      WRITE(8,8)'BRANCH CALLED'
      GOTO 70
67      CALL DELP(J,A,Q,P,NS,DP)
      CALL PUMP(J,B,CH,CP,DP,NS,OP,PP,OPU)
C      WRITE(8,8)'PUMP CALLED'
      GOTO 70
69      CALL PULSE(J,B,T,W,NS,QU,CP,CH1,PP,OP,OPU)
70      CONTINUE
C
C      END CONDITIONS
C
75      CONTINUE
C      IF (T.LE.0.2) THEN
C          POR=4.944E+5-2.472E+68T
C      ELSE
C          POR=0.
C      IF (T.LE.0.2.OR.T.GE.1.65) THEN
C          POR=5.91E+5
C      ELSEIF (T.GT.0.2.AND.T.LE.0.55) THEN
C          POR=5.91E+5-1.2395E+68(T-0.2)
C      ELSEIF (T.GT.0.55.AND.T.LT.1.45) THEN
C          POR=1.374E+5-3.268E+48(T-0.55)
C      ELSE
C          POR=1.079E+5+2.414E+68(T-1.45)
C      ENDIF
C      PP(1,1)=POR
C      J=1
C      I=1
C      CALL FCH(I,J,Q,QU,P,B,R,FF,ZETA,CH)
C      OP(1,1)=CH+PP(1,1)8B(1)
C      OPU(1,1)=OP(1,1)
C      J=N
C      I=NS(N)
C      CALL FCP(I,J,Q,QU,P,B,R,FF,ZETA,CP)
C      PP(J,I)=P(J,I)
C      OP(J,I)=CP-PP(J,I)8B(J)
C      I=T/TC+
C
C      IF (I.GE.NTA) GOTO 79
C      TH=(T-(I-1)8TC)/TC
C      TAU(N,2)=TA(I)8(1-TH)+TH8TA(I+1)
C      IF (T.GT.TC) GOTO 79
C      TAU(N,2)=(1-T/TC)88TX
C      GOTO 80
79      TAU(N,2)=TA(NTA)
80      CV(N,2)=CVP(N,2)8TAU(N,2)882/B(N)
      OP(N,NS(N))=-CV(N,2)+88RT((CV(N,2))882+28CV(N,2)8CP)
      PP(N,NS(N))=(CP-OP(N,NS(N)))/B(N)

```

```

C      X=CV(M,2)/2
C      PP(M,NS(M))=(-SQRT(X)/B(M)+SQRT(X+B(M)*(CP+QU*SIN(WST)))
C      * /B(M))**2
C      QP(M,NS(M))=CP-PP(M,NS(M))*B(M)
C      QOR=QO*SQRT(PP(M,NS(M))/PO)
C      QPU(M,NS(M))=QP(M,NS(M))
C      IF (MB.NE.M) THEN
C          DO 85 J=M1,MB
C              I=NS(J)
C              CALL FCP(I,J,Q,QU,P,B,R,FF,ZETA,CP)
C              QP(J,I)=0.
C              QPU(J,I)=0.
C              PP(J,I)=CP
85      CONTINUE
C          ENDIF
C
C      RESET VALUES FOR NEXT ITERATION
C
C          DO 90 J=1,MB
C              DO 90 I=1,NS(J)
C                  Q(J,I)=Q(J,I)
C                  QU(J,I)=QU(J,I)
C                  Q(J,I)=QP(J,I)
C                  QU(J,I)=QPU(J,I)
C                  P(J,I)=PP(J,I)
C                  IF (P(J,I).GT.PMAX) THEN
C                      PMAX=P(J,I)
C                      IMAX=I
C                      JMAX=J
C                      TMX=T
C                  ENDIF
C                  IF (P(J,I)+PB.LT.PV) THEN
C                      P(J,I)=-PB+PV
C                  ENDIF
90      CONTINUE
C          IF (K/IPR*IPR-K.EQ.0) THEN
C              GOTO 40
C          ELSE
C              GOTO 50
C          ENDIF
99      STOP
C          END
C
C      SUBROUTINE FCH(I,J,Q,QU,P,B,R,FF,ZETA,CH)
C      REAL Q(17,150),P(17,150),ZETA(17),B(17),FF(17)
C      REAL QU(17,150),R(17)
C
C      QS=Q(J,I)-ZETA(J)*(Q(J,I)-Q(J,I+1))
C      PS=P(J,I)-ZETA(J)*(P(J,I)-P(J,I+1))
C      CH=QS-R(J)-PSSB(J)-FF(J)*ABS(QS)*QS
C      RETURN
C      END

```

```

C
C
SUBROUTINE FCP(I,J,Q,QU,P,B,R,FF,ZETA,CP)
  REAL Q(17,150),P(17,150),ZETA(17),B(17),FF(17)
  REAL QU(17,150),R(17)
C
  QR=Q(J,I)-ZETA(J)*(Q(J,I)-Q(J,I-1))
  PR=P(J,I)-ZETA(J)*(P(J,I)-P(J,I-1))
  CP=QR-R(J)+PR*B(J)-FF(J)*ABS(QR)*QR
RETURN
END
C
C
C
SUBROUTINE DELP(J,A,QP,PP,NS,DP)
  REAL QP(17,150),PP(17,150),A(17)
  INTEGER NS(17)
  COMMON/DELTAP/ B0,B1,B2,B3,QPO,PPO,DPPO
C
  J1=J-1
  I=NS(J1)
  DP=DPPO-B0*((QP(J,1)-QPO)/A(J))**2-B1+(PP(J1,I)-PPO)
  * /((B2+B3*(PP(J1,I)-PPO))
RETURN
END
C
C
C
SUBROUTINE VALUE(J,B,NS,CP,CH,CV,QP,PP,QPU)
  REAL B(17),CV(17),QP(17,150),PP(17,150),QPU(17,150)
  INTEGER NS(17)
C
  J1=J-1
  I=NS(J1)
  X=CP/B(J1)-CH/B(J)
  IF (X.GE.0) THEN
    QP(J1,I)=-CV(J)*(1/B(J)+1/B(J1))+SQRT((CV(J)*(1/B(J)
  * +1/B(J1))**2+2*CV(J)*X)
  ELSE
    QP(J1,I)=CV(J)*(1/B(J)+1/B(J1))-SQRT((CV(J)*(1/B(J)
  * +1/B(J1))**2-2*CV(J)*X)
  ENBIF
  PP(J1,I)=(CP-QP(J1,I))/B(J1)
  QPU(J1,I)=QP(J1,I)
  QP(J,1)=QP(J1,I)
  QPU(J,1)=QPU(J1,I)
  PP(J,1)=(QP(J,1)-CH)/B(J)
RETURN
END
C
C
C
SUBROUTINE BRANCH(J,J2,B,NS,CP,CH,CH1,QP,PP,QPU)
  REAL B(17),QP(17,150),QPU(17,150),PP(17,150)
  INTEGER NS(17)

```



```

C
  J1=J-1
  I=NS(J1)
    PP(J,1)=(CP-CH-CH1)/(B(J)+B(J1)+B(J2))
    PP(J2,1)=PP(J,1)
    PP(J1,I)=PP(J,1)
    OP(J,1)=PP(J,1)*B(J)+CH1
    OP(J2,1)=PP(J2,1)*B(J2)+CH
    OP(J1,I)=CP-PP(J,1)*B(J1)
    OPU(J,1)=OP(J,1)
    OPU(J2,1)=OP(J,1)
    OPU(J1,I)=OP(J,1)
  RETURN
  END

```

```

C
C
C
SUBROUTINE PUMP(J,B,CH,CP,DP,NS,OP,PP,OPU)
  REAL B(17),OP(17,150),OPU(17,150),PP(17,150)
  INTEGER NS(17)

```

```

C
  J1=J-1
  I=NS(J1)
    PP(J,1)=(CP-CH+B(J1)*DP)/(B(J)+B(J1))
    PP(J1,I)=PP(J,1)-DP
    OP(J1,I)=CP-B(J1)*PP(J1,I)
    OP(J,1)=OP(J1,I)
    OPU(J,1)=OP(J,1)
    OPU(J1,I)=OP(J,1)
  RETURN
  END

```

```

C
C
C
SUBROUTINE PULSE(J,B,T,W,NS,OV,CP,CH,PP,OP,OPU)
  REAL B(17),PP(17,150),OP(17,150),OPU(17,150)
  INTEGER NS(17)

```

```

C
  J1=J-1
  I=NS(J1)
    PP(J,1)=(CP-CH-OV*ABS(SIN(W*T)))/(B(J)+B(J1))
    PP(J1,I)=PP(J,1)
    OP(J,1)=PP(J,1)*B(J)+CH
    OP(J1,I)=CP-PP(J1,I)*B(J1)
    OPU(J,1)=OP(J,1)
    OPU(J1,I)=OP(J1,I)
  RETURN
  END

```

```

C
C
C
SUBROUTINE ACCUM(J,B,P,Q,CP,CH,DT,NS,PAO,VAO,TOL,PP,OP,OPU)
  REAL B(17),TOL(17),P(17,150),Q(17,150),PP(17,150),OP(17,150)
  REAL OPU(17,150),OLDCP(17),OLDCH(17),PAO(17),VAO(17)
  INTEGER NS(17)

```

COMMON/OLD/ OLDCN,OLDCP

C

```
J1=J-1
CMNID=(OLDCN(J)+CH)/2
CPNID=(OLDCP(J1)+CP)/2
PEND=P(J,1)
PD1=PEND
CALL PNEW(J,B,P,DT,PAO,VAO,PEND,CMNID,CPNID,PN,QIN,QOUT)
PN1=PN
PD2=PEND*1.00001
CALL PNEW(J,B,P,DT,PAO,VAO,PD2,CMNID,CPNID,PN,QIN,QOUT)
10 A=(PN1-PN)/(PD1-PD2)
A1=PN1-A*PD1
PEND=A1/(1-A)
PD1=PD2
PN1=PN
CALL PNEW(J,B,P,DT,PAO,VAO,PEND,CMNID,CPNID,PN,QIN,QOUT)
IF (ABS(PN-PEND).GT.TOL(J)) THEN
  PD2=PEND
  GOTO 10
ENDIF
PP(J,1)=PEND
PP(J1,NS(J1))=PP(J,1)
QP(J,1)=QOUT
QP(J1,NS(J1))=QIN
QPU(J,1)=QP(J,1)
QPU(J1,NS(J1))=QP(J1,NS(J1))
OLDCN(J)=CH
OLDCP(J1)=CP
RETURN
END
```

C

C

C

```
SUBROUTINE PNEW(J,B,P,DT,PAO,VAO,PEND,CMNID,CPNID,PN,QIN,QOUT)
REAL P(17,150),B(17),PAO(17),VAO(17)
INTEGER NS(17)
```

C

```
J1=J-1
PHID=(P(J,1)+PEND)/2
QIN=CPNID-PHID*NS(J1)
QOUT=PHID*NS(J)+CMNID
VDOT=QIN-QOUT
PN=P(J,1)+DT*VDOT*PHID**2/(PAO(J)*VAO(J))
RETURN
END
```

## Appendix B: Additional Boundary Conditions

### Branch Connection

For the purposes of this work, any branching junctions were considered to consist of one pipe flowing into two (Fig. B-1). In this type of connection the continuity equation was used, a common head was assumed after neglecting losses as minor effects, and the characteristic equations at the pipe ends were needed: Eq. (2.18) for pipe 1, and Eq. (2.19) for pipes 2 and 3 (14:45). Rewriting the characteristic equations

$$P_p = P_{p1} = P_{p2} = P_{p3} \quad (\text{B.1})$$

$$Q_{p1} = C_p - B P_{p1} \quad (\text{B.2})$$

$$Q_{p2} = C_{M1} + B P_{p2} \quad (\text{B.3})$$

$$Q_{p3} = C_M + B P_{p3} \quad (\text{B.4})$$

A summation of Eq. (B.1) through (B.4) provided a simple solution for the common pressure,  $P_p$ :

$$P_p = (C_p - C_{M1} - C_M) / \Sigma B \quad (\text{B.5})$$

The flow in each pipe would then be found by use of the appropriate characteristic equation. If required, this method could be expanded to any other number of pipes by the addition of more characteristic equations to the summation in Eq. (B.5).

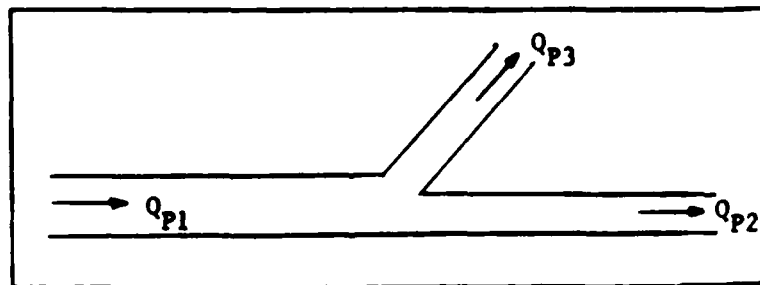


Fig. B-1. Branch Connection

### Instantaneous Pressure Rise

The end conditions created by a nonreciprocating pump may be approximated by a lumped rise in pressure of magnitude,  $\Delta P$ , as long as the dimensions of the pump are small compared to those of the other system elements (3:16). The end conditions take the form

$$\begin{aligned} Q_{P1} &= C_P - B_1 P_{P1} & Q_{P2} &= C_M - B_2 P_{P2} \\ Q_{P1} &= Q_{P2} & P_{P2} &= P_{P1} + \Delta P \end{aligned} \quad (B.5)$$

Solving simultaneously

$$P_{P1} = (C_P - C_M - B_2 \Delta P) / (B_1 + B_2) \quad (B.6)$$

Here again the remaining unknowns would be calculated directly from the appropriate equation. Note, however, that no loss term was used at the interface. These losses should be taken into account when assigning the functional form of  $\Delta P$ . One such form of  $\Delta P$  was given by Fashbaugh and Streeter (11:1014) as

$$\Delta P = \Delta P_0 - B_0 (Q_d - Q_{d0}) / A - [B_1 - (P_u - P_{u0}) / (B_2 + (P_u - P_{u0}) B_3)]^2 \quad (B.8)$$

in which  $Q_d$  is the outlet flow and  $P_u$  the pressure at the inlet of the pump. The constants  $\Delta P_0$ ,  $B_0$ , and  $Q_{d0}$  are constants determined from the steady-state pressure rise versus flow rate curve. While  $P_{u0}$ ,  $B_1$ ,  $B_2$ , and  $B_3$  are constants obtained from the steady-state pressure rise versus inlet pressure curve (11:1014).

## Vita

First Lieutenant William F. Berrier, Jr. was born in Harrisburg, Pennsylvania on 12 June 1962. In June of 1980 he graduated from Huntingdon Area High School in Huntingdon, Pennsylvania. In September of 1980 he entered the Pennsylvania State University, College of Engineering, on a four year scholarship from the Air Force ROTC program. Upon completion of his studies on 19 May 1984, he received a Bachelor of Science degree in Aerospace Engineering and a commission in the USAF. On 22 May 1984 he entered the School of Engineering, Air Force Institute of Technology at Wright-Patterson AFB, Ohio.

Permanent Address: 11-19th Street

Huntingdon, Pa 16652


UNCLASSIFIED

SECURITY CLASSIFICATION OF THIS PAGE

REPORT DOCUMENTATION PAGE

1a. REPORT SECURITY CLASSIFICATION <b>UNCLASSIFIED</b>		1b. RESTRICTIVE MARKINGS	
2a. SECURITY CLASSIFICATION AUTHORITY		3. DISTRIBUTION/AVAILABILITY OF REPORT <i>Approved for public release; distribution unlimited</i>	
2b. DECLASSIFICATION/DOWNGRADING SCHEDULE		4. PERFORMING ORGANIZATION REPORT NUMBER(S) <b>AFIT/GA/AA/85D-2</b>	
5. MONITORING ORGANIZATION REPORT NUMBER(S)		6a. NAME OF PERFORMING ORGANIZATION <b>School of Engineering</b>	
6b. OFFICE SYMBOL <i>(If applicable)</i> <b>AFIT/ENY</b>		7a. NAME OF MONITORING ORGANIZATION	
6c. ADDRESS (City, State and ZIP Code) <b>Air Force Institute of Technology Wright-Patterson AFB, Ohio 45433</b>		7b. ADDRESS (City, State and ZIP Code)	
8a. NAME OF FUNDING/SPONSORING ORGANIZATION		8b. OFFICE SYMBOL <i>(If applicable)</i>	
8c. ADDRESS (City, State and ZIP Code)		9. PROCUREMENT INSTRUMENT IDENTIFICATION NUMBER	
11. TITLE (Include Security Classification) <b>See Box 19</b>		10. SOURCE OF FUNDING NOS.	
		PROGRAM ELEMENT NO.	PROJECT NO.
		TASK NO.	WORK UNIT NO.
12. PERSONAL AUTHOR(S) <b>William F. Berrier Jr., B.S., 1LT, USAF</b>			
13a. TYPE OF REPORT <b>MS Thesis</b>	13b. TIME COVERED FROM _____ TO _____	14. DATE OF REPORT (Yr., Mo., Day) <b>1987 May</b>	15. PAGE COUNT <b>104</b>
16. SUPPLEMENTARY NOTATION			
17. COSATI CODES		18. SUBJECT TERMS (Continue on reverse if necessary and identify by block number)	
FIELD	GROUP	SUB GR.	<b>Fluid Transients, Unsteady Flow, Method of Characteristics, Propellant Feedlines</b>
19. ABSTRACT (Continue on reverse if necessary and identify by block number)			
<p>Title: <b>DYNAMICS OF PROPELLANT FEEDLINE SYSTEMS</b></p> <p>Thesis Chairman: <b>Dr. Milton E. Franke, Professor Department of Aeronautics and Astronautics</b></p>			
20. DISTRIBUTION/AVAILABILITY OF ABSTRACT <b>UNCLASSIFIED/UNLIMITED</b> <input checked="" type="checkbox"/> SAME AS RPT. <input type="checkbox"/> DTIC USERS <input type="checkbox"/>		21. ABSTRACT SECURITY CLASSIFICATION <b>UNCLASSIFIED</b>	
22a. NAME OF RESPONSIBLE INDIVIDUAL <b>Dr. Milton E. Franke</b>		22b. TELEPHONE NUMBER <i>(Include Area Code)</i> <b>513-255-2362</b>	22c. OFFICE SYMBOL <b>AFIT/ENY</b>

Approved for public release: IAW AFR 100-4.  
 BY: *[Signature]*  
 E. WOLAVER 3 Sept 87  
 Dir. for Research and Professional Development  
 Air Force Institute of Technology  
 Wright-Patterson AFB, OH 45433



In this investigation, a generalized computer code for the simulation of fluid transients was assembled, verified, and applied. The solution method developed for the program was based on a method of characteristics solution of the equations of motion for one-dimensional fluid flow in pipelines. The differential equations were solved using a first-order finite difference technique. Boundary conditions for the equations of motion were developed or directly included from available component models. The computer routines were verified by comparison of results with published results from several sources. The agreement between the results of this study and the published data was quite good for a wide range of boundary conditions and pipe systems. Recommendations were made for improvement of some models and the replacement of others to further improve the accuracy of the results.

